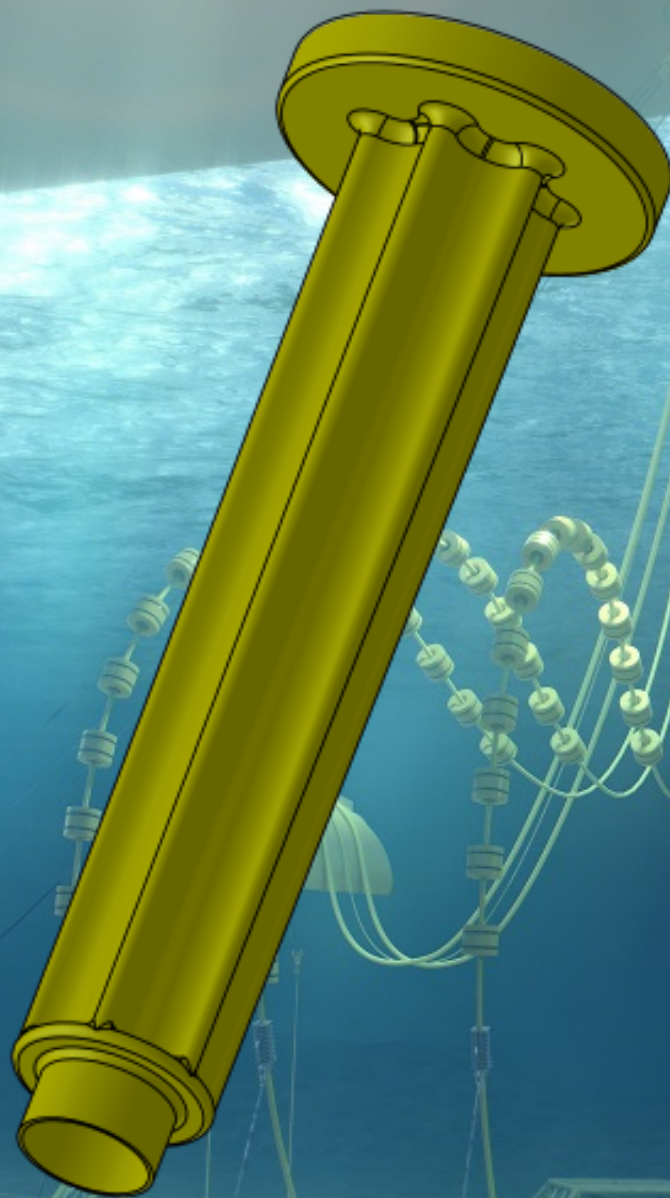


---

# **Design and Development of a Bend Stiffener for Flexible Pipelines in Offshore Industries**

---

*In collaboration with National Oilwell Varco Denmark I/S*



**Master Thesis**  
**Design of Mechanical Systems**  
**Aalborg University**  
**June 2015**

Source frontpage picture: [https://www.nov.com/Segments/Completion\\_and\\_Production\\_Solutions/Subsea\\_Production\\_Systems/Flexibles/Products\\_and\\_Solutions/10\\_Reasons\\_for\\_Choosing\\_Flexible\\_Pipes.aspx](https://www.nov.com/Segments/Completion_and_Production_Solutions/Subsea_Production_Systems/Flexibles/Products_and_Solutions/10_Reasons_for_Choosing_Flexible_Pipes.aspx)

Download date: 03-06-2015





**Study Board of Industry and Global Business Development**  
Fibigerstraede 16 - DK-9220 Aalborg East - Phone +45 99 40 93 09  
swe@me.aau.dk - www.industri.aau.dk

**Titel:** Design and Development of a Bend Stiffener for Flexible Pipelines in Offshore Industries  
**Semester theme:** Design of Mechanical Systems  
**Semester:** Master Thesis - 10<sup>th</sup> semester  
**Project period:** 02-02-2015 to 03-06-2015  
**ECTS:** 30 points  
**Supervisor:** Jan Schjødt-Thomsen and Jens H. Andreasen  
**Project group:** DMS4 - 2.209A

**Group members:**

---

Peter Tinggaard Sørensen  
Student no.: 20103698

---

Lean Ravnkilde Johansen  
Student no.: 20102483

**Printed copies:** 6 pcs.  
**Pages:** 99  
**Appendix:** 20 pages  
**Annex:** 4 CD

**Synopsis:**

This project is focused on the design development of a bend stiffener, for flexible pipelines in the oil industry. The problem with the old design is that it is too insulating, which causes the outer wall of the pipe to fail. The design is developed through a design process consisting of several iterations. The final design is based on a combination of the current design and a conceptual design developed through the report. The design is optimized towards a desired behaviour, where the current bend stiffener design is used as reference. A model of the equivalent stiffness of the flexible pipe was needed in order to evaluate the strength of the bend stiffener. A pipe model was therefore developed. The stresses determined in the strength analysis was too high, and it was concluded that the design could not be dimensioned to withstand the stresses without compromising the mechanical behaviour. The reports leaves an open design process, ready for further development. All necessary data and models have been developed in this project to continue the process. The design fulfilled the mechanical behaviour and the temperature requirement.

# Resume

Denne rapport omhandler udviklingen af et nyt design, af en bøjningsstiver til fleksible rør i olieindustrien. Arbejdet er udført i samarbejde med National Oilwell Varco Denmark I/S (NOV), som har leveret opgavebeskrivelsen for projektet. Rapporten er udarbejdet, som en speciale afhandling på kandidatuddannelsen i Design af Mekaniske Systemer på Aalborg Universitet.

Formålet med projektet er at udvikle og designe en ny bøjningsstiver, med lavere isolationsevne. Dette skyldes, at det nuværende design er årsag til, at overfladen på de fleksible rør nedbrydes, fordi temperaturen er for høj ved bøjningsstiveren. Rørets overflade der er lavet af polyamid ældes og hydrolyse processen (reaktion med vand) fremskyndes, når temperaturen er for høj. Det nuværende design af bøjningsstiveren er lavet af polyuretan, som har en relativ høj isolationsevne. Virksomheden, NOV, ønsker et nyt design med den samme mekaniske opførsel, som den nuværende bøjningsstiver. Rapporten lægger ud med, at bestemme opførslen af den nuværende bøjningsstiver for, at etablere en reference opførsel, der kan benyttes til, at tilpasse opførslen af det nye design. Derudover analyseres det nuværende design også termisk, for at bevise, at temperaturen er et reelt problem. Dernæst undersøges de omgivelser og ydre påvirkninger der kunne have indflydelse på designet af bøjningsstiveren. Analysen af den nuværende bøjningsstiver efterfølges af en kravspecifikation, der er delt op i primære og sekundære krav, som designet skal opfylde.

Designfasen tager form efter kravspecifikationen og bygger på en metode udviklet til industriel produkt design. Designfasen går gennem nogle trin, hvorved de bedste intuitive design forslag kommer videre. Denne del af projektet slutter med et konceptdesign, der består af næsten udelukkende af stål, hvilket har forholdsvis ringe isolationsegenskaber. Dette design optimeres mod den rette mekaniske reference opførsel bestemt tidligere i projektet. Ved denne optimering opstår nogle problemer i opførslen, som er design betinget. Herefter bliver designet ændret til en kombination af konceptdesignet og det nuværende design. Dette design optimeres ved brug af Finite Element Methods og optimeringsalgoritmer. Dette gøres for at opnå den ønskede opførsel. En termisk analyse udføres hvor konvektion er inkluderet, for at bevise at temperatur kravet er overholdt i det nye design. Dette design raffineres i forhold til design detaljer, formålet med disse detaljer er bl.a. at undgå styrkemæssige problemer, som fx kærvfølsomhed.

Oprindeligt var det ikke en del af projektet, at modellere det fleksible rør, da en model af denne skulle være givet fra projektstart. Denne model udeblev imidlertid og derfor blev en model udviklet i projektet. Denne model har til formål, at bestemme den ækvivalente bøjningsstivhed af røret. Modellen er baseret på en række videnskabelige artikler omhandlende modellering af rør. Kapitlet om rørmodellering beskriver tre ækvivalente stivheder, baseret på forskellige bøjningstilfælde af røret.

Efter at røret er modelleret, kan styrken af det nye design evalueres. Det viser sig, at det nye design ikke er stærkt nok og kan ikke dimensioneres til den rette styrke uden at gå på kompromis med den mekaniske opførsel, hvilket er uhensigtsmæssig. En procedure for udmattelses beregninger var udarbejdet, men da den statiske styrke ikke var overholdt, var der intet incitament for, at bestemme udmattelses levetiden. Dog er udmattelses proceduren præsenteret i appendiks for den interesserede læser.

Projektet efterlader et åbent designforslag, med basis for videreudvikling. Med dette projekt er alt forarbejdet gjort, for at kunne udvikle en ny bøjningsstiver. Alle nødvendige data og modeller er udviklet og samlet, hvilket ikke var tilgængeligt før dette projekt. Især bør det bemærkes at projektet bidrager med en modellering af det fleksible rør, som kan anvendes til, at bestemme en ækvivalent stivhed for røret.

# Preface

This master thesis is the outcome of development work carried out between the 1st of February to the 3rd of June 2015, and is written at the Department of Mechanical and Manufacturing Engineering (M-tech), Aalborg University.

## **Reading guide**

All the references throughout the report are displayed using the Vancouver reference system; hence references are stated with a number in a square bracket. A list of references can be found in the back of the report. Be aware that figures are modified to fit the layout of the report, even though these are based on a source. All figures inspired from a source is added with Vancouver reference system.

Also included is a collection of appendices that complement the report and an Annex-CD, containing various software routines and other material relevant for the report. The contents of the Annex-CD are listed on page 121.



# Contents

<b>Nomenclature</b>	<b>xii</b>
<b>1 Introduction</b>	<b>1</b>
1.1 Consequences Due to Failure of Energy Plants . . . . .	1
1.2 Main Purpose of The Project . . . . .	3
<b>2 Case</b>	<b>7</b>
2.1 National Oilwell Varco . . . . .	7
2.2 Main Issue and Task Description . . . . .	11
2.3 Materials, Dimensions and Load Cases of The Current Bend Stiffener and Pipe . . . . .	12
2.4 Summary . . . . .	16
<b>3 Project Objective and Methodology</b>	<b>17</b>
3.1 Project Objective . . . . .	17
3.2 Project Strategy and Methodology . . . . .	17
<b>4 Analysis of Current Structure and Surroundings</b>	<b>21</b>
4.1 Scope of Analysis . . . . .	21
4.2 Environment and Surroundings . . . . .	22
4.3 Standards . . . . .	25
4.4 Basis Structural Analysis . . . . .	26
4.5 Summary . . . . .	45
<b>5 Requirements for The New Design</b>	<b>47</b>
5.1 Primary Requirements . . . . .	47

5.2	Secondary Requirements . . . . .	48
<b>6</b>	<b>Development of a Conceptual Design</b>	<b>49</b>
6.1	Description of The Design Procedure . . . . .	49
6.2	Material Selection . . . . .	50
6.3	Implementation of The Design Procedure . . . . .	52
6.4	Presentation of The Initial Design Concept . . . . .	57
6.5	Summary . . . . .	58
<b>7</b>	<b>Initial Design Evaluation And Development</b>	<b>59</b>
7.1	Optimisation of Deflection Curve . . . . .	59
7.2	Design Changes due to Behaviour Issues . . . . .	60
<b>8</b>	<b>Final Design Optimisation and Development</b>	<b>63</b>
8.1	Optimisation . . . . .	63
8.2	Thermal Analysis of The Final Design . . . . .	66
8.3	Refinement of The Design . . . . .	70
8.4	Summary and Discussion . . . . .	71
<b>9</b>	<b>Analytical Modelling of the Bending Stiffness of a Flexible Pipe</b>	<b>73</b>
9.1	Pipe Structure . . . . .	73
9.2	Contribution from Polymer Layers . . . . .	74
9.3	Contribution from Helical Steel Layers . . . . .	75
<b>10</b>	<b>Static Strength Analysis</b>	<b>83</b>
10.1	Analysis Setup . . . . .	83
10.2	Results and Discussion of the Analysis . . . . .	84
<b>11</b>	<b>Conclusion and Discussion</b>	<b>87</b>
11.1	Modelling of the Current Bend Stiffener . . . . .	87
11.2	Design Procedure . . . . .	87
11.3	Optimisation of New Design and Strength Analysis . . . . .	88
11.4	Stiffness Modelling of the Pipe . . . . .	88

11.5 Overall Outcome of the Project . . . . .	89
<b>12 Future Work</b>	<b>91</b>
12.1 New Design Proposals . . . . .	91
12.2 Load Scenarios and Experiments . . . . .	91
<b>Bibliography</b>	<b>92</b>
<b>Appendix</b>	<b>101</b>
<b>A Shore hardness scale</b>	<b>101</b>
<b>B Preliminary Finite Element Model</b>	<b>103</b>
<b>C The Theory of FE Contact Formulations</b>	<b>107</b>
<b>D Fatigue Evaluation</b>	<b>113</b>
D.1 The Setup of a Corrected S-N Curve . . . . .	113
D.2 Considerations and the Overall Approach . . . . .	115
D.3 The Approach for The Fatigue Calculations . . . . .	117
<b>Annex-CD</b>	<b>121</b>
D.4 Report (pdf-version) . . . . .	121
D.5 Optimisation Scripts . . . . .	121
D.6 Thermal Models . . . . .	121
D.7 Nonlinear Stress Analysis . . . . .	121
D.8 3D Pipe Model . . . . .	121
D.9 New Design 3D Model . . . . .	121
D.10 Fatigue Script . . . . .	121

# Nomenclature

Symbol	Description	Page	Unit
$[T]$	Transformation matrix	111	—
$\alpha$	Lay angle of helical layer	76	<i>rad</i>
$\alpha_k$	Step size in the descent direction	65	—
$\Delta\sigma_{i \text{ Element}}$	Range stress tensor for load case i	118	—
$\Delta_L$	Element displacement vector	111	—
$\Delta T$	Temperature difference	66	<i>K</i>
$\Delta u$	Relative displacement in the tangential direction	110	—
$\Delta v$	Relative displacement in the normal direction	110	—
$\kappa$	Global bending curvature	75	$\frac{1}{m}$
$\kappa_b$	Local binormal curvature of a tendon	81	$\frac{1}{m}$
$\kappa_n$	Local normal curvature of a tendon	81	$\frac{1}{m}$
$\kappa_t$	Local torsional curvature of a tendon	81	$\frac{1}{m}$
$\kappa_{cr}^{min}$	Minimum critical curvature	79	$\frac{1}{m}$
$\kappa_{ns}$	Critical curvature for the initiation of slip	78	$\frac{1}{m}$
$\lambda_i$	Langrangian	64	—
$\mu$	Friction coefficient	110	—
$\mu_i$	Inner friction coefficient of helical layer	79	—
$\mu_o$	Outer friction coefficient of helical layer	79	—
$\nabla$	Gradient	65	—
$\phi$	Angle between helical tendon and xy-plane	76	—
$\phi_{cr}$	Critical angle at which slip initiates	79	<i>rad</i>

$\mathbf{d}$	Unit vector - feasible descent direction	65	–
$\mathbf{H}_k$	Hessian matrix	65	–
$\mathbf{s}$	Slack variable vector	65	–
$\mathbf{x}_k$	Design variable vector	65	–
$\sigma'_{ai}$	Equivalent alternating stress for load case i	116	<i>Pa</i>
$\sigma'_{mi}$	Equivalent mean stress for load case i	116	<i>Pa</i>
$\sigma_{1a}$	Maximum principal stress	117	<i>Pa</i>
$\sigma_{ai} \text{ Element}$	Alternating stress tensor for load case i	118	–
$\sigma_f$	Stress in full slip range	79	<i>MPa</i>
$\sigma_{iL} \text{ Element}$	Lower stress tensor for load case i	118	–
$\sigma_{iU} \text{ Element}$	Upper stress tensor for load case i	118	–
$\sigma_{mi} \text{ Element}$	Mean stress tensor for load case i	118	–
$\sigma_{ns}$	Stress in no slip range	79	<i>MPa</i>
$\sigma_{xa}$	Alternating normal stress in x direction	116	<i>Pa</i>
$\sigma_{xm}$	Mean normal stress in x direction	116	<i>Pa</i>
$\sigma_{ya}$	Alternating normal stress in y direction	116	<i>Pa</i>
$\sigma_{ym}$	Mean normal stress in y direction	116	<i>Pa</i>
$\sigma_{za}$	Alternating normal stress in z direction	116	<i>Pa</i>
$\sigma_{zm}$	Mean normal stress in z direction	116	<i>Pa</i>
$\tau_{xya}$	Alternating shear stress	116	<i>Pa</i>
$\tau_{xym}$	Mean shear stress	116	<i>Pa</i>
$\tau_{yza}$	Alternating shear stress	116	<i>Pa</i>
$\tau_{yzm}$	Mean shear stress	116	<i>Pa</i>
$\tau_{zxa}$	Alternating shear stress	116	<i>Pa</i>
$\tau_{zxm}$	Mean shear stress	116	<i>Pa</i>
$\theta$	Angle	109	<i>rad</i>
$\varepsilon$	axial strain of a helical tendon	77	–
$\xi$	Constant used to determine $\phi_{cr}$	79	–
$^{\circ}C$	Celsius	22	–

$A$	Area	66	$m^2$
$A$	Coefficient presenting the value of $S_{Nf}$ at one cycle	119	$Pa$
$B$	Coefficient presenting the slope of a S-N curve	119	—
$b$	Width of a tendon in a helical layer	79	$m$
$C_{Load}$	Correction factor for loading effects	114	—
$C_{Reliab}$	Correction factor for reliability	114	—
$C_{Size}$	Correction factor for size effects	114	—
$C_{Surf}$	Correction factor for surface effects	114	—
$C_{Temp}$	Correction factor for temperature effects	114	—
$D$	Displacement	108	$m$
$D_{PM}$	The Palmgren-Miner sum	119	—
$E$	Young's modulus	34	$Pa$
$E_{poly}$	Young's Modulus for polymer layers	75	$GPa$
$EI_{bt}$	Equivalent stiffness due to local bending and torsion	81	$Nm^2$
$EI_{ns}$	Equivalent stiffness for the no slip range	78	$Nm^2$
$EI_{ps}$	Equivalent stiffness in the partial slip range	80	$Nm^2$
$F$	Force	34	$N$
$f_c$	Fill factor for a helical layer	79	—
$F_j$	Strip force	32	$N$
$F_L$	Element force vector	111	—
$g$	Gab	108	$m$
$g_i$	Inequality constraint equation	64	—
$h$	Convection heat transfer coefficient	66	$\frac{W}{m^2} \cdot K$
$h$	Height	32	$N$
$I$	Moment of inertia	34	$m^4$
$i, j$	Index	118	—
$I_{poly}$	Area moment of inertia of polymer layers	75	$m^4$
$k$	Element stiffness	108	$m$
$k^{th}$	Iteration	65	—

$L$	Length	34	$m$
$L$	Length of a helical tendon	77	$m$
$M$	Moment	32	$Nm$
$m$	Coefficient used in fatigue calculation	117	—
$m$	The number of inequality constraints	65	—
$M_b$	Global bending moment	75	$\frac{1}{m}$
$n$	Normal direction	109	—
$n$	Number of tendons in a helical layer	79	—
$n_i$	Number of load cycles	119	—
$N_{fi}$	Number of cycles for a specific fatigue strength	119	—
$P_i$	Inner surface/contact pressure of helical layer	79	$Pa$
$P_o$	Outer surface/contact pressure of helical layer	79	$Pa$
$q$	heat transfer per unit time	66	$W$
$R$	Radius of helical layer	76	$m$
$r$	Radius	34	$m$
$S_{e'}$	Uncorrected endurance limit	113	$Pa$
$S_e$	Corrected endurance limit	113	$Pa$
$S_{N_{fi}}$	Uniaxial fully reversed fatigue strength for load case i	117	$Pa$
$S_{ut}$	Ultimate tensile strength	119	$Pa$
$t$	Tangential direction	109	—
$U$	Strain energy	77	$J$
$W$	Work done by the bending moment	78	$J$
$w$	Deflection in z direction	34	$m$
$k_g$	Element artificial stiffness	108	—



## Introduction

One of the largest political and industrial issues in the last century, has been the utilization of the energy resources available on earth. Thus, in the last 100 years there has been an increased focus on the exploitation of wind power, sun energy and the world's oil and gas deposits. This vital need for energy has led to a worldwide energy industry, which is known for large production facilities, placed all over the world. This chapter will give an introduction to these facilities and failures which can appear on such facilities. The consequences due to these failures will also be discussed. All this leads to a final description of the main purpose of this project.

### Contents

---

<b>1.1</b>	<b>Consequences Due to Failure of Energy Plants . . . . .</b>	<b>1</b>
<b>1.2</b>	<b>Main Purpose of The Project . . . . .</b>	<b>3</b>

---

### 1.1 Consequences Due to Failure of Energy Plants

The worldwide energy industry began in the early 1900s with the invention of the combustion engine, and in the following years was oil and gas the primary source of energy instead of coal, this industry is known for worldwide companies such as Shell and BP. The utilization of wind energy and the use of solar cells started in the 1970s, especially because of two oil crises which caused a decrease in the oil production.

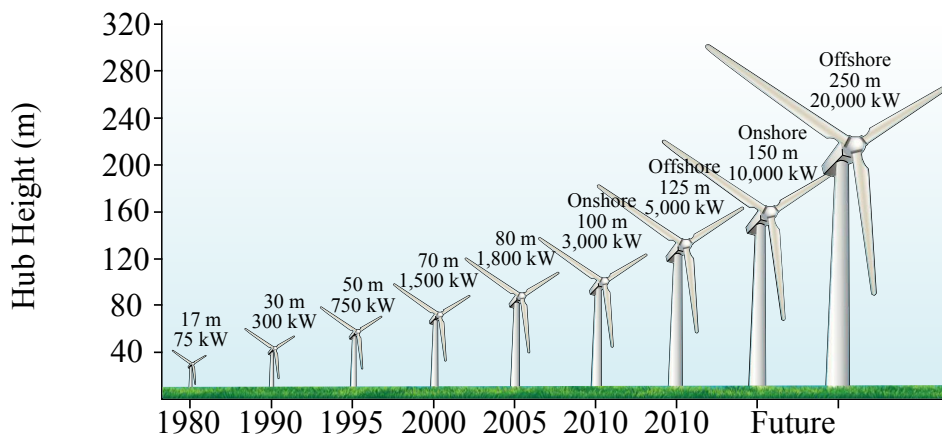


**Figure 1.1:** Development of typical commercial wind turbine [54].

These alternatives to oil and gas energy grew through the 1990s, mainly caused by the growing concern about the use of fossil fuels. Over the years, wind turbines and oil

---

production have been developed to extract more energy, which usually means that the physical size of these plants have been enlarged. This trend can be seen particularly in the development of wind turbines, see figure 1.1 [13; 14; 47; 60].

On figure 1.1, the rotor diameter and the turbine size is specified with meters and kilowatt are specified above each development step, which indicates the growth in size of typical wind turbines. As energy plants has become larger over time, failure of these plants are also associated with major consequences, both social and economic. One example would be the Deepwater horizon accident in 2010, where 4.9 million barrels of oil was released from the well, and the cleanup costed BP more than 14 billion USD, see figure 1.2.



**Figure 1.2:** The Deepwater horizon accident [17].

The accident occurred because high pressure methane gas from the well was ignited, which led to an explosion on the Deepwater horizon oil rig. The accident caused more than just financial losses, 11 workers on the oil rig was never found, and it is assumed that they died in the explosion. The following spill of the 4.9 million barrels of oil, or 780,000 m<sup>3</sup>, directly affected 180,000 km<sup>2</sup> of ocean [58].

The Deepwater horizon episode was rated to be the largest accidental oil spill, and was a major and unusual accident, but also small technical errors can cause significant damage and economic losses. An example can be read in an article from from the Danish magazine *Ingeniøren*. The article describes the magnitude of economic losses associated with an interrupted energy production. It reports how a broken valve on a Norwegian oil rig in 2012 forced a stop to the oil production. As the rig daily produced about 11,854 barrels of oil at a market price of 116 USD per barrel, the daily loss due to missing income was about 1,38 million USD per day. In the article it is not stated how many days of production that was lost, but it is clear that the production was stopped in at least seven days, which means that the losses of income in this period was about 10 million USD [27].

## 1. Introduction

---

Another technical problem related to oil production, is the failure of flexible oil pipe. The magnitude of this problem is described in a report from The Petroleum Safety Authority Norway (PSA) [55]. The flexible pipes have been used for more than 30 years, and was developed to be used in both static and dynamic applications. The flexible pipe consists of several layers of steel and polymers, and is therefore a complex structure compared to a rigid pipe manufactured of a solid material. According to the report from PSA Norway are the flexible pipes related to high failure rate, because of the complexity of the structure. In the period from 1995 to 2013, PSA has reported 85 failures of flexible pipes, and 60 of these were classified as a major incident, meaning that there was a high risk of injury or pollution. The failure of the pipes was due to a number of different errors in the different layers, like fatigue of metal layers and failure of the polymer due to ageing or hydrolysis. An example of failure of the flexible pipe is shown on figure 1.3.



**Figure 1.3:** Failure of the outer layer of the flexible pipe [55].

The failure shown on figure 1.3 is cracking of the outer polymer layer of the flexible pipe. This failure is due to a high temperature on the surface of the flexible pipe under a bend stiffener, which ensures a proper bending radius of the pipe. As the outer layer serves as protection of the inner layers, damage or cracking of this layer will cause failure of the flexible pipe, which might lead to serious accidents.

The issue with a high temperature between a flexible pipe and the bend stiffener is also the main topic in this project, and the main purpose of the project is outlined in the next section.

### 1.2 Main Purpose of The Project

This project is a collaboration with the danish division of the worldwide wellknown oil company National Oilwell Varco, which is a manufacturer of flexible oil pipes. These flexible pipes are equipped with a bend stiffener located at the vicinity of the oil rig, shown on figure 1.4.

The purpose of the bend stiffener is to gradually increase the bending stiffness of the pipe and transfer the loads between the flexible pipe and the stiff rig construction. The current bend stiffener design has a high insulating effect, which causes the pipe to suffer from a hydrolysis process which is accelerated above 70°C. This process leads to decomposition of the outer fluid barrier of the pipe. The local division of NOV flexibles has requested a new design of the bend stiffener that lowers the insulating effect and thus the temperature of the outer wall of the pipe.

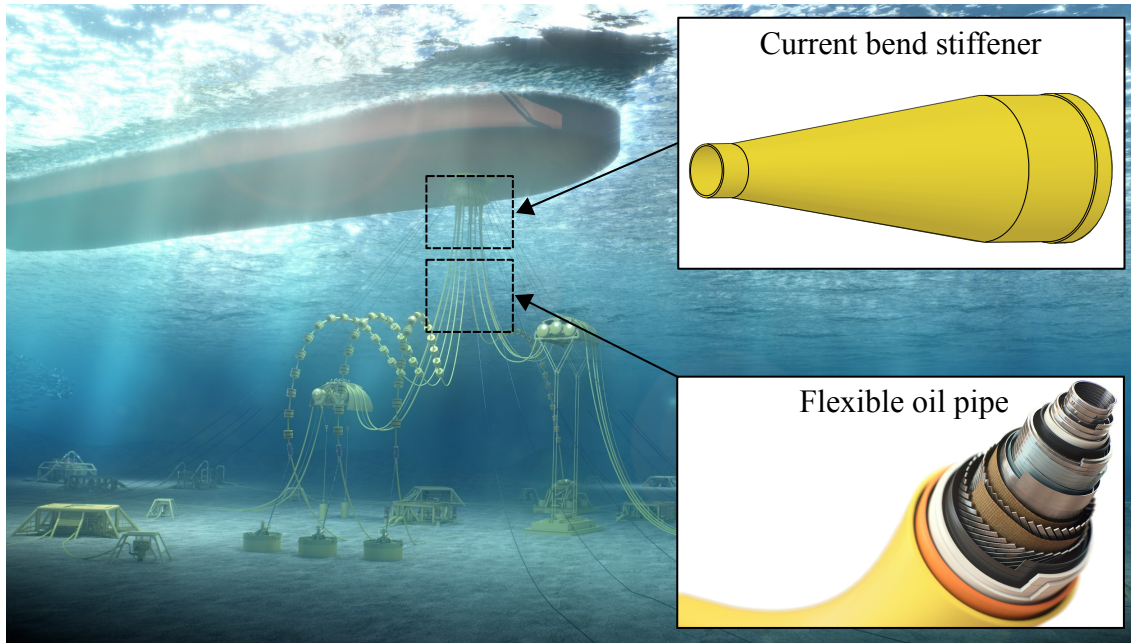


**Figure 1.4:** Oil production plant with the location of the oil pipes and the bend stiffeners [42].

This report describes how a new design of a bend stiffener is developed. The project ended with the design shown on figure 1.5, this design needs further development in order to be full operational. As there are different sizes of tubes, there are also various sizes of bend stiffeners, and therefore, the development work must be limited to one type of bend stiffeners. Therefore is this project based on a current bend stiffener that fits a pipe with an outer diameter of 308 mm.

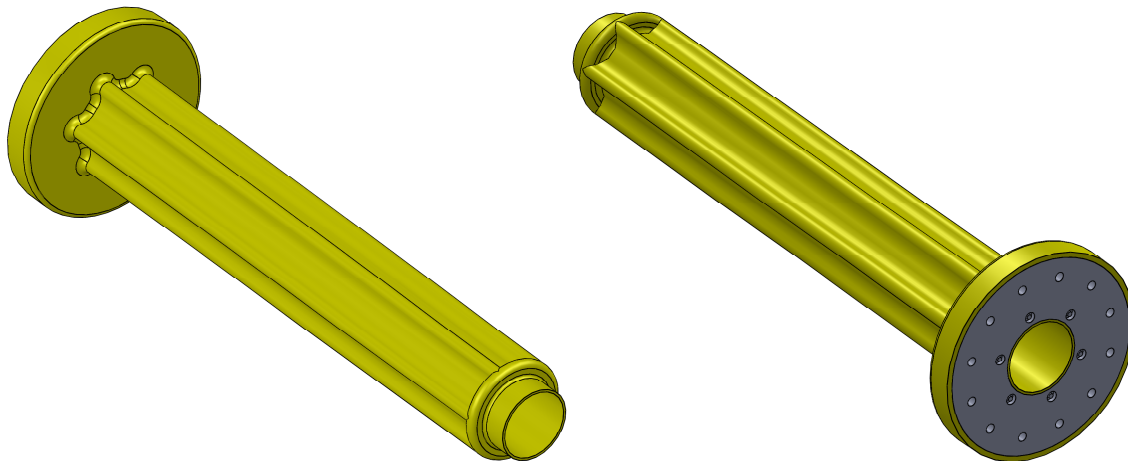


**Figure 1.5:** The new developed design of the bend stiffener

Each chapter in the report describes a step in the development of a new bend stiffener, and the following text briefly states what is presented to the reader through the report. Initially, the reader will be introduced to National Oilwell Varco and the structure of the flexible oil pipes, it will also be revealed how the current bend stiffener is designed, and which materials are used to manufacture the bend stiffener. This leads to determination of the extent of the problem, which is conducted by an analysis of current structure and

## *1. Introduction*

---

surroundings. In the analysis the structure of the current bend stiffener is investigated, but also issues that influence the development of a new design are considered.

Based on this analysis, the full extent of the project is revealed, and the objectives of the project will be outlined. In order to achieve these goals, a development strategy with associated methods will be explained. The rest of the report covers the application of the development methods with the aim of creating a new and useful design of a bend stiffener.

In the next chapter, National Oilwell Varco, their product and the main task of this project be introduced.



## Case

The purpose of the project is to design a bend stiffener for flexible pipes, and this task is stated by the company, National Oilwell Varco. In this chapter the company is presented, and the extent of the task is described. First, National Oilwell Varco, its products and the challenges associated with the product are presented, and afterwards the essence of the task is outlined.

### Contents

---

<b>2.1 National Oilwell Varco</b> . . . . .	<b>7</b>
<b>2.2 Main Issue and Task Description</b> . . . . .	<b>11</b>
<b>2.3 Materials, Dimensions and Load Cases of The Current Bend Stiffener and Pipe</b> . . . . .	<b>12</b>
2.3.1 Materials . . . . .	12
2.3.2 Dimensions . . . . .	13
2.3.3 Load Cases . . . . .	15
<b>2.4 Summary</b> . . . . .	<b>16</b>

---

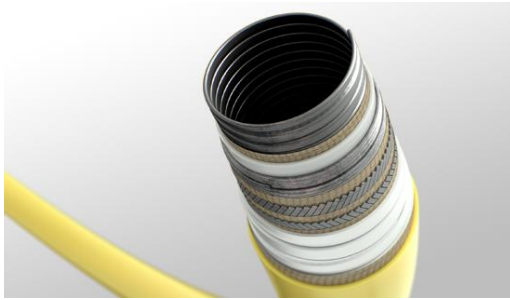
### 2.1 National Oilwell Varco

National Oilwell Varco, also known as NOV, is an American multinational company, which provides solutions, equipment and components for the oil and gas drilling industries, and its activities are spread out over six continents [59].

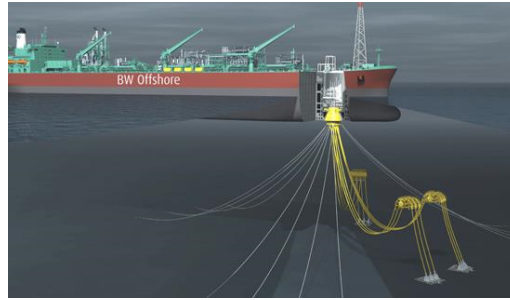
This project is conducted in collaboration with the danish division of National Oilwell Varco. The company has three locations in Denmark, where the Danish headquarter is placed in Brøndby at Sealand, the production facilities are placed in Kalundborg and a small research and development office is placed in Aalborg. The task for this project is stated by the office in Aalborg and all collaboration is done with this office.

The Danish division, National Oilwell Varco Denmark I/S, is also called NOV Flexibles, and produces flexible pipe systems as a part of a complete floating production system, see figure 2.1(a) and figure 2.1(b) [28; 41].

The pipes manufactured by NOV Flexibles consist of different layers, and combining the properties for each individual layer, constitute all the features of the pipe, that are necessary to operate satisfactorily when submerged into water.



(a) Flexible pipe [41].



(b) Floating production system [41].

**Figure 2.1**

There are various types of pipes for different applications. The number of layers varies, depending on the specific pipe model. However, the structure is relatively similar among the different types of pipes, and there are normally five basic layers in a flexible pipe, these are shown on figure 2.2 [11].

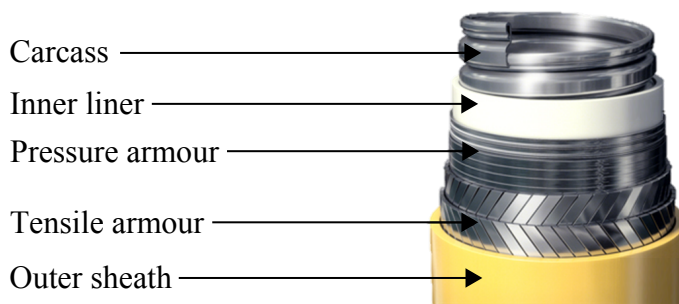
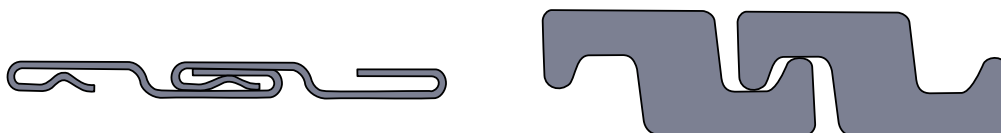


**Figure 2.2:** The basic layers in the pipes manufactured by NOV Flexibles [41].

The innermost layer is the carcass, which consist of stainless steel flat strips, these are shaped to have an interlocking profile, see figure 2.3(a). The purpose of the carcass is to resist the hydrostatic pressure from the sea, and a secondary property is to withstand corrosion caused by the fluid in the pipes.

Next layer is the inner liner, which is a layer of polymer acting as inner fluid barrier. The third layer is the pressure armour, and its main function is to resist the circumferential stress caused by the internal pressure in the pipe.



(a) Standard design of carcass [11].

(b) The Z shaped pressure armour [11].

**Figure 2.3**

## 2. Case

---

This layer is constructed by rolled carbon steel wires, which are formed as Z shaped profiles, so that the layer has an interlocking property, shown on figure 2.3(b). This layer also provides protection against external pressure and crushing damage caused by the next outer lying layer, known as the tensile armour.

The tensile armour consist of two layers that are cross lapped, and the layers are made of flat rectangular carbon steel wires. These layers are used to resist loads in the axial and torsional directions, meaning that the layers carry the weight of the flexible pipe when the pipeline is connected to the surface vessel. Layers of lubricating thermoplastics are inserted between the metal layers, to avoid wear. These are not shown on figure 2.2.

The outer layer is a polyamide layer, which is a thermoplastic material, and the main purpose with this layer is to seal and protect the metal layers against sea water, abrasion damage and corrosion.

The basic concept with the floating production system is to pump oil or gas from the well to a production ship at the surface through the flexible pipes produced by NOV Flexibles, shown on figure 2.1(b). At the connection between the ship and the flexible pipe, or other mechanical transition, a bend stiffener surrounds the pipe to avoid kinks and fatigue, this is shown on figure 2.4.

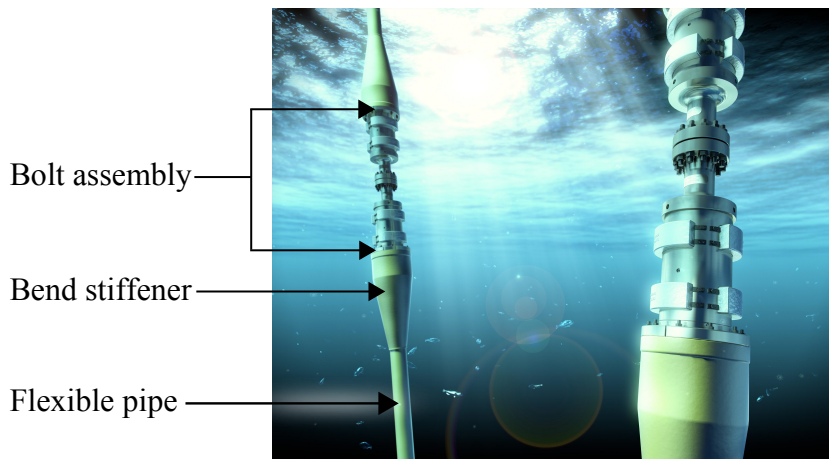


**Figure 2.4:** The mechanical transition between two flexible pipes, where bend stiffeners are mounted to avoid damage to the pipes [46].

The bend stiffener can both be placed in seawater and above sea level, which means it is hanging in the air. Placement of the bend stiffener depends on how it is used, and on which type of vessel the bend stiffener is mounted.

The bend stiffener can be formed as a hollow truncated cone with a steel mounting flange placed in one of the ends. By this flange is the bend stiffener assembled to a mechanical transition by bolts. The hollow truncated cone form and the mounting flange of the bend stiffeners produced by National Oilwell Varco is displayed on figure 2.5.

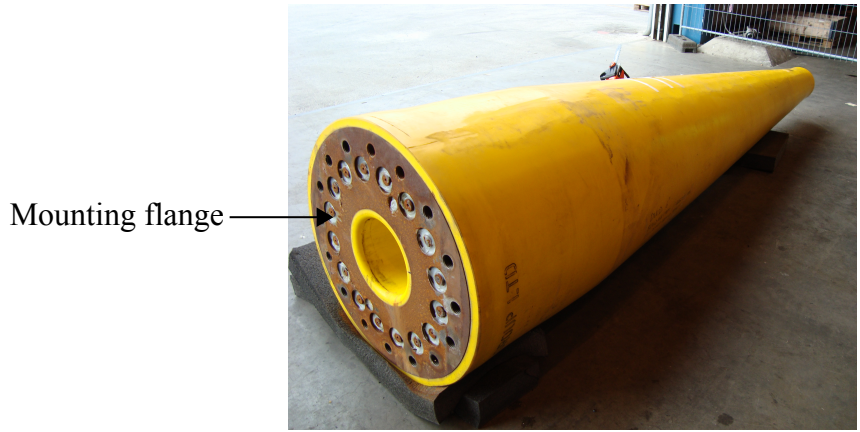


**Figure 2.5:** A typically bend stiffener produced by National Oilwell Varco [46].

The bend stiffener is assembled with a male connector at the mounting flange, and this is locked to a female connection in the vessel. Together these parts constitute the mechanical transition to the vessel, a typical male connector can be seen on figure 2.6.

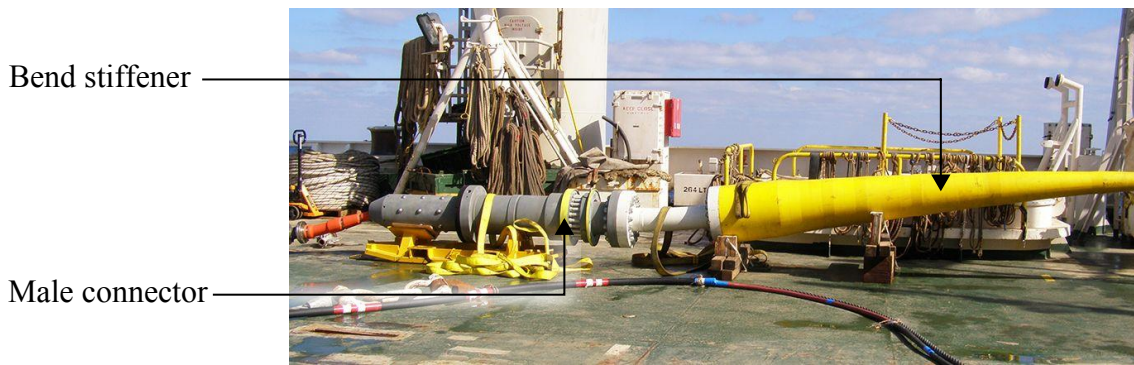


**Figure 2.6:** A typically assembly between the bend stiffener and the male connector [24].

The flexible pipe is guided through the bend stiffener and further through the mechanical connection to the vessel, and the flexible pipe is not locked in this transition. Therefore the pipe can slide through the connection and bend stiffener, and thereby is it ensured that the pipe can be moved depending on various operational requirements and maneuvers. The bend stiffener is constructed of polyurethane, and the steel mounting flange is molded into the construction. The flexible pipe is guided by the inner wall of the bend stiffener and the tolerance between the pipe and bend stiffener allows for a small gap. A conceptional drawing of the mechanical transition is shown on figure 2.7.

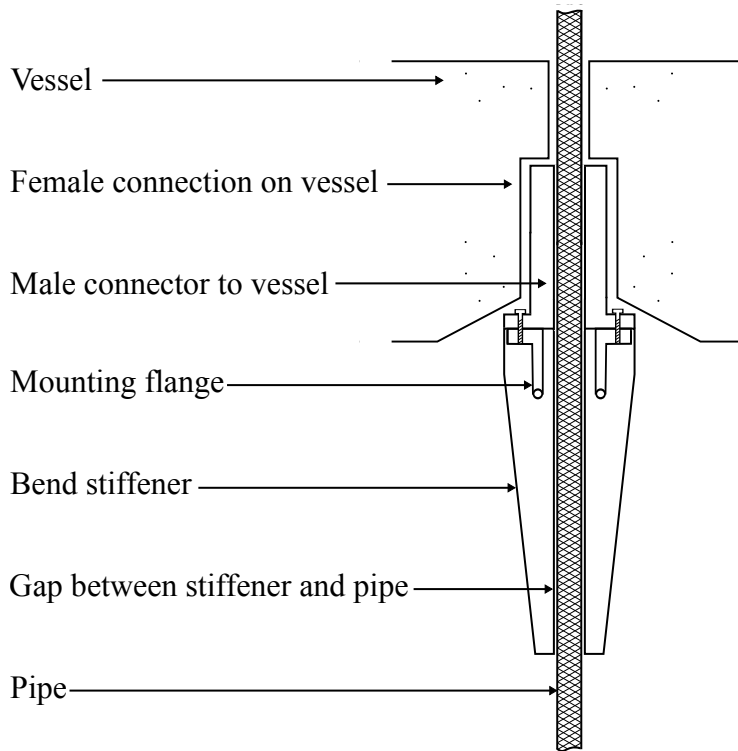


**Figure 2.7:** Sectional view of the mechanical transition between sea and vessel. The drawing is inspired by [33].

This type of bend stiffener design is causing damage to the surface material of the flexible pipe, which is the reason for making a new design of the bend stiffener. Further description and clarification of this problem is outlined in the next section, where the main task is stated.

### 2.2 Main Issue and Task Description

The damage to the flexible pipe occurs at the bend stiffener, and the following text describes the cause of the damage. The liquid is pumped through the pipeline with a temperature about 100°C to 130°C, and the surface of the pipe is cooled by the sea water. However, at the bend stiffener the surface temperature of the pipe rises because the bend stiffener has a thermal insulating effect. The increase in temperature causes the hydrolysis process to accelerate, and the surface of the pipe reacts chemically with the water between the pipe and bend stiffener, whereby the outer layer of pipe decomposes. As the surface layer of the pipe decomposes, water is passed on to the underlying layers, which are mainly constructed of metal, and damage occurs thereby progressively through each layer [29].

If failure to a flexible pipe occurs, then economic losses are mainly due to lost profit and costs related to installation of material replacements. NOV flexibles estimate that repair work due to a pipe failure at the bend stiffener would take from one week to two weeks, and to conduct the repair work, an installation vessel is required as the oil producing vessel is not able to lift the pipe. According to NOV flexibles, a repair operation is also depending on the weather conditions, so the economic loss associated with a production breakdown, could in worst case exceed two weeks. It is NOV Flexibles goal to avoid

hydrolysis by designing a new type of bend stiffener, which has a lower thermal insulating effect compared to the existing design. This new design, must have some of the same properties as the current design, and furthermore have either a cooling capacity or be manufactured in one or more materials which has a larger thermal conductivity [29]. As described in chapter 1 *Introduction*, is the project based on a specific bend stiffener, and next details about this bend stiffener is outlined.

## 2.3 Materials, Dimensions and Load Cases of The Current Bend Stiffener and Pipe

This section will give an overview of the materials used and the dimension of the current bend stiffener design. At the end of this section a presentation of the load cases are given, from which the current design is constructed.

### 2.3.1 Materials

The current design of the bend stiffener is made of a combination of a thermoplastic polyurethane (TPU) and steel. The bend stiffener is moulded in one part where the steel flange is inserted in the mould and the polymer is injected into the mould and surrounds the steel. The flexible pipe is made of layers of different materials where some of them are steel and some are polymers. The most widely used polymer for the pipes is polyamide 11 which is a certain type of nylon that has been developed to have good resistance against various types of fluids which makes it suitable for flexible pipes that is exposed to sea water on the outer side and crude oil inside the pipe. The inner carcass of the pipe is made of AISI 316 steel and the tensile and pressure armours are made of AISI 304 steel. Anti-wear layers of polymers are inserted between the steel layers and for the analyses made in this report it is assumed that these layers have the same properties as polyamide 11. The materials used for pipes and bend stiffener are listed in table 2.1.

**Table 2.1:** Material Properties - Bend Stiffener and Flexible Pipes

Properties	Unit	TPU S-60D	Polyamide 11	AISI 304	AISI 316
E-Modulus at 23°C	Pa	$186 \cdot 10^6$	$320 \cdot 10^6$	$193 \cdot 10^9$	$193 \cdot 10^9$
Flex. Modulus at 23°C	Pa	$151 \cdot 10^6$	$280 \cdot 10^6$	-	-
Yield Strength at 23°C	Pa	$36 \cdot 10^6$	$27 \cdot 10^6$	$215 \cdot 10^6$	$193 \cdot 10^6$
UTS at 23°C	Pa	$50 \cdot 10^6$	$30 \cdot 10^6$	$505 \cdot 10^6$	$580 \cdot 10^6$
Density	$\frac{\text{kg}}{\text{m}^3}$	1250	1050	8000	8000
Thermal Conductivity	$\frac{\text{W}}{\text{m}\cdot\text{K}}$	0.58	(61–142°C) 0.24	16.2	16.3
Poisson's Ratio	-	0.4	0.4	0.29	0.29
Source		[8; 26; 38] [29; 48]	[37; 56] [29]	[35]	[36]

All strength parameters are given at 23°C, because this is the assumed average temperature for the test conducted by NOV Flexibles which yields the load data used in this project. UTS is an abbreviation for ultimate tensile strength.

## 2. Case

The bend stiffener is mainly constructed of polyurethane, and according to technical data sheet on the polyurethane, the material exhibits relatively good wear and tear resistance and has a relatively high toughness. It also has good heat, oil, fuel, and solvent resistance, and has a relatively good damping characteristics. These properties indicates the reason to use polyurethane as the main material in the bend stiffener, which may be exposed to an environment containing damages corresponding to the above described effects. Given by information from NOV flexibles, it is known that the hardness of the polyurethane is 60 on the Shore Hardness D scale. The hardness of different plastic products and the Shore hardness scale is shown in Appendix A *Shore hardness scale*.

### 2.3.2 Dimensions

As mentioned in previous sections, the bend stiffener is composed of a steel part and a polyurethane part. The dimensions of the two parts are presented in this section, the complete bend stiffener design can be seen on figure 2.8.

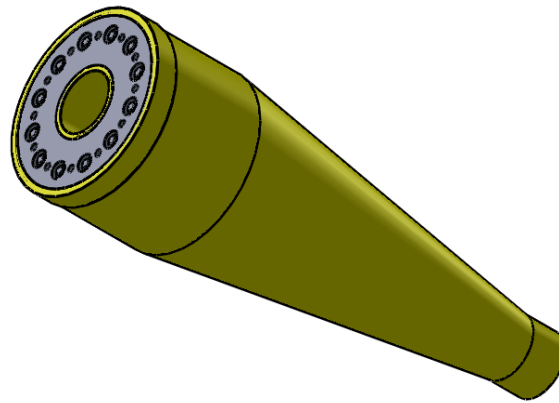


**Figure 2.8:** The current bend stiffener design, drawn with inspiration from [46].

The dimensions of the bend stiffener can be seen on figure 2.9. This figure shows all outer dimensions of the TPU part.

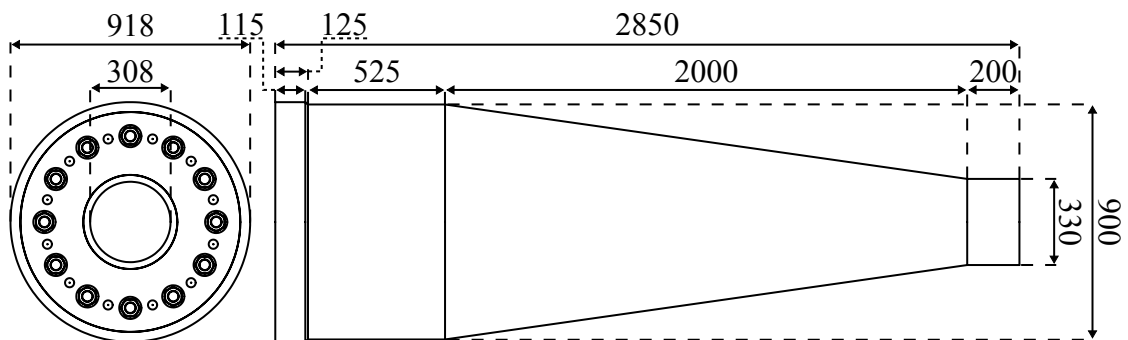


**Figure 2.9:** Outer dimensions of the TPU part of the bend stiffener, all dimensions are in mm. Drawn with inspiration from [46].

The design of the steel part can be seen below. This part is composed of a flange and a ring which is welded onto steel rods which are bolted on to the flange.

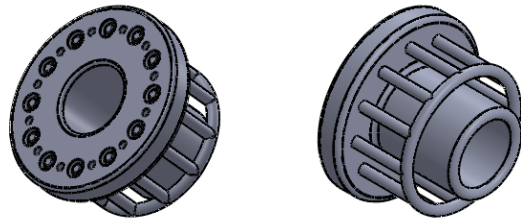


**Figure 2.10:** Design of the steel flange, drawn with inspiration from [46].

The dimensions of the steel part is given in figure 2.11. It should be noted that, the dimension of 120mm in section A on the figure, is not the thickness of the steel flange, but the length of the threaded part in the bolt connection.

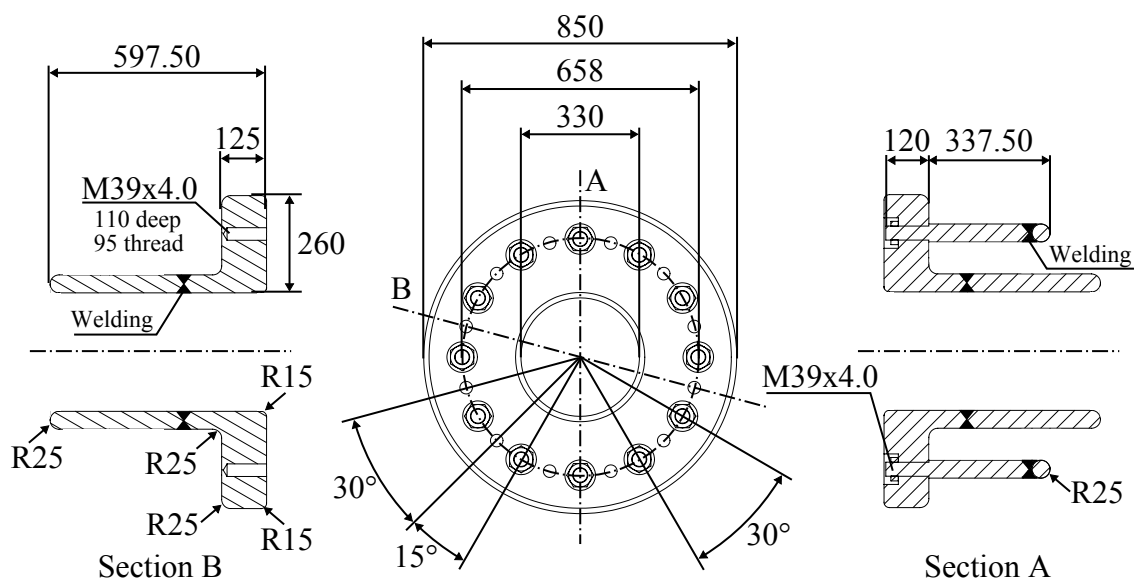


**Figure 2.11:** Dimensions of the steel flange, all dimensions are in mm. Drawn with inspiration from [46].

The pipe is build of several layers of different material. Layup of layers and their dimension and materials can be seen on figure 2.13. A complete 3D drawing of a pipe segment can be seen on figure 2.12.

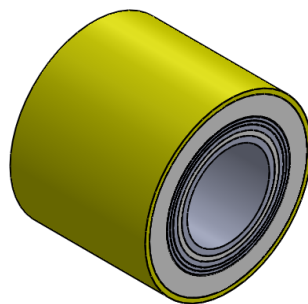


**Figure 2.12:** Pipe design, drawn with inspiration from [29].

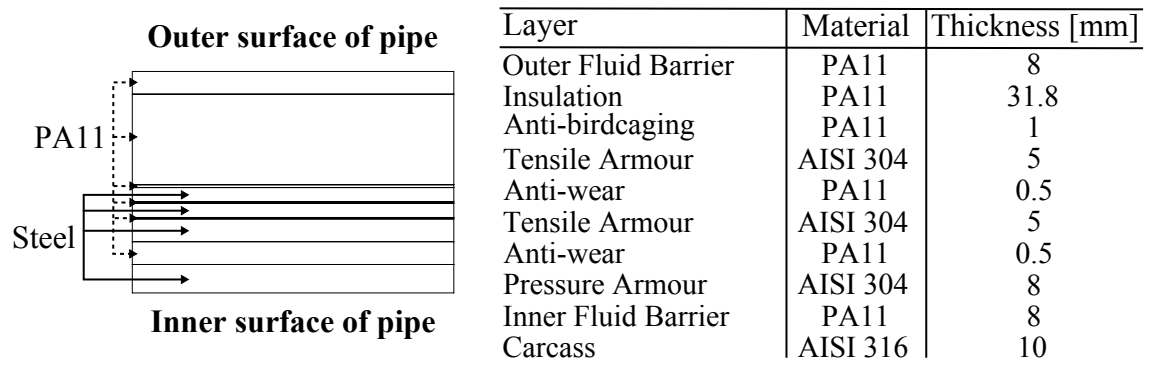


**Figure 2.13:** Dimensions and material of the different layers of the pipe, drawn with inspiration from [29].

The materials of the anti-wear and anti-birdcaging layers are unknown, but they are assumed to have the same properties as PA11. The same is assumed for the insulation layer.

### 2.3.3 Load Cases

NOV Flexibles I/S has performed some tests on their bend stiffener, where it has been exposed to different load cases with a different number of cycles. These test data are used as load cases for dimensioning the new design in this project. A setup of the test rig is illustrated on figure 2.14.



**Figure 2.14:** Test setup for testing the bend stiffener with different load cases [46].

The load cases are a combination of moment, shear and tension forces. An overview of load directions on the structure is given in figure 2.15.

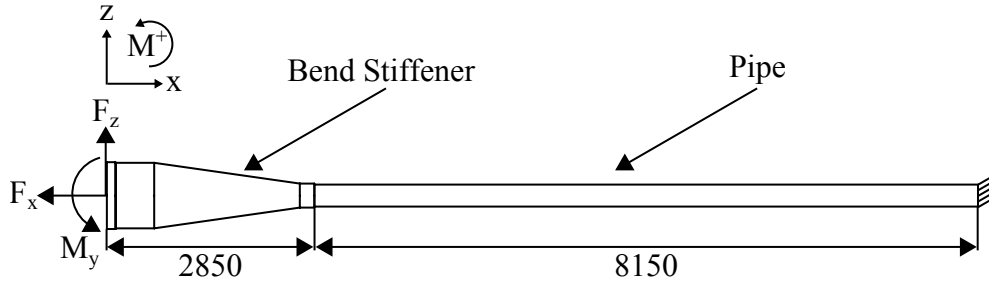


**Figure 2.15:** Direction of the loads exerted to the bend stiffener and pipe assembly in the test on figure 2.14. The figure is drawn with inspiration from [46].

The test was performed with six different load cases, where the force and moment range were change as well as the number of load cycles also was changed. The magnitudes of the loads are listed below in table 2.2.

**Table 2.2:** Load cases - Bend stiffener and pipe assembly

Load Case	No. of Cycles	Min. Tens.	Max. Tens.	Tens. Range	Min. Shear	Max. Shear	Shear Range	Min. Mom.	Max. Mom.	Mom. Range
-	-	kN	kN	kN	kN	kN	kN	kNm	kNm	kNm
1	1065600	1100	1300	200	-30.7	20.65	51.35	-74.4	69.01	143.41
2	586000	1080	1320	240	-35.09	26.51	61.6	-89.05	82.84	171.89
3	267000	1060	1340	280	-39.23	32.5	71.73	-103.7	94.83	198.53
4	80000	1050	1350	300	-41.21	35.54	76.55	-111.1	100.2	211.4
5	1000	933.1	1463	529.9	-67.43	83.04	150.47	-223.2	170.2	393.4
6	400	893.8	1491	597.2	-112	160.5	272.5	-405.2	288	693.2

All tension forces are along the x-axis, shear forces are along the z-axis and all moments are around the y-axis, see the axes on figure 2.15. All data in this table are from [46].

NOV Flexibles are using a static safety factor of two, and a fatigue safety factor of ten.

## 2.4 Summary

In this chapter were the company and the main problem of the project presented. The company, NOV Flexibles, produces flexible pipes for offshore floating oil systems, and each pipe consists of several layers of polymer and metal. The outer layer is a sealing layer that is protecting the underlying layers. This layer is made of polyamide, and due to the insulating effect of the bend stiffener, is the outer layer decomposed by hydrolysis. NOV Flexibles aims to design a new bend stiffener with less insulating properties.

As the extent of the project has been clarified, the main objectives and the methods are outlined in the next chapter.

## Project Objective and Methodology

Based on Chapter 2 *Case*, the project objective, a selected solution strategy and the chosen methodology are specify in this section. After this section it should be clear what is to be achieved through the project and what methods are used to obtain the objective.

### Contents

---

<b>3.1</b>	<b>Project Objective . . . . .</b>	<b>17</b>
<b>3.2</b>	<b>Project Strategy and Methodology . . . . .</b>	<b>17</b>

---

### 3.1 Project Objective

The main objective for this project is stated as:

*Design a bend stiffener that ensures a minimum bending radius of 2,2 m and a maximum surface temperature 70°C of the part of the flexible pipe, which is covered by the bend stiffener.*

### 3.2 Project Strategy and Methodology

To design a new bend stiffener, a model of the flexible pipe is required, in order to ensure a correct interaction between these two parts. As stated in the objective are there two main goals, these are basically to ensure the right bending behaviour and to lower the temperature of the surface of the flexible pipe. Therefore are two models required, one model of the mechanical behaviour and one of the thermal behaviour of the flexible pipe. At the first meeting with NOV Flexibles, the project group asked if the company had any models of the mechanical model of the flexible pipe. The company could not provide any model at the time.

It is decided to set up a basic model of the flexible pipe and the current bend stiffener, in order to examine the main thermal properties and the deflection over the length of the current bend stiffener. The flexible pipe is therefore modelled as a solid pipe with the layers shown in figure 2.13, well knowing that the pipe is too stiff. It should be possible to replicate the behaviour of the current design to a new design, regardless of the pipe inserted in the model. Later will a model of the flexible pipe be developed, in order to evaluate the design concepts. Based on this decision, a strategy to achieve the objectives for the project is setup, and the strategy consists of four main steps to ensure a proper design, which together constitute the methodology. These steps are; analysis of the current bend stiffener, a design procedure, structural engineering methods and evaluation,

---

which together constitute the methodology. A detailed description of each step is given below.

### **Analysis of The Current Bend Stiffener**

The purpose is to investigate if thermal insulation is the main problem, but also to determine the thermal and mechanical behaviour of the current bend stiffener, and furthermore to examine the operational environment for the bend stiffener. Therefore, a thermal and static structural analysis are conducted using finite element method, in order to examine the mechanical behaviour and the level of the bend stiffeners insulating effect. Several models and analytical expressions will be setup and compared to each other, in order to evaluate the steps in the modelling procedure and to ensure that the models are properly setup.

### **Determine the requirements for a new design of a bend stiffener**

The requirements obtained from the analysis of the current bend stiffener, together with the requirements from the company, will be divided into primary and secondary requirements. The requirements which are directly linked to the development of an useful design will be stated as primary requirements. The rest will be stated as secondary requirements, meaning that they are desirable, but not mandatory to fulfil. The primary focus is to develop a new design, and when this objective is obtained, the next aim is to fulfil the complete set of requirements.

### **Design Procedure**

A design procedure in four steps will be conducted, in order to develop a design concept. The basic idea with the procedure is to create a simple initial concept, and develop the design through the process, by adding shapes and details. Each step of the design procedure will be outlined in chapter 6 *Development of a Conceptual Design*.

### **Structural Engineering Methods**

Based on the primary requirements and the design concept, a new design is developed by using different structural engineering methods. The steps of this development and the methods that will be used are listed below.

#### **Step 1: Optimization**

Optimization will be used to refine the initial design concept.

#### **Step 2: Thermal FE Analysis**

The design concept is analysed to investigate the thermal behaviour of the new design.

#### **Step 3: Static and FE Analysis**

The final design is analysed from a static point of view, meaning that it should be dimensioned to withstand the static load cases. For this analysis a proper model of the flexible pipe is needed.

#### **Step 4: Fatigue Analysis**

The lifetime of the outcome of the static analysis is determined with respect to the load cycles that the structure is exposed to. The structure will be dimensioned to have the required lifetime, described in product requirements.

### ***3. Project Objective and Methodology***

---

#### **Evaluation of the new design**

When the final design is developed, it will be evaluated to ensure that the requirements are fulfilled.

The first step in the project strategy is initiated with analysis of the current bend stiffener, and this analysis is described in the next chapter.



## Analysis of Current Structure and Surroundings

This chapter deals with the behaviour of the structure described in the previous chapter, referred to as the *current structure*. The purpose of the analysis is to identify the thermal and mechanical behaviour of the current structure in order to reveal the designs advantage and disadvantage. Furthermore, should issues that are important for a new design be clarified. This chapter ends with a summary of the significant flaws in the current structure and design issues, which should lead to a specific list of requirements.

### Contents

---

<b>4.1 Scope of Analysis . . . . .</b>	<b>21</b>
<b>4.2 Environment and Surroundings . . . . .</b>	<b>22</b>
<b>4.3 Standards . . . . .</b>	<b>25</b>
<b>4.4 Basis Structural Analysis . . . . .</b>	<b>26</b>
4.4.1 Thermal Analysis . . . . .	26
4.4.2 Deflection Analysis . . . . .	28
4.4.3 Results . . . . .	41
<b>4.5 Summary . . . . .</b>	<b>45</b>

---

### 4.1 Scope of Analysis

The full extent and the limitations for the analysis are outlined in this section. The analysis is to narrow down all issues that are considered to be necessary to establish an initial design concept, so a requirements specification can be setup. The scope of the analysis is to assess the structural failures by determining the mechanical performance and temperature characteristics of the bend stiffener. Furthermore, to determine issues that are important for the new design. The full extent of the analysis are described below.

The first issue to examine is the environment, in which the bend stiffener must be able to operate in. Based on interview with NOV flexibles, it is known that the bend stiffener must be able to operate worldwide, and can be subjected to the effects caused by a sea environment. Therefore the global temperatures and the salinity condition in seawater are examined. The bend stiffener can also be affected by the surroundings on the vessel, and therefore, surroundings are also examined. The new design of the bend stiffener must fulfil the standards for products in offshore industries, and the standards related to bend stiffeners are studied and briefly outlined.

In order to determine main mechanical and heat properties of the current design of the bend stiffener, the Finite Element Method is used. Based on the Finite Element Analysis

it will be possible to assess how the heat flow is through the structure and how the structure deforms under the load described in section 2.3.3 *Load Cases*.

The limitations related to the objectives above, are that NOV flexibles has provided the overall load data, and therefore are the effect of weather conditions as winds and storms not addressed. The analysis starts with an examination of the effects from the environment and the surroundings.

## 4.2 Environment and Surroundings

In this section the operational environment temperatures, salinity conditions and surroundings are considered, as these issues might affect the properties of the bend stiffener. First the operational environment temperatures are studied, and since the bend stiffener must be able to act worldwide, a temperature interval must be determined. There are two sets of intervals studied, the first set describes the world temperature extremes, while the last set describes the global mean temperature for a year.

To assess the extreme temperatures a list describing continental weather extremes is considered. This list is published by Arizona State University (Based on work done by World Meteorological Organization), and according to this the maximum temperature was measured in North America to  $56.7^{\circ}\text{C}$ , while the lowest was measured in Antarctica to  $-89.2^{\circ}\text{C}$ . As it is unlikely that the bend stiffener will be used in Antarctica, the next lowest is sought on the list, and it was measured in Russia to  $-67.8^{\circ}\text{C}$ . As the extreme temperatures are determined, the worldwide mean air and sea temperature will be considered. These considerations are based on annual measurements for the period between January and December 2014, and the air temperature (temperature measured in 2 m height), is shown on figure 4.1(a), while the sea surface temperature is shown on figure 4.1(b).

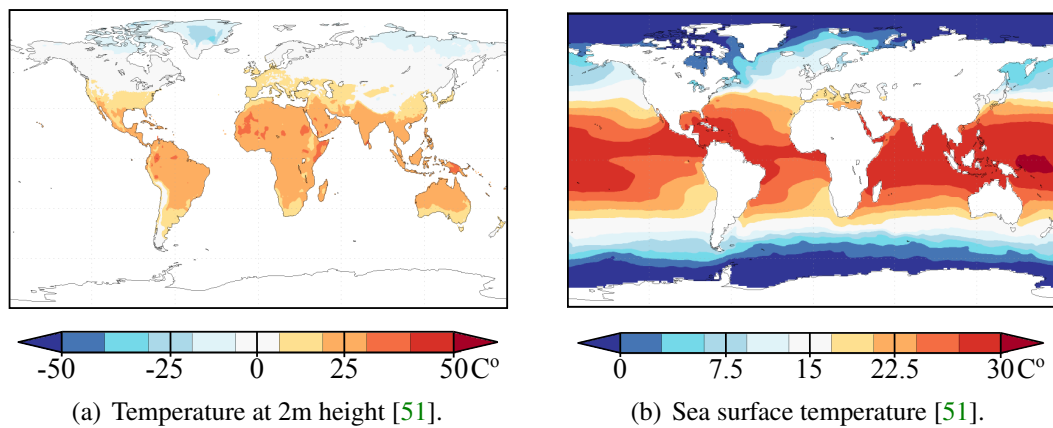


**Figure 4.1:** Overview of the world average air and sea temperature measured in Celsius of January-December 2014 [51].

From figure 4.1(a) it can be seen that the air temperature in most parts of the world is between  $-25^{\circ}\text{C}$  and  $25^{\circ}\text{C}$ , while the lower or higher temperatures are occurring at locations where the project specific type of oil production not is suitable or likely possible, for example in the middle of Greenland.

#### 4. Analysis of Current Structure and Surroundings

---

The Contour plot on figure 4.1(b) shows that large parts of the world are covered by seawater with temperatures that are contained in the entire scale, meaning that the bend stiffener must be able to operate in sea water temperature between 0°C and 30°C.

One could argue against the use of an average temperature consideration, as the bend stiffener is used at different global locations with different weather conditions, which likely will affect the mechanical properties, so it behaves differently depending on the location. As the aim is to design a new type of bend stiffener, the focus is on all the general conditions that must be fulfilled, then later could an extensive temperature analysis be conducted. Based on these considerations, and by assuming that the bend stiffener will be used in average air and sea temperatures, it is chosen to continue with the following temperature intervals:

Air temperature interval

- -25°C to 25°C.

Sea water temperature interval

- 0°C to 30°C.

The extreme temperatures will be considered, if the new design is made in a significant temperature sensitive material. This could be an issue if the bend stiffener and the pipe for example is stored onshore, and hereby exposed to extreme temperatures for a long period before it is transported to the production vessel on sea.

The level of salinity must be considered briefly, since the sea is a saline environment and can thereby cause accelerated corrosion for some materials. The salinity conditions are measured in practical salinity unit (PSU), which is salinity in water measured in parts per thousand. The world's sea salinity conditions measured in the PSU are shown on figure 4.2.

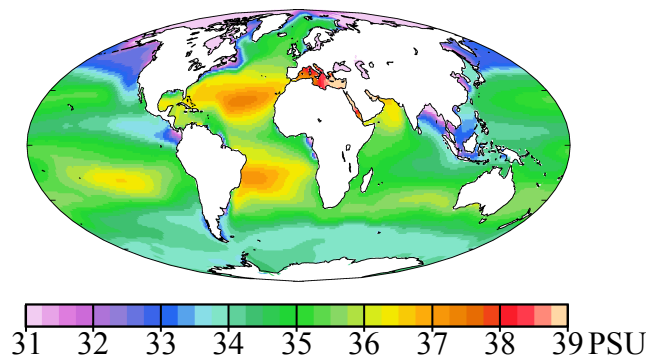


**Figure 4.2:** The worldwide seawater salinity conditions [61].

By considering figure 4.2 it is concluded that the bend stiffener must be designed to operate in a seawater environment with a PSU between 0.034 to 0.036 corresponding to 0.034kg - 0.036kg salt in one liter of water. Next are the surroundings which the bend

stiffener is a part of considered. When the bend stiffener is mounted to a vessel or floating oil rig, it is assumed that the surroundings will not have any effect on the bend stiffener, as there are normally relatively large space around the stiffener, an example is shown on figure 4.3.



(a) Closeup of a collection of bend stiffeners [53].



(b) A bend stiffener relative to the surroundings [53].

**Figure 4.3**

From figure 4.3(a) and figure 4.3(b) it is seen that surroundings from the vessel or rig does not normally constitute an obstacle to the bend stiffener, as long as the dimensions of the bend stiffener are kept within some limitations. These limitations given by NOV flexibles, and the dimensions of a new design shall be within a cylinder of 1 meter in diameter and 6 meters in length. These restraints are set due to the transport procedure. Before transportation, the bend stiffener is mounted on the flexible pipe, and pipe with bend stiffener is rolled on a cable drum. The cable drum is afterwards transported and mounted on the production vessel. The cable drum with pipe and the bend stiffener is seen on figure 4.4(a), and on figure 4.4(b) the transportation of a NOV flexible cable drum is shown.



(a) Cable drum with pipe and bend stiffener [43].



(b) Transportation of the cable drum [9].

**Figure 4.4**

The bend stiffener must not be too long, because it will protrude out over the edge of the cable drum, which is not preferable during transport. Neither must the diameter of the bend stiffener be too large, because it has to fit into a installation tool, and this tool is able to handle bend stiffener with a diameter up to 1 meter [29].

During transport or installation the surroundings could damage the bend stiffener, however, it is assumed these operations do not constitute any risk to the current design, as the polyurethane has a hardness of 60 on the Shore Hardness D scale, which is considered to withstand the wear associated with transportation and installation. A new design should include a material which has the same or better hardness to avoid damage or wear from such operations. All the surroundings have been investigated and a brief description of the standards, regarding the design of a bend stiffener, will be presented in the next section.

### 4.3 Standards

A set of standards has been written, in order to control the quality and safety aspects related to the products developed for the offshore industries. The purpose of the standards are to ensure that the products does not affect environment, safety etc. In this project the standards will be used more as guidelines than actual rules and requirements. The standards used in this project are API (American Petroleum Institute) standards, as it is requested from NOV flexibles to use these standards. It is especially the API 17L1 [2] and API 17L2 [3] which are used. The first is a set of specifications for flexible pipe ancillary equipment, the latter is recommended practice, related to the products described in 17L1. Only the most vital parts of the standard will be included in this section. There are four overall requirements to the ancillary equipment for flexible pipes. The following are citations taken directly from the standard [2].

- *"The ancillary equipment shall be capable of withstanding all design loads defined in the design requirements section applicable to the ancillary equipment in question."*
- *"The ancillary equipment shall perform its function for the specified service life."*
- *"The ancillary equipment materials shall be compatible with the environment to which the material is exposed."*
- *"Ancillary equipment metallic materials shall conform as a minimum to the corrosion requirements specified in 4.3.11 and in the corrosion requirements section applicable to the ancillary equipment in question."*

Where section 4.3.11 in the standard describes corrosion requirements for materials and especially for fasteners. The most vital requirements are

- The bend stiffener shall maintain the operating minimum bending radius of the pipe at all time during the service life.
- The bend stiffener shall transfer the loads from the flexible pipe to the supporting structure.

The standards provides a relatively large design freedom, as they are not directly specifications, but more serves as general guidelines to design of the bend stiffener. The next section deals with a basic structural analysis of the current design of the bend stiffener.

## 4.4 Basis Structural Analysis

A basic structural analysis is conducted, in order to investigate the behaviour of the current design. This analysis will include a thermal analysis, with the purpose of determining the steady state temperature through the bend stiffener under average operational conditions. Furthermore, an analysis of the behaviour due to static loads will be conducted, in order to investigate the deflection behaviour and determine a workspace for the bend stiffener.

### 4.4.1 Thermal Analysis

The purpose of the analysis is to predict the temperature distribution through the flexible pipe and the current bend stiffener. As mentioned earlier, the current design is too insulating, as the temperature rises above 70°C and thereby accelerates the hydrolysis process significantly. The analysis in this section will give an estimate of the temperature through the assembly of pipe and bend stiffener. This is simply to prove that temperature is really an issue, before conducting a design phase based on this assertion.

The analysis is set up as a steady-state analysis where the following material properties are used.

**Table 4.1:** Parameters used for steady-state thermal analysis

Material	Abbreviation	Thermal Conductivity $\frac{W}{m \cdot K}$	Density $\frac{kg}{m^3}$	Source
TPU Elastollan® S-60D	TPU	0.58	1250	[8; 48]
Polyamide 11	PA11	0.24	1050	[37; 56]
Steel AISI 304 & AISI 316	Steel	16.2	8000	[35; 36]

AISI 304 & AISI 316 has the same thermal conductivity and is therefore summarized to the abbreviation, steel, in this analysis. TPU is an abbreviation for thermoplastic polyurethane.

The analysis is set up as a 2D analysis with the geometry shown on figure 4.5. It can be seen that the bend stiffener is made of a cone formed polyurethane part where a steel flange is moulded into it.

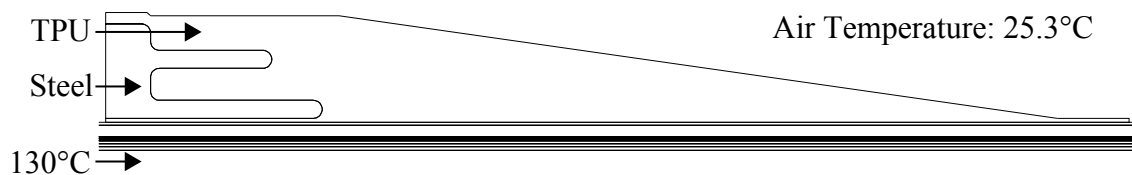


**Figure 4.5:** The geometry used in the heat transfer analysis.

The air temperature is set to 25.3°C as an average value, since this is the average temperature in a year in Brazil [63]. Brazil is one of the hottest places that the company delivers the bend stiffener to [29]. The temperature at the surface of the bend stiffener is set to be the same as the air temperature, even though that is a bit optimistic, since the surface temperature will probably get higher than the air temperature due to heat transfer from

#### 4. Analysis of Current Structure and Surroundings

the pipe and heating from the sun. The fluid inside the pipe is set to a temperature of 130°C [29]. The dimensions of pipe and bend stiffener used for this analysis can be seen in Annex D.3 *Annex-CD*. The material layup for the pipe can be seen on figure 4.6.

##### Air, Sea Water or Bend Stiffener

Outer Fluid Barrier: PA11
Insulating Layer: PA11
Anti-birdcaging Layer: PA11
Tensile Armour: Steel
Antiwear Layer: PA11
Tensile Armour: Steel
Antiwear Layer: PA11
Pressure Armour: Steel
Inner Fluid Barrier: PA11
Carcass: Steel

##### Fluid or Gas

**Figure 4.6:** The material layup for the flexible pipe used in the heat transfer analysis.

#### Results

An analysis is conducted in Ansys APDL with the materials and set up described previously. The analysis gives a temperature distribution as follows from figure 4.7.

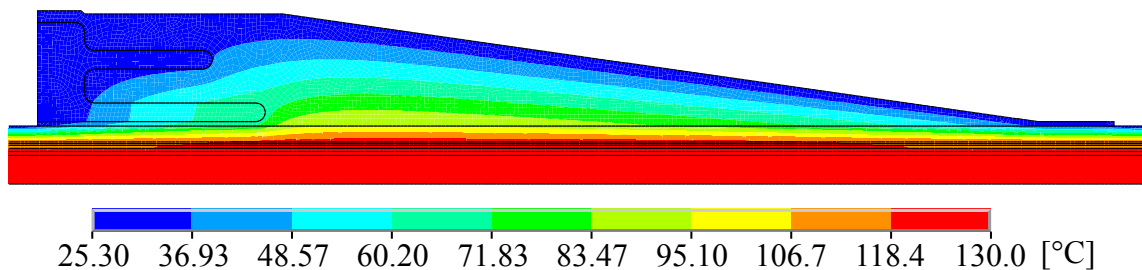


**Figure 4.7:** Temperature distribution through the bend stiffener and pipe assembly.

It is seen that the steel flange acts as a cooling body, this is due to the poor insulating properties of steel compared to polymers. The interesting area in this project are the temperatures at the surface of the flexible pipe, since it is this area that suffers from

hydrolysis failure. This area is examined more thoroughly by plotting the temperatures at the surface of the pipe along the length of the bend stiffener, see figure 4.8.

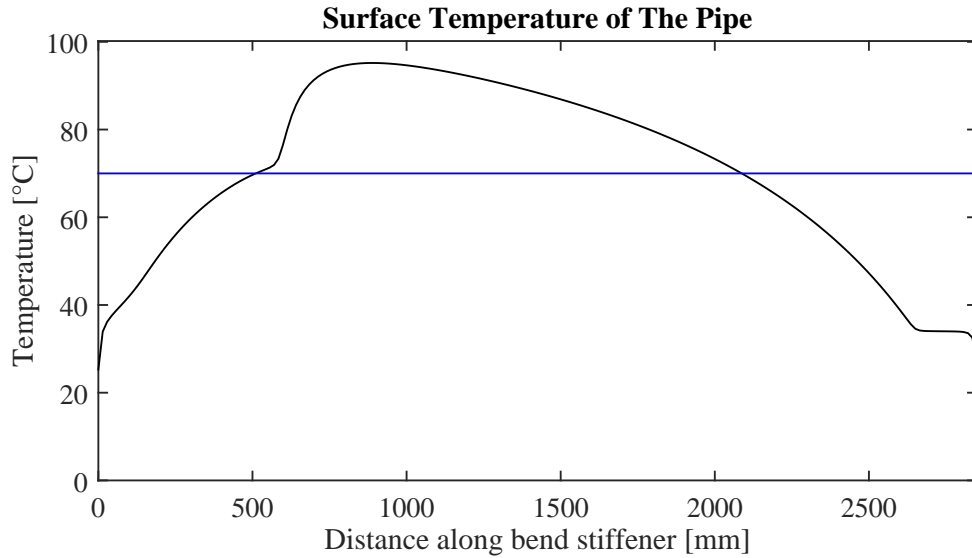


**Figure 4.8:** Temperature at the surface of the pipe under the bend stiffener. **Black line:** Surface temperature of the pipe. **Blue line:** Maximum allowable temperature at the surface of the pipe.

As it is seen on the figure, the temperature of the surface of the pipe beneath the bend stiffener gets much higher than the allowable temperature of 70°C. This proves that temperature really is an issue, even though a very optimistic case is chosen for the heat transfer analysis. This means that a new design has to be found in order to decrease the surface temperature of the flexible pipe.

#### 4.4.2 Deflection Analysis

Next a static analysis is conducted with the purpose to determine the deflection of the bend stiffener, when this is affected by the loads described in section 2.3.3 *Load Cases*. This analysis is used to determine the mechanical behaviour of the current design, which leads to knowledge about the advantages and disadvantages for the current design. Such information may be useful in a design procedure of a new bend stiffener, as distinctive advantages or weaknesses would be known. In the section, the setup of a model in ANSYS APDL and the approach of modelling are first explained, this is followed by a description of how the model is evaluated in order to ensure a proper model, the steps in this evaluation procedure will be explained in section 4.4.2 *Evaluation of the model*. Last the results obtained from the model are outlined and compared with a model setup in ANSYS workbench.

#### Model Setup and Considerations

All considerations regarding the setup of a model of the current design, and the approach of modelling are outlined in this subsection. The dimensions and geometry of the model

#### 4. Analysis of Current Structure and Surroundings

is based on a technical drawing provided by NOV flexibles [29]. The model is based on a preliminary model, that was rejected, since the model was relatively complex, and therefore required a higher computing power compared to the used model. The setup of the preliminary model is described in Appendix B *Preliminary Finite Element Model*.

To simulate the load situation, described in section 2.3.3 *Load Cases*, the model is setup so it consist of both the current bend stiffener and a piece of the pipe, as the pipe constitute a structural part inside the bend stiffener, and the forces are transferred to the bend stiffener through the pipe.

Initially, it must be considered, if a 2D or a 3D analysis should be used, and as the steel structure inside the bend stiffener is too complex to be modelled in 2D, it is chosen to setup a 3D model. The final model of the bend stiffener with the pipe is shown on figure 4.9.

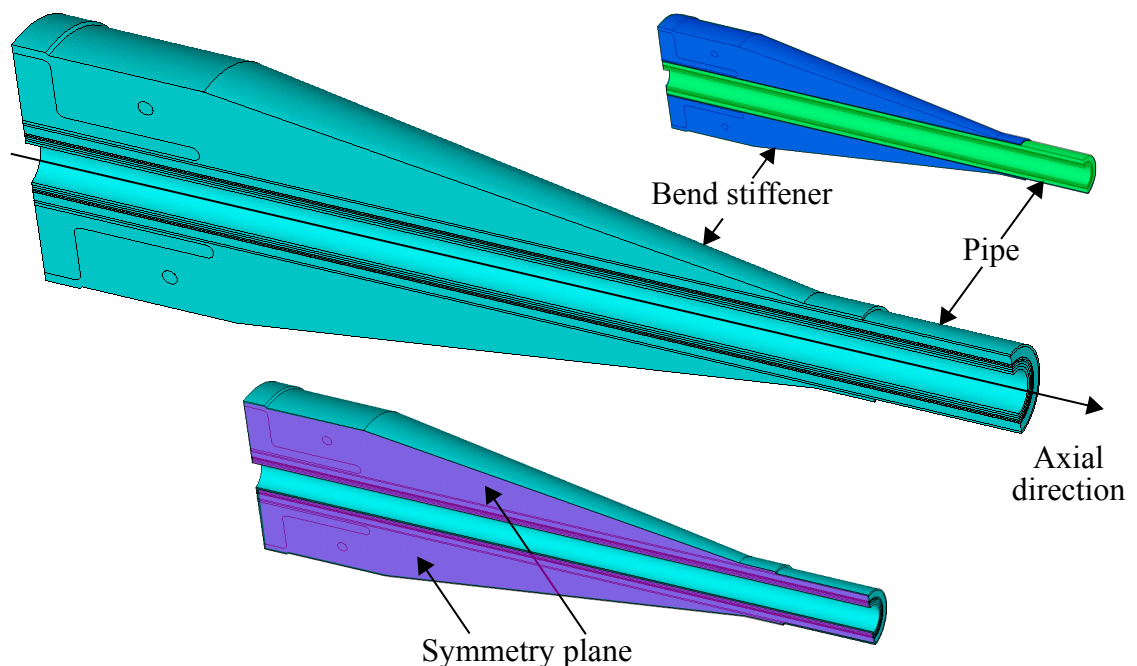


**Figure 4.9:** The final model of the bend stiffener with the flexible pipe. **Blue marking:** *The bend stiffener.* **Green marking:** *The flexible pipe.* **Violet marking:** *The used symmetry plane.*

The next step is to consider how to model the bend stiffener. As the bend stiffener and the pipe are symmetric around the axial direction, symmetry planes can be used to setup a model consisting of only one half or one quarter of the entire bend stiffener with pipe. One half of a model is chosen, as the bend stiffener is affected by both shear forces, tension and moment at the same time, and a moment can only be simulated with one symmetry plane.

The location of the symmetry plane with respect to the axial direction is shown on figure 4.9. To create the model, the cross sectional area of the bend stiffener and the pipe is drawn, then rotated around the axial direction by  $180^\circ$  to generate the volumes, this procedure is shown on figure 4.10.

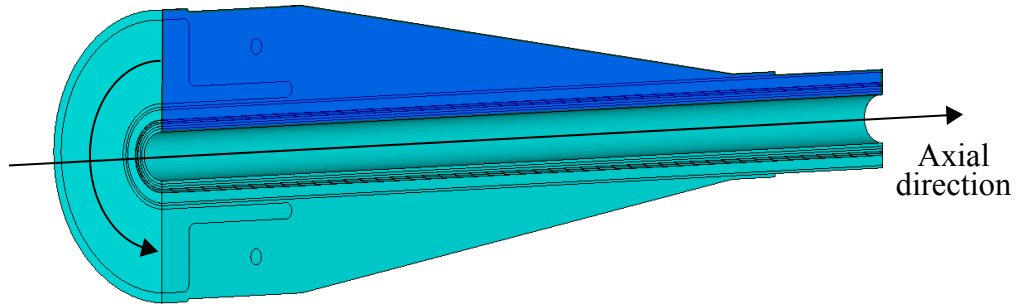


**Figure 4.10:** Rotation of the cross sectional area. **Blue marking:** *Cross sectional area.*

After the volumes are created, the steel structure inside the bend stiffener is applied with steel rods, so the entire steel structure is complete. The steel structure is displayed on figure 4.11.

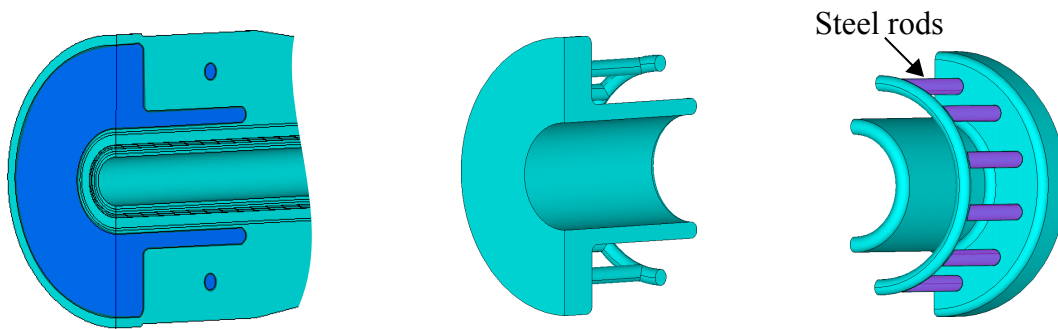


**Figure 4.11:** The steel structure inside the bend stiffener. **Blue marking:** *The steel structure inside the bend stiffener.* **Violet marking:** *The steel rods.*

It is chosen to use the 3D element SOLID186 in the model, which is a 20 node quadratic element. The element is suitable for 3D solid models and among other things suitable for analysis for structures exposed to large deflection. Each node has three degrees of freedom, which is translations in the x, y, and z nodal directions. The element can be formed as tetrahedral shaped element with 10 nodes, which is used in free mesh, while the quadratic shape is used in sweep mesh or mapped mesh. The different shapes are shown on figure 4.12 [4].

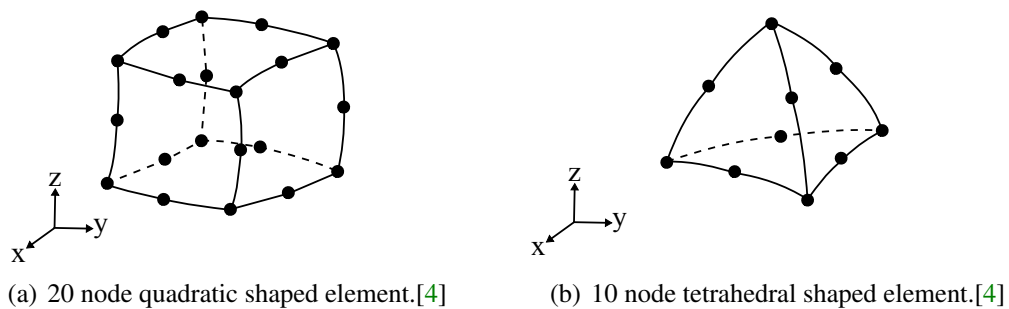


**Figure 4.12**

#### 4. Analysis of Current Structure and Surroundings

Therefore the discretization of the model can be conducted with both quadratic and tetrahedral shaped elements. Quadratic shaped elements are used to create a mapped or sweep mesh on square or rectangular volumes, but mapped mesh can not be used to mesh very curved or round structures, while sweep mesh can be used on semi curved objects or an irregular volumes. The tetrahedral elements are used in free mesh on curved volumes. However to fit the tetrahedral elements to the structure, it is often seen that the element size is reduced to avoid distortion of the elements, which also means that more elements are required. The model is deliberate setup to be as simple as possible, and as it consists mostly of curved volumes is the model meshed with tetrahedral shaped elements.

It is now considered how the loads should be applied to the model. From NOV flexibles it is informed that the safety factor for static load analysis should be set to two, and as the model is modelled with symmetry, the applied load is set to half the magnitude, as the symmetry will ensure a simulation of the deflection caused by the entire load. The values from the load case is therefore used directly on the model. The load case of the test rig is seen on figure 4.13.

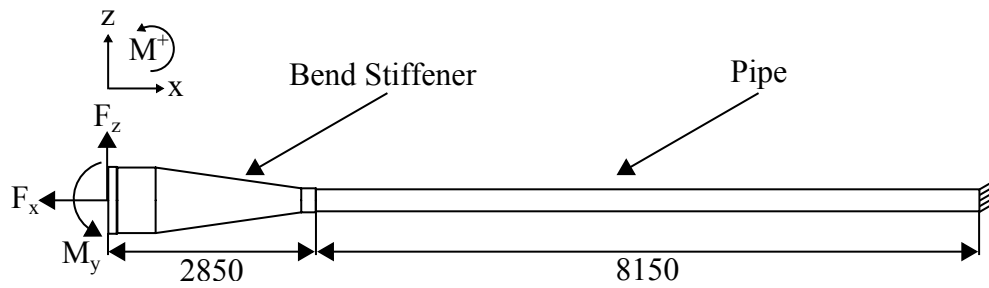


**Figure 4.13:** Direction of the loads exerted to the bend stiffener and pipe assembly in the test on figure 2.14. The figure is drawn with inspiration from [46].

As it is seen from figure 4.13, the load test is conducted with a pipe with a length of 2850+8150 mm, and to avoid a large model that require high computational power, the length of the pipe in the model is reduced. So the FE model is setup with a pipe with a length of 2850+500 mm in order to reduce the number of elements in the model, see figure 4.14, and the model is applied with recalculated loads and boundary conditions, which are equivalent to the loads and boundary conditions on the test rig. Therefore model is affected in the same manner as the load test.

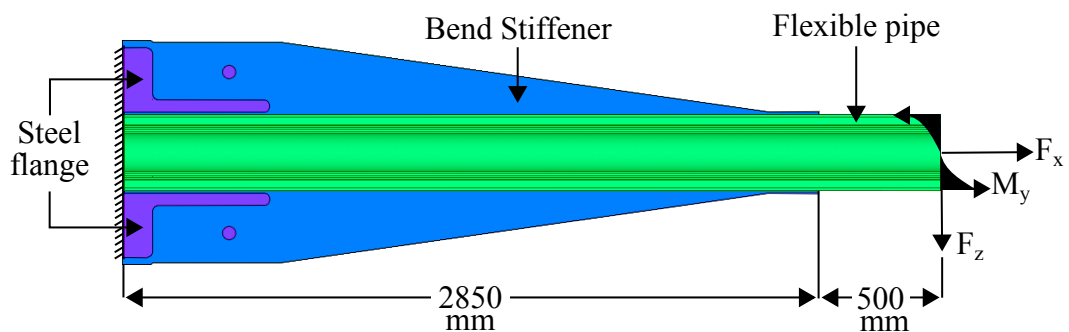


**Figure 4.14:** Boundary conditions and loads situation on the FE model.

**Blue marking:** Polyurethane surrounding the steel structure. **Green marking:** The flexible pipe. **Violet marking:** Steel structure.

Because SOLID186 only has translational degrees of freedom, a bending moment cannot be applied directly. Therefore must a bending moment be expressed as force pairs.

### Calculation of Moment - Force Pairs

The moment is transformed into force pairs, in order to apply it to the FE model. This is due to the fact that a moment cannot be applied to the SOLID186 element in ANSYS® APDL. A moment can be described as a set of force pairs, and for the end of the pipe this is done by dividing the cross section into small strips, where each strip is assigned with a force as a part of a force pair, see figure 4.15.

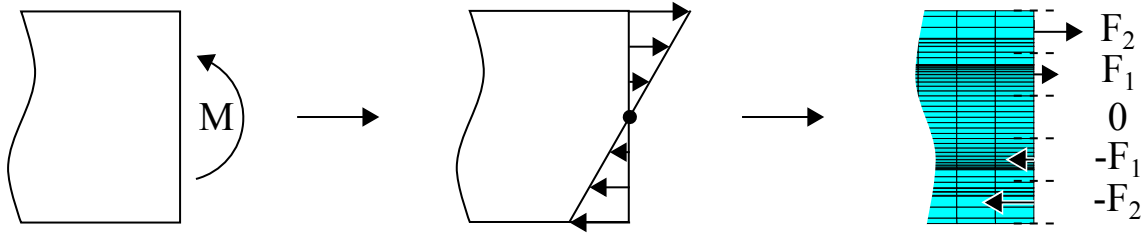


**Figure 4.15:** Moment transformed into force pairs.

The strip forces are found from the following two relationships

$$M = \sum_{j=1}^n F_j z_j \quad (4.1)$$

$$F_j = \frac{2z_j}{h} F_n \quad (4.2)$$

Where  $M$  is the applied moment,  $F_j$  is the  $j^{\text{th}}$  strip force and  $z_j$  is the distance from the center line to the strip force.  $h$  is the height of the cross sectional area, and  $F_n$  is the outer most strip force, and thereby also the largest strip force.  $F_n$  can be determined by combining equation (4.1) and (4.2).

$$F_n = \frac{Mh}{2 \sum_{j=1}^n z_j^2} \quad (4.3)$$

All the strip forces can now be determined, by inserting the right hand side of equation (4.3) in equation (4.2). A number of nodes is placed within each strip, and the sum of node forces should equal the total strip force. Therefore are the number of nodes in each strip determined and the strip force are distributed equally between all nodes in the strip.

### Evaluation of the model

To assess if the model is properly setup, the model must be evaluated. As it is considered to be difficult to evaluate the entire model with other tools than Finite Element Analysis, the evaluation procedure is conducted in two steps, where two basic FE models are established and compared with analytical expressions.

The comparison is based on a determination of the deflection of the different models. The first step is to model only the truncated cone, and compare it with an analytical

#### 4. Analysis of Current Structure and Surroundings

expression, and afterwards, the entire bend stiffener without pipe is evaluated in the same manner as the cone. All models are considered as a cantilever beam affected by a point load at the free end of the beam. The load is selected to be 100,000 N, this magnitude is chosen because it is in the same range as the loads on the test rig, and hereby will the models provide an initial prediction of the behaviour of the bend stiffener. The material for all models are thermoplastic polyurethane (TPU) and steel for the grid inside the bend stiffener. The first step in the evaluation procedure is to compare results from a FE model of the cone setup in ANSYS® with an analytical calculation.

##### Evaluation of the Cone

The cone is modelled with symmetry, and the cone has the geometry shown on figure 4.16. To setup the model, the cross sectional area of the cone is drawn, then rotated around central axis or the axial direction by 180 ° to generate one volume, afterwards the model is meshed with tetrahedral shaped elements.

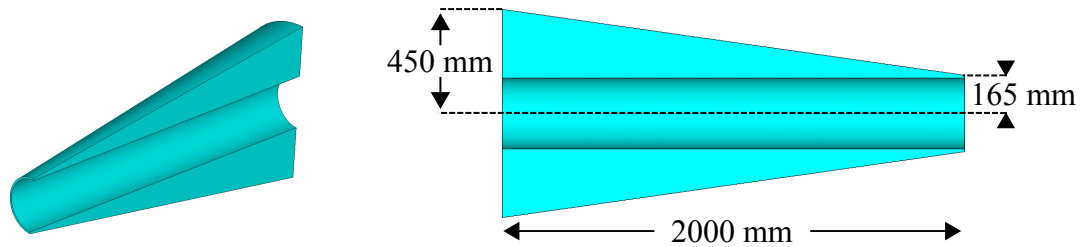


Figure 4.16: The FE model of the cone.

The analytical and FE model responds differently to a point load, the FE model will simulate both the local and global deformation, while the analytical model only calculates the global deflection. Since it is expected that the point load will cause a large local deformation, the analysis is conducted with two different load cases, to examine the effect of the point load. Load case one is a point force on the end of the cone, while at the second load case the load is distributed on the inside areas that covers the first 200 mm of the cone. These load cases are shown on figure 4.17(a) and figure 4.17(b).

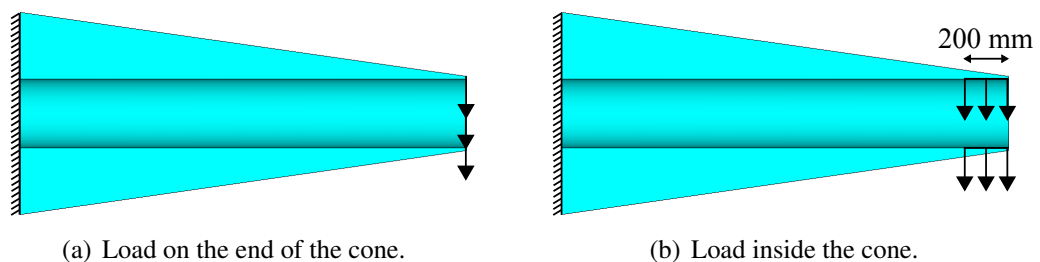
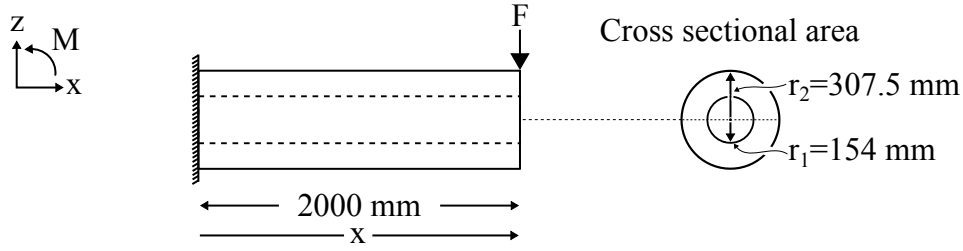


Figure 4.17

In order to compare the deflection of the cone with a well known behaviour, the deflection of a pipe with a corresponding cross sectional area to the cone is calculated. The calculation is setup as shown on figure 4.18.



**Figure 4.18:** The setup used to calculate the deflection of a pipe with a corresponding cross sectional area to the cone. The different radii are shown on the cross sectional area.

The calculation is done with the data described in section 2.3 *Materials, Dimensions and Load Cases of The Current Bend Stiffener and Pipe*, and the used expressions of the deflection of a beam with a point load and the moment of inertia are given by equation (4.4) and equation (4.5)[25].

$$w(x) = -\frac{Fx^2}{6EI}(3L - x) \quad (4.4)$$

$$I = \frac{\pi}{4} (r_2^4 - r_1^4) \quad (4.5)$$

$$w(2000 \text{ mm}) = -218 \text{ mm} \quad (4.6)$$

$E$  is Young's modulus,  $I$  is the moment of inertia of a pipe,  $F$  is point force and  $w$  is deflection. In the expression of the moment of inertia  $r_2$  is the outer radius of the pipe and  $r_1$  is the inner radius, these are displayed on figure 4.18. The maximum deflection of the pipe is calculated and the result is stated in equation (4.6). The FE model is compared with an analytical expression for the deflection of the cone, and setup of the analytical model is based on figure 4.19.

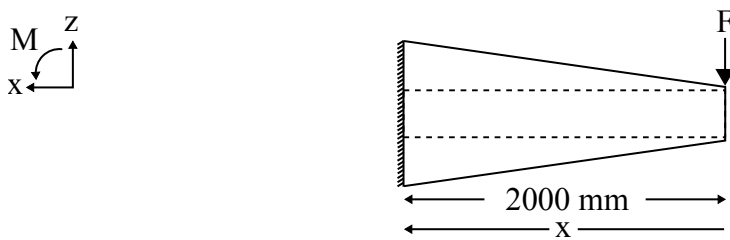


**Figure 4.19:** The setup for the analytical model.

The calculation of the deflection, is based on the differential equation for a beam, equation (4.7), and the expression for the second moment of area of a pipe, equation (4.5).

$$EI \frac{d^2w}{dx^2} = M \Rightarrow w = \frac{1}{E} \int \int \frac{M}{I} dx dx \quad (4.7)$$

$E$  is Young's modulus,  $I$  is the second moment of area of a pipe,  $M$  is moment and  $w$  is deflection. An expression for the moment of inertia varying throughout the length must be stated, as the cone is a non prismatic beam. From figure 4.19 it is seen that the inner radius

#### 4. Analysis of Current Structure and Surroundings

is constant throughout the length, while the outer radius is varying. The increase between the smallest and largest outer radius is calculated, and used to express the moment of inertia as shown in equation (4.8). Notice that the calculation direction goes from the load end to the fixed end on figure 4.19. This is chosen, because the expression for the moment of inertia must be formulated positive, as the integration of the differential equation for a beam result in a function containing the natural logarithm, and the natural logarithm of a negative number, results in a complex number. Therefore is the expression for the moment of inertia increasing in x direction, instead of decreasing if the calculation direction was opposite, which will cause a negative number in the expression. It can be shown that the moment affecting the cone is calculated by equation (4.9), and the deflection of the cone is stated by equation (4.10).

$$I(x) = \frac{\pi}{4} \left( \left( \frac{57}{400}x + 165 \text{ mm} \right)^4 - 154 \text{ mm}^4 \right) \quad (4.8)$$

$$M(x) = Fx \quad (4.9)$$

$$w(x) = \frac{4}{E\pi} \int \int \frac{Fx}{\left( \left( \frac{57}{400}x + 165 \text{ mm} \right)^4 - 154 \text{ mm}^4 \right)} dx dx \quad (4.10)$$

Using the boundary condition, the integration constants are determined, and the deflection is calculated using the software Maple. So four models are setup, an analytical expression of the deflection of a equivalent pipe and the cone, and two FE models with different load cases, and the deflection curves from the different expressions/models are shown in figure 4.20.

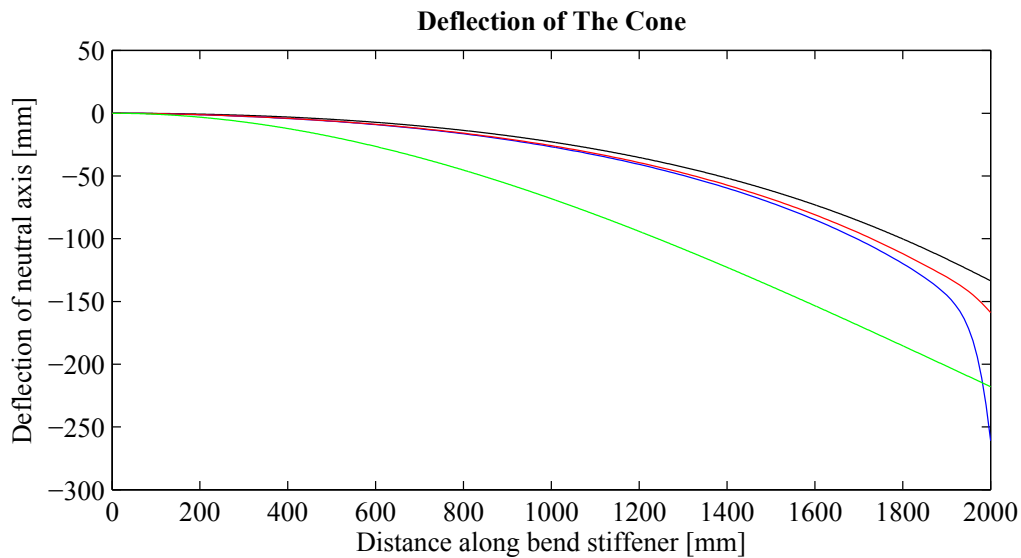


**Figure 4.20:** Results from the different analytical expressions/models. The primary axis is the length, the secondary axis is the deflection of the cone. **Black line:** The analytical expression for the cone. **Red line:** FE model with load inside the cone. **Blue line:** FE model with load on the end of the cone. **Green line:** The analytical expression for the equivalent pipe.

From figure 4.20 it can be seen that the FE model with the point load results in a larger deflection compared to the other models. This is due to the simulation of the locally deformation of the end, this is seen on figure 4.21.

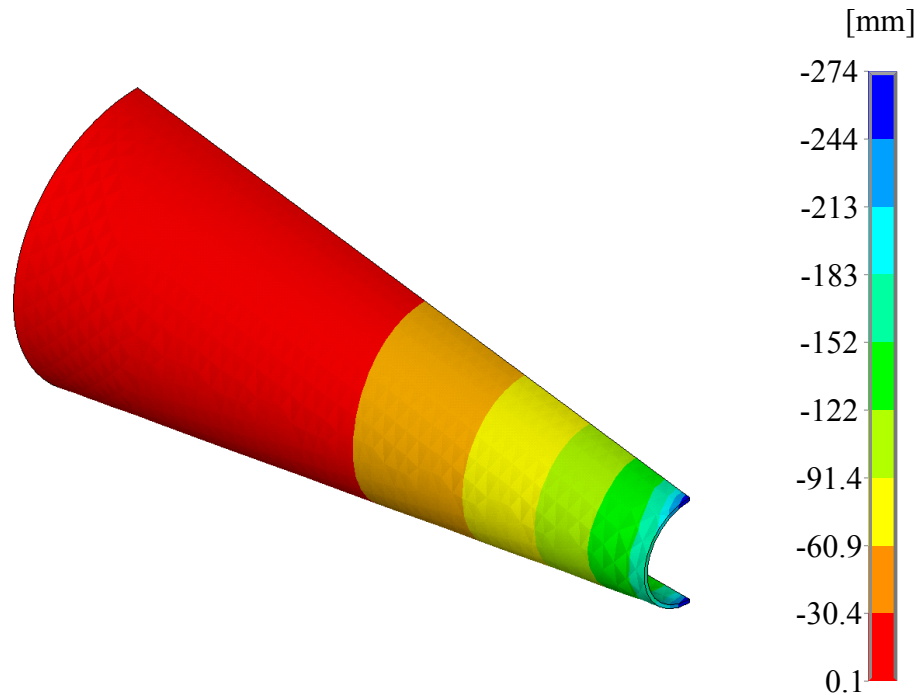


**Figure 4.21:** Deformation of the end of the cone.

From the graphs on figure 4.21, it is seen that FE models and the expression for the cone have a similar behaviour, except at the free end. The FE model with the distributed load, shows that the larger deflection at the free end, is caused by the locally deformation as expected. It can also be seen that the deflection of the models of the cone is overall lesser than the deflection of a pipe with an equivalent cross sectional area, which shows the advantage of the cone shaped structure compared to a pipe shaped structure.

#### Evaluation of the Bend Stiffener

A FE model and an analytical model of the bend stiffener is compared. The FE model of the bend stiffener is setup without the pipe, but the bend stiffener is modelled in the same manner as described in section 4.4.2 *Model Setup and Considerations*. The load is placed on the free end of the bend stiffener. The boundary condition is applied by fixing all degrees of freedom at the mounting interface of the steel structure, the boundary condition and load are shown on figure 4.22.

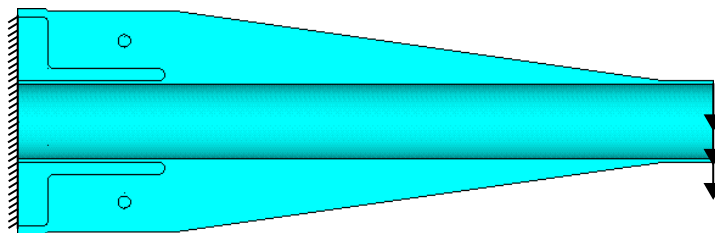


**Figure 4.22:** The FE model of the bend stiffener with load and boundary conditions.

#### 4. Analysis of Current Structure and Surroundings

Again, an expression for the deflection of a pipe with an equivalent cross sectional area is setup, and the calculation is conducted with equation (4.4) and equation (4.5).

The entire pipe is modelled with the Young's modulus for polyurethane (TPU), and the setup is shown on figure 4.23 [25].

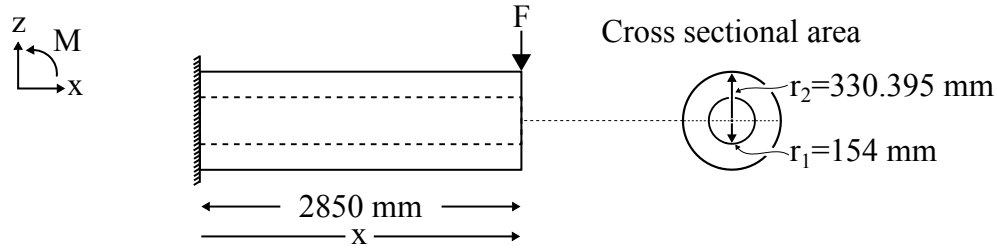


**Figure 4.23:** The setup for the deflection of a pipe with an equivalent cross sectional area.

The analytical model of the bend stiffener is modelled with polyurethane as material, and is a piecewise function, setup by four functions. Each function covers a part of the bend stiffener, where the part has a constant moment of inertia.

The cone is considered to have a constant moment of inertia, as the change is constant throughout the length of the cone. The four parts are displayed with numbers on figure 4.24, which shows the setup for the analytical model.

It is seen from figure 4.24, that there are three cylindrical parts (number 1, 3 and 4) and the cone (number 2).

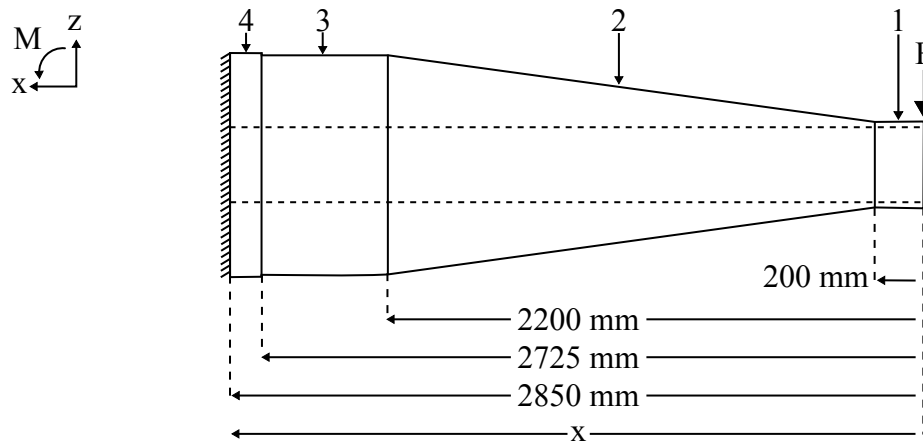


**Figure 4.24:** The setup for the analytical model.

To setup the piecewise function, an expression for the deflection of each part is setup by using the differential equation for a beam, equation (4.4), and moment of inertia of a pipe, equation (4.5).

The deflection for each part is expressed by equation (4.11) to equation (4.14).

$$w_1(x) = \frac{4}{E\pi} \int \int \frac{Fx}{(165 \text{ mm}^4 - 154 \text{ mm}^4)} dx dx \quad (4.11)$$

$$w_2(x) = \frac{4}{E\pi} \int \int \frac{Fx}{\left(\left(\frac{57}{400}x + \frac{273}{2} \text{ mm}\right)^4 - 154 \text{ mm}^4\right)} dx dx \quad (4.12)$$

$$w_3(x) = \frac{4}{E\pi} \int \int \frac{Fx}{(450 \text{ mm}^4 - 154 \text{ mm}^4)} dx dx \quad (4.13)$$

$$w_4(x) = \frac{4}{E\pi} \int \int \frac{Fx}{(459 \text{ mm}^4 - 154 \text{ mm}^4)} dx dx \quad (4.14)$$

Then, the boundary conditions for each function is used to determine the eight integration constants. The calculations are conducted in four steps, where one function and the related integration constants are determined.

These calculations are conducted from the fixed end and forward to the free end, so the function and integration constants for part number four is the first function to be determined, and the function for part one is the last. The order of these calculation steps, the range for each function and the boundary conditions for each step are outlined in table 4.2.

**Table 4.2:** Calculations Steps.

Step	Function	Range of the function [mm]	Boundary condition for deflection	Boundary condition
1	4	$2750 \leq x \leq 2850$	$w_4(2850) = 0$	$w_4'(2850) = 0$
2	3	$2200 \leq x \leq 2725$	$w_3(2750) = w_4(2750)$	$w_3'(2750) = w_4'(2750)$
3	2	$200 \leq x \leq 2200$	$w_2(2200) = w_3(2200)$	$w_2'(2200) = w_3'(2200)$
4	1	$0 \leq x \leq 200$	$w_1(200) = w_2(200)$	$w_1'(200) = w_2'(200)$

After the integration constants are determined, the models are compared and the deflection curves are displayed on figure 4.25.

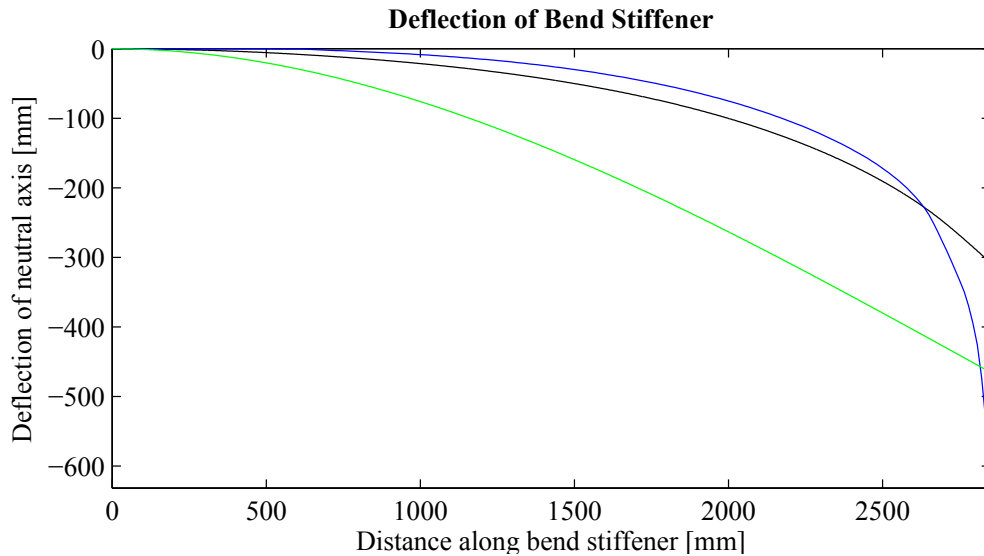


**Figure 4.25:** The deflection curve from the different models. The primary axis is the length, the secondary axis is the deflection of the bend stiffener. **Black line:** The analytical model of the bend stiffener. **Blue line:** The FE model. **Green line:** The analytical model of the equivalent pipe.

From 4.25, it is seen that the FE model have an overall stiffer behaviour compared to the analytical calculation of the deflection of the bend stiffener and the pipe, which is considered to be due to the steel structure inside the bend stiffener which is only included in the FE model. However the deflection curves from the FE model and the analytical model of the bend stiffener are in the same range and has a overall similar curvature, and the model is therefore considered to be properly setup, as the steel structure only covers the first part of the bend stiffener and has therefore a minor effect on the shape of the entire deflection curve. The large deflection on the free end of the bend stiffener for the FE model is again due to a simulation of the locally deformation, the true scale of the deflection is shown on figure 4.26.

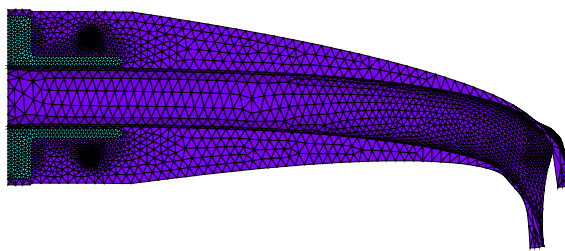


**Figure 4.26:** Deflection of the bend stiffener.

It can also be concluded that the effect of the steel grid and the shape of the bend stiffener has a significant effect on the stiffness compared to a pipe shaped structure without internal support.

#### Ansys Workbench Model

To evaluate the full model setup in ANSYS® APDL, is a corresponding model setup in ANSYS Workbench®. The Workbench model is created by drawing, generating and assemble all volumes in SolidWorks, and import the model into Workbench afterwards.

The main difference between the APDL model and Workbench model, is that all volumes in APDL model are glued, meaning that the volumes shares areas, also the pipe and bend stiffener shares areas. This results in a model where the element shares nodes across the volume boundaries. While the ANSYS® Workbench model is made with contact elements between all volumes. Examples of contact between volumes are shown on figure 4.27(a) and figure 4.27(b). The contact between the volumes are modelled without friction and are calculated with a nonlinear solver, while the deformation of the volumes is solved with a linear solver. The theory of a contact problem in FEA, is outlined in appendix C *The Theory of FE Contact Formulations*.

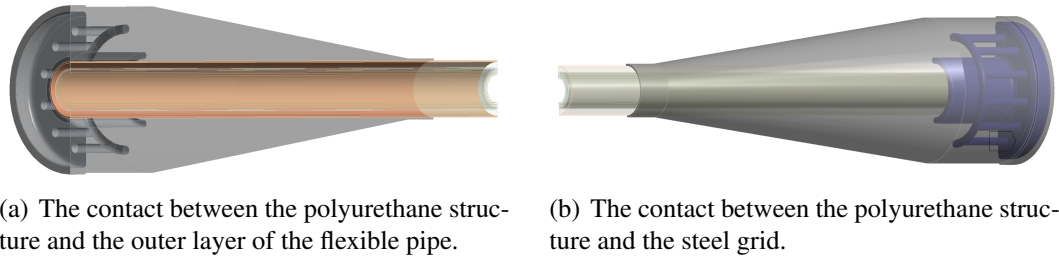


**Figure 4.27**

The boundary conditions are applied by fixing all degrees of freedom on the areas covering the widest end of the bend stiffener, see figure 4.28(a), while loads are applied on the areas covering the opposite end of the flexible pipe, shown on figure 4.28(b).

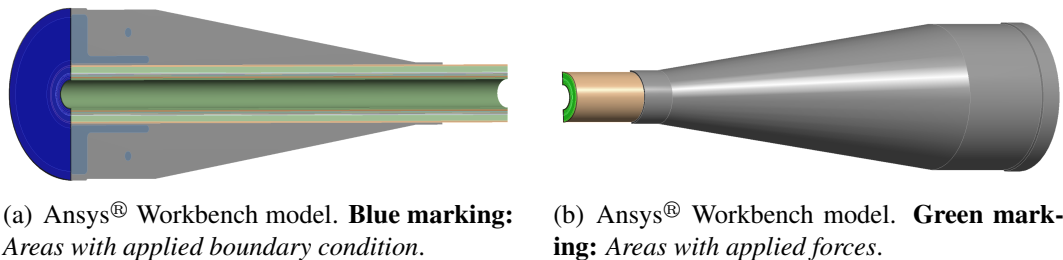


**Figure 4.28**

The APDL and Workbench model represent two extremes compared to the right solution, and the right solution probably lies in between these models. The APDL model simulates the situation where the flexible pipe and bend stiffener are bonded, while the Workbench model simulates the opposite situation; the flexible pipe is not bonded inside the bend stiffener, not even by friction, but the contact elements prevent penetration of the different bodies. Friction is not applied to the model, since the value is unknown. The right solution is considered to permit movement of the flexible pipe, but it is likely that the pipe and the bend stiffener has a tolerance, which results in a friction between them. For example in the Workbench model, is it possible for the flexible pipe to be exposed to a pure traction without it has any effect on the bend stiffener, while this will have resulted in deformation of the bend stiffener in the APDL model. As two different models are setup, the results from these will be compared in the following section.

4.4.3 Results

The results of the two FE Analyses described in the previous sections are presented here. The main purpose of these results is to show the behaviour of the current bend stiffener design, and the workspace in which a new design is allowed to operate. As the workspace for the new design is based on the static deflection of the current design, including safety factor.

Only the three most extreme load cases are shown as they will be governing in determining the workspace. For each load case will the contour plots of the lateral deflection for the models be shown first. A comparison of the lateral deflection of the neutral axis will be shown afterwards.

Load Cases used for The Results

As mentioned previously, the models are setup with load cases equivalent to the ones described in section 2.3.3 *Load Cases*. The three load cases which are used, has been selected from load case no. 6 in table 2.2. The model are setup as shown on the following figure.

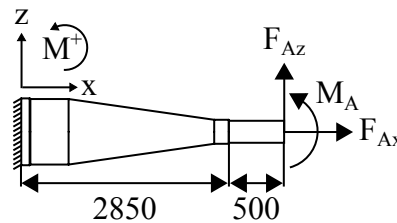


Figure 4.29: Setup for evaluating the load cases given in table 2.2.

The loads given in table 2.2 are actually the reaction forces that should be achieved at the fixed end of the bend stiffener on figure 4.29. The forces at point A on the figure, are the equivalent forces needed to achieve these reaction forces. Table 4.3 shows the magnitudes of the forces needed in point A.

Table 4.3: Equivalent Load cases - Bend stiffener and pipe assembly

Load Case	Original $F_x$	Original $F_z$	Original $M_y$	Equivalent $F_{Ax}$	Equivalent $F_{Az}$	Equivalent $M_A$
-	kN	kN	kNm	kN	kN	kNm
Lower limit	-893.8	-112	-405.2	893.8	112	30
Upper limit	-1491	160.5	288	1491	-160.5	249.675
Extreme Values	-1491	160.5	-405.2	1491	-160.5	942.875

All loads in this table has been given their sign according to the positive and negative directions defined by the coordinate system given in figure 4.29. The original loads are taken from load case no. 6 in table 2.2 and the equivalent forces are calculated based on the setup in figure 4.29.

All loads in table 4.3 are applied to the FE models with a safety factor of two, as this is the safety factor given by NOV Flexibles [46]. The reason for choosing these three load cases is to investigate the behaviour within the extreme range of loads, presented in load case 6 in table 2.2. The third load case is an extreme set of values where all the largest values in the particular range are selected.

This load case is most unlikely to happen, but as long as it does not violate any other requirements regarding the bend stiffener and pipe, it is still useful for determining a workspace for the bend stiffener, and it will also bring the bend stiffener on the conservative side when evaluating the load cases that are more likely to happen.

#### Load Case: Lower Limit

This load case are the lower limits of the range of loads in load case no. 6 in table 2.2. Figure 4.30 and 4.31 shows the contour plots of the lateral deflection for the solid model made in ANSYS® APDL and the contact model made in ANSYS® Workbench, respectively.

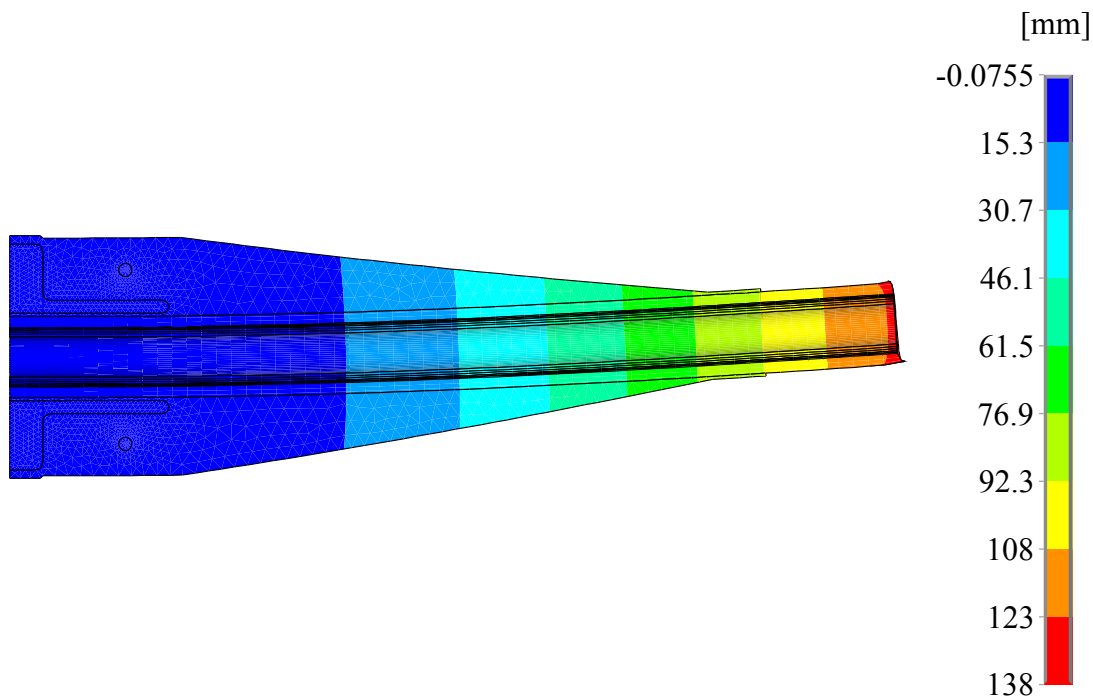


**Figure 4.30:** Deflection in the lateral direction of the bend stiffener. This is the result of the solid model in ANSYS® APDL.

As it can be seen on the figure above, the model gives a maximum lateral deflection of approximately 93 mm at the end of the bend stiffener. It should also be noticed that the way the loads are applied gives a small local deformation of the end of the pipe, but this is neglected, as the purpose of this model is to predict the behaviour of the bend stiffener.

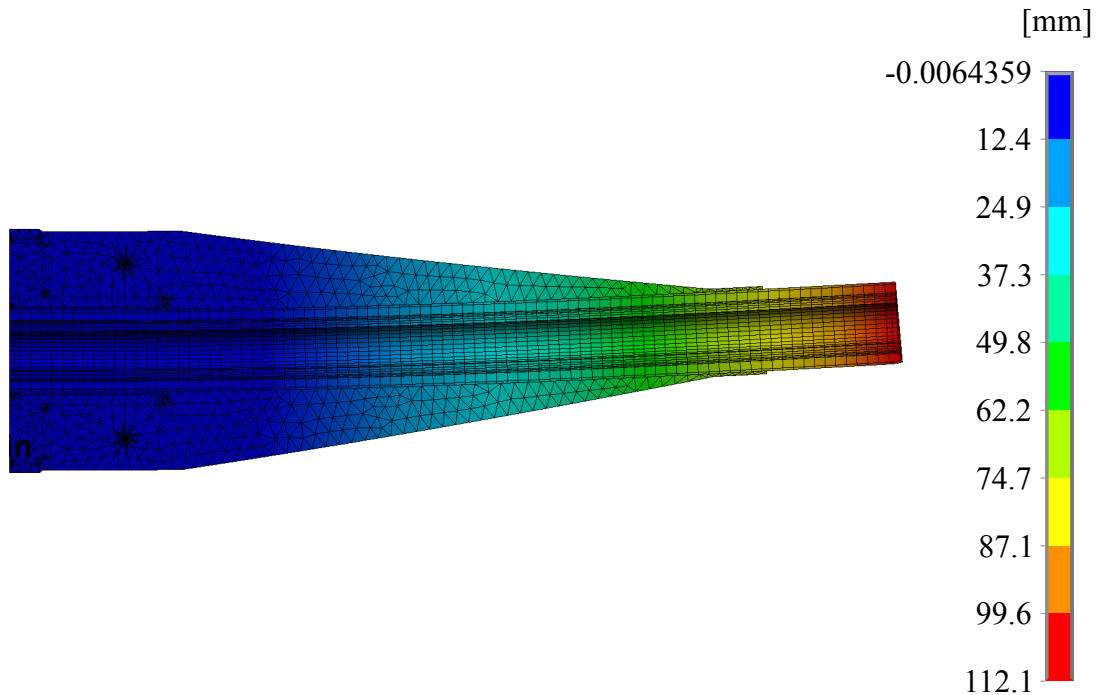


**Figure 4.31:** Deflection in the lateral direction of the bend stiffener. This is the result of the contact model in ANSYS® Workbench.

The contact model gives a slightly smaller deflection at the end of the bend stiffener which is also clear from figure 4.32, which compares the deflection of the neutral line throughout the length for both models.

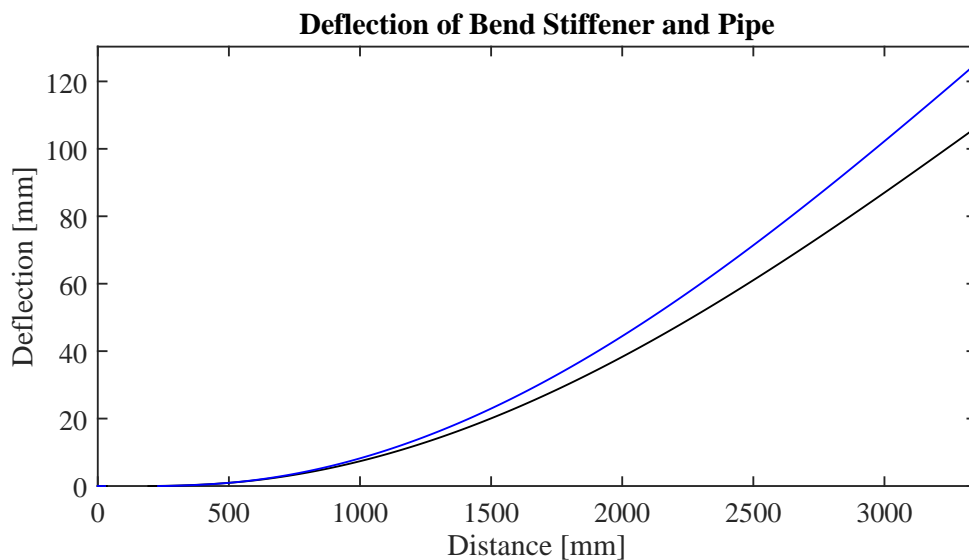


**Figure 4.32:** Deflection in the lateral direction of the neutral line of the bend stiffener. **Blue line:** Solid model in ANSYS® APDL. **Black line:** Contact model in ANSYS® Workbench.

It is clear that the solid model gives a larger deflection than the contact model. The difference of these models are acceptable, as the behaviour looks similar and a difference was also expected, since the models are not equally setup (e.i. solid versus contact).

### Load Case: Upper Limit

The following deals with the results obtained from the upper limits of the loads from table 4.3. Similar to the previous section are the contour plots of the lateral deflection for both the solid and contact model shown in figure 4.33 and 4.34, respectively.

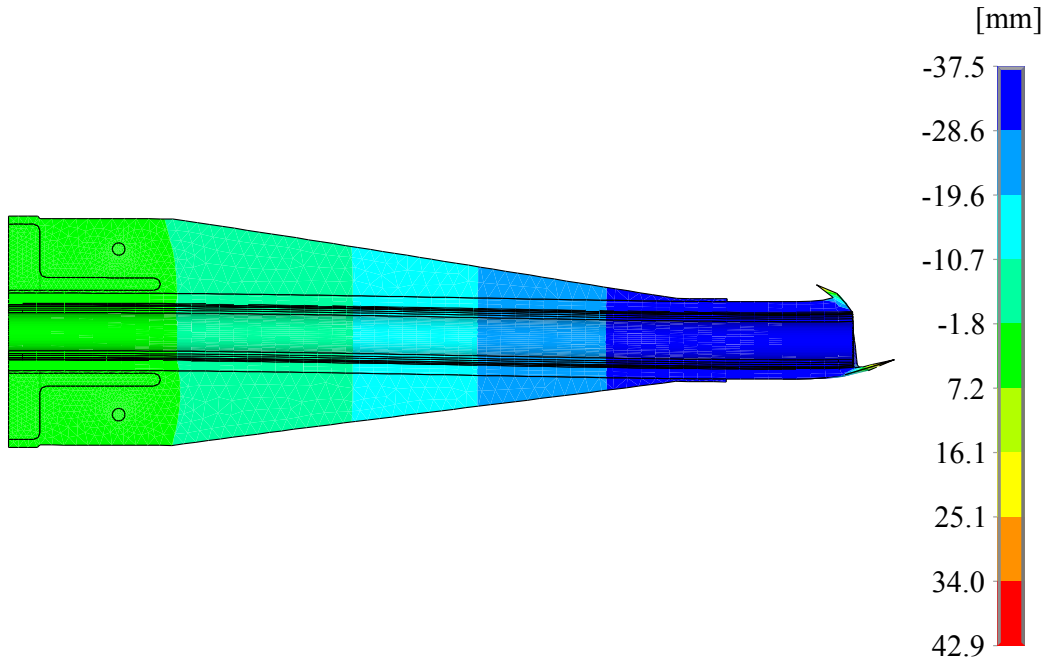


**Figure 4.33:** Deflection in the lateral direction of the bend stiffener. This is the result of the solid model in ANSYS® APDL.

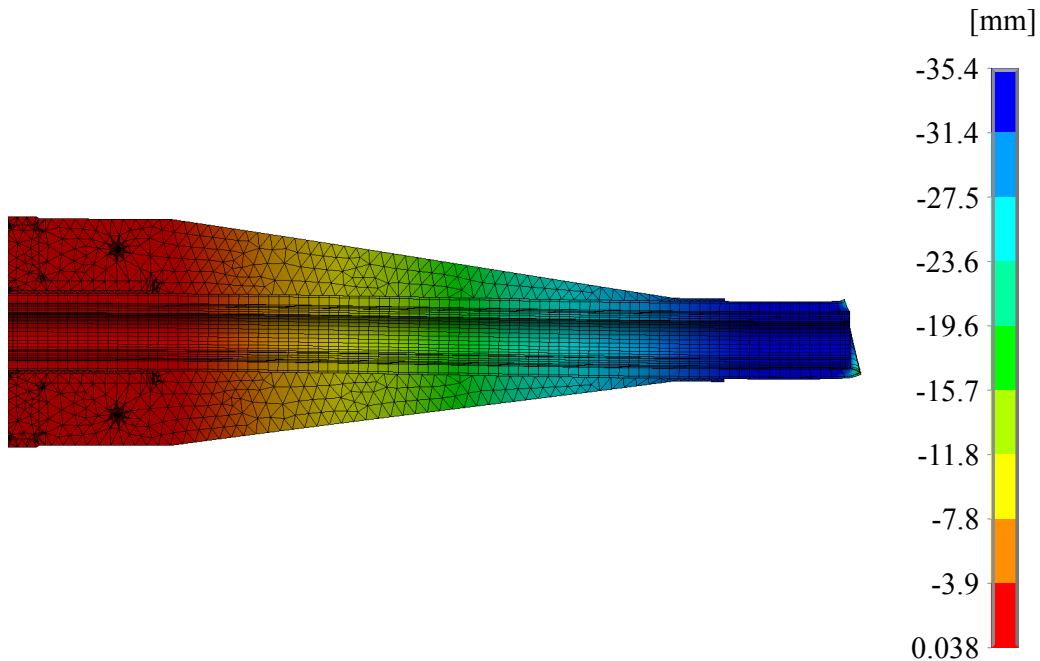


**Figure 4.34:** Deflection in the lateral direction of the bend stiffener. This is the result of the contact model in ANSYS® Workbench.

By observing the two plots in figure 4.33 and 4.34, it is seen that this load case does not lead to very large deflections, as the moment and shear force are cancelling each other out. In the same way as the previous load case, it can be seen that the moment leads to

a local deformation of the end of the pipe, which is most clear on the solid model. A comparison of the deflection of the neutral line can be seen on figure 4.35.

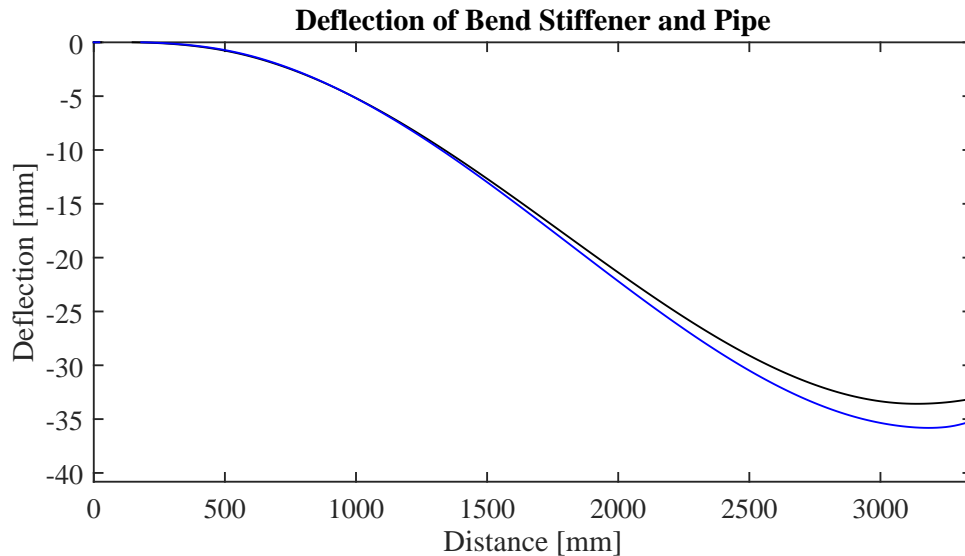


**Figure 4.35:** Deflection in the lateral direction of the neutral line of the bend stiffener. **Blue line:** Solid model in ANSYS® APDL. **Black line:** Contact model in ANSYS® Workbench.

The two models are very close to each other in their behaviour. The deflection is relatively small for this load case, which means that this load case will not contribute significantly to the determination of the workspace for the bend stiffener.

The workspace are determined by the deflection of the solid model in APDL for the lower load case, presented in figure 4.32. Now that the workspace have been determined, a brief summary of the analysis will be presented.

#### 4.5 Summary

Through this chapter, the world wide air and water temperatures affecting the bend stiffener as well as the salinity of the sea water has been determined. The surroundings effect on the bend stiffener has also been investigated, and the maximum dimensions of the bend stiffener has been specified. Different Finite element analysis has been conducted, and it has been proven that the insulating effect of the bend stiffener is the base of the problem, and the deformation due to loads and the structural behaviour of the bend stiffener has been examined. Also has the requirements stated by the standards been outlined, and the following chapter contains all requirements for a new design of a bend stiffener.



## Requirements for The New Design

A list of requirements will be established for the new design of the bend stiffener. The requirements mainly consist of two parts, requirements from the analysis of the current structure and surroundings, and requirements stated by NOV Flexibles. As mentioned in chapter 3.2 *Project Strategy and Methodology*, all requirements divided into two groups, primary and secondary requirements.

### Contents

---

<b>5.1 Primary Requirements</b> . . . . .	<b>47</b>
5.1.1 Requirements based on Analysis of Current Structure . . . . .	47
5.1.2 Requirements to The Bend Stiffener from NOV Flexibles . . . . .	47
<b>5.2 Secondary Requirements</b> . . . . .	<b>48</b>

---

### 5.1 Primary Requirements

#### 5.1.1 Requirements based on Analysis of Current Structure

Primary requirements from the analysis are outlined below.

**Operational Environment:**

The bend stiffener must be able to operate in an environment with the following temperature and salinity conditions.

- Air temperature interval: -25°C to 25°C.
- Sea water temperature interval: 0° to C 30°C.
- Salinity level: 0.034 to 0.036 PSU

**Manufacturing:**

The bend stiffener must be designed in a material with a hardness corresponding to or higher than 60 on the Shore D Hardness scale.

#### 5.1.2 Requirements to The Bend Stiffener from NOV Flexibles

Primary requirements from NOV Flexibles are described in this section [29].

**Operational Environment:**

The bend stiffener must be designed in such a way that the part of the flexible pipe, which

---

is covered by the bend stiffener, has a surface temperature below 70°C. Furthermore must the bend stiffener be designed to operate in air.

**Dimensions and Weight:**

The exterior dimensions shall be within a cylinder of 1 meter in diameter with a length of 6 meters, and the inner diameter must be 308 mm, (Pipe diameter), including a tolerance of +3/-0 mm. The total weight of the bend stiffener must not exceed 1000 kg.

**Mechanical Properties:**

The bend stiffener must not cause the bending radius of the pipe to exceed 2.2 m, in addition to this, is a safety factor of 1.5 required by the company and thereby increases the actual minimum bending radius to 3.3 m.

**Manufacturing and Environmental issues:**

The bend stiffener nor the manufacturing process may not contain mercury.

**Requirements for installation:**

The bend stiffener must be mounted to the vessel with bolts, in the same way as the old design.

## 5.2 Secondary Requirements

The secondary requirements are listed below, and these are all stated by the company. Each requirement is stated, and an explanation of why it is categorized as a secondary requirement is given afterwards.

**Operational Environment:**

If possible should the bend stiffener be designed to operate in both air and in seawater. This requirement will be fulfilled, when a design for operation in air is ensured, as this is the main goal for NOV Flexibles.

**Service time:**

The bend stiffener must be designed for a lifetime of 30 years, but as the full extent of the load situations for the bend stiffener is unclear, as the loads in this project are described by the load situations from the test rig, can a lifetime of 30 years not be guaranteed. However, fatigue calculations will be used to develop a new design.

**Manufacturing price:**

The manufacturing cost of the bend stiffener must be maximum 1 million DKK. A maximum manufacturing cost cannot be guaranteed, but an estimated price will be stated.

**Requirements from legislation/standards:**

The bend stiffener must be designed to fulfil the standards stated by The American Petroleum Institute (API). The standards from the API serves more as guidelines rather than directly requirements, and will therefore be followed in the extent it is possible.

In the following chapter, a conceptual design procedure is initiated.

## Development of a Conceptual Design

The development of a new design of the bend stiffener is described in this chapter. The chapter starts with a description of the design procedure, which is followed by the selection of the main material for a new design. Afterwards, the design procedure is conducted, and the outcome of each step in the process is presented. Last, the initial design concept is introduced, and this design will be evaluated and further refined in order to fulfil the requirements, this will be conducted in the next chapters.

### Contents

---

<b>6.1 Description of The Design Procedure</b>	<b>49</b>
<b>6.2 Material Selection</b>	<b>50</b>
<b>6.3 Implementation of The Design Procedure</b>	<b>52</b>
6.3.1 Principal Structure	52
6.3.2 Quantitative Structure	54
6.3.3 Total Form	56
6.3.4 Detailed Design	56
<b>6.4 Presentation of The Initial Design Concept</b>	<b>57</b>
<b>6.5 Summary</b>	<b>58</b>

---

### 6.1 Description of The Design Procedure

The chosen design procedure is based on a method described in "Systematisk udformning af industriprodukter" [57]. In this method, the development of a design is conducted in steps. The purpose of each step is to gradually increase the complexity of the design, which ends up in a useful design. At each step, different designs are created and evaluated, and a design is selected based on the evaluation.

The selected design is the basis for the next design step, where complexity and details are added, and a new evaluation of the changed design is conducted. To avoid an initial design with a high level of complexity, which could be difficult to manufacture or be related to a relatively high manufacturing cost, a design with a simple shape is sought throughout the design procedure.

Thus, a design is developed from a basic concept to a complete and useful design through steps. The design procedure consists of four steps, which are; Principal structure, quantitative structure, total form and detailed design. The content of each step is described below.

---

**Step 1: Principal structure**

The purpose with this step is to develop a simple structure where the main functions of the product are obtained, while dimensions, details and spatial distribution of components are left out. This means that the outcome of this step, is a basic and dimensionless concept which only sketches the main function of the design.

**Step 2: Quantitative structure**

In this step, the principal design is improved, by determining the number and the spatial distribution of the subparts of the design, but the design is still dimensionless.

**Step 3: Total form**

This level deals with relative dimensions of the design and the sub parts, thereby the overall conceptual form of the design is determined.

**Step 4: Detailed design**

After the Total form stage, the detailed design can take place. This step is about detailed functional design, for example the shape and initial dimensions of connections, links, etc. This is the final stage of the conceptual design.

The next section describes the selection of a main material for the new design of a bend stiffener.

## 6.2 Material Selection

The material selection is based on the stainless steel and the polyurethane used in the current design, since the materials have properties suitable for a bend stiffener. For example, polyurethane is relatively good to withstand oil and fuel as described in section 2.3 *Materials, Dimensions and Load Cases of The Current Bend Stiffener and Pipe*. These materials have also been tested for a number of years, and it is assumed that experience due to live tests, would have clarified most of the issues related to the use of these materials in a bend stiffener. If new materials should be used, it is considered to require assessment of a number of issues and properties, for example chemical reactions and resistance to fuel and oil, which require a comprehensive study and is out of the scope for this project.

Stainless steel 304 AISI is chosen as main material for a new design, the arguments and the considerations behind this choice is described in this following. From the thermal analysis, it is known that the current design combined with the polyurethane is causing an insulating effect. However, the areas of the flexible pipe that are partly covered by steel, is not exposed to the same level of insulation as with the polyurethane, due to the thermal conductivity of the steel.

Compared to polyurethane, steel has several advantages. Steel has a worldwide standardized quality, while the quality of the polyurethane is more uncertain, as there is no specific standardized quality.

The price difference between the two materials is not an issue, as the average price of steel is 2.08 EUR per kg steel [40], while the average price for one kg of polyurethane is estimated to be 1,98 EUR [21].

## 6. Development of a Conceptual Design

It is known from the data described in table 2.1 that steel has a higher stiffness and higher density compared to polyurethane, but it is unknown if the relationship between stiffness and density for polyurethane is corresponding to the relationship for steel. If the stiffness/density relation for steel is lower than for polyurethane, it might result in a design with an unacceptable high mass. Therefore is a stiffness/density chart used to compare the two materials, see figure 6.1.

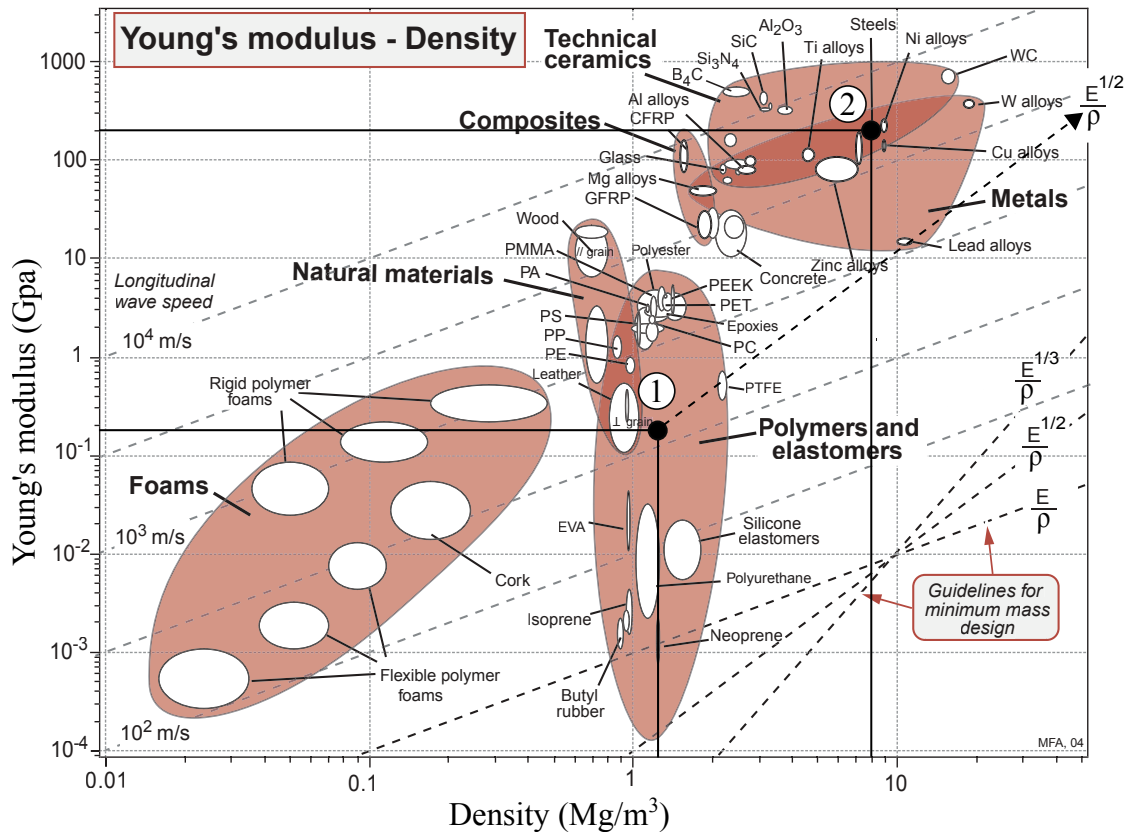


**Figure 6.1:** Material chart for the relation between stiffness and density [6].

To compare the two materials, their properties are plotted on the chart, where the black dots denoted with point one and two respectively outlines the properties of polyurethane and stainless steel. The guidelines on the chart,  $\frac{E}{\rho}$ ,  $\frac{E^{1/2}}{\rho}$  and  $\frac{E^{1/3}}{\rho}$  outlines a rod pulled in tension, a beam in bending and a plate in bending, respectively. To indicate the difference between the materials, the guideline for a beam in bending is selected,  $\frac{E^{1/2}}{\rho}$ , as bending of a beam is assumed to represent the load on most parts in a new design. The guideline is drawn with a starting point in the properties of polyurethane. The guideline is shown as a dashed arrow on the chart, and all materials above the guideline, performs better compared to the materials below the line. It is clear that steel has a higher stiffness/density relation compared to polyurethane. Another issue is the materials ability to resist the damage caused by the environment. The overall ability to resist four vital environmental factors, are listed in table 6.1, for the two materials. The letter, A, indicates a high level of resistance, while C indicates a lower level of resistance.

**Table 6.1:** Environmental resistance [10].

Material	Fresh water	Salt water	Sunlight (UV)	Wear resistance
Stainless Steel	A	A	A	B
Polyurethane	A	A	B	C

Overall, stainless steel has a higher level of resistance compared to polyurethane. It is also considered to be easier to find production facilities which can produce a steel design compared to polyurethane, as manufacturing processes in steel is widely used. This could be an advantage, if repair parts should be manufactured in a hurry, where the transport of a molded polyurethane bend stiffener could cost production time. Furthermore, the tools used to analyse the ability of a steel design to withstand static load and fatigue are well known, compared to a design in polyurethane. It is also required that the new bend stiffener are bolted to the production vessel, which altogether leads the selection of steel as the main material for the new design. However, polyurethane has a wide variety of suitable properties, which might be useful in an overall steel design, for example, the polyurethane can be used as a protection layer between the steel and the pipe. As the main material is determined, the design procedure is initiated.

### 6.3 Implementation of The Design Procedure

The steps in the design procedure are outlined in the following subsections.

#### 6.3.1 Principal Structure

The first step in the design procedure, principal structure, is initiated by considering the design of the current bend stiffener, see figure 6.2(a). This design in steel will have a relatively high weight. Thus, the material must be removed, in order to lower the mass, as shown on figure 6.2(b). This will also have a positive effect on the insulating properties of the design.

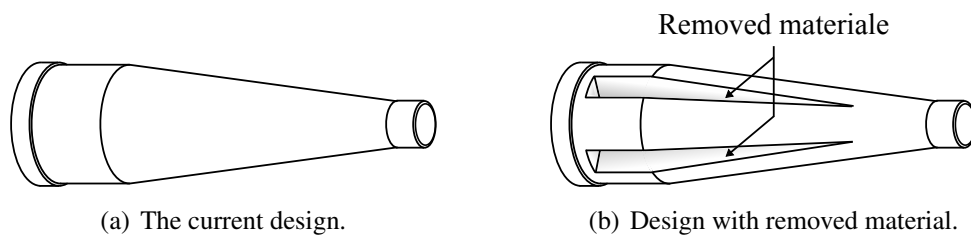


**Figure 6.2**

This idea is the basis for the development of a principal structure. The functions of the current bend stiffener are considered first. This is done by dividing the current design into three parts, two flanges and a bending part, which is the cross sectional area, see figure 6.3(a). The cross sectional area provides the right stiffness in order to avoid a violation of the minimum bending radius of the pipe, while the flanges guides the pipe and works as a connection to the vessel. A number of basic principal structures are setup,

## 6. Development of a Conceptual Design

based on the aforementioned main functions, three of these are shown on figure 6.3(b), figure 6.4(a) and figure 6.4(b).

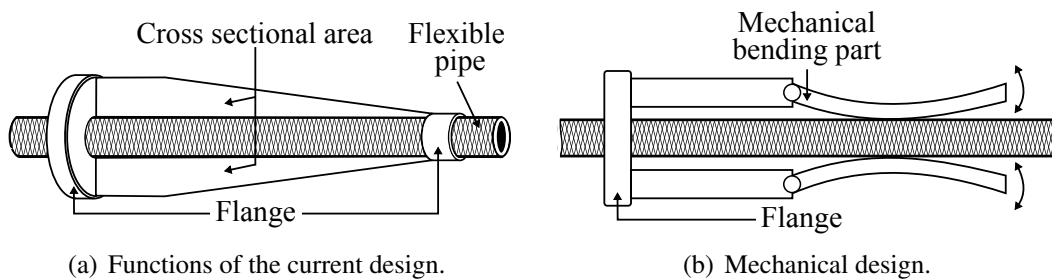


Figure 6.3

The first design proposal is to make a mechanical bending part, see figure 6.3(b). This design functions with moveable rods or plates connected to springs, so the wall of the bend stiffener can guide the flexible pipe in the transverse direction.

The next solution is to construct the bend stiffener as a spine, where the bend stiffener is build up of small parts which are linked together, but can move independently, this design is shown on figure 6.4(a).

A third concept is to use the current design, and to remove material as well as to lower the temperature, the design of the bend stiffener is manufactured with hollow channels. With the channels, air or water can be directed to the surface of the flexible pipe, and apply a cooling effect. Another opportunity is to fill the channels with a thermal conducting material to transfer heat from the surface of the pipe to the surrounding environment.

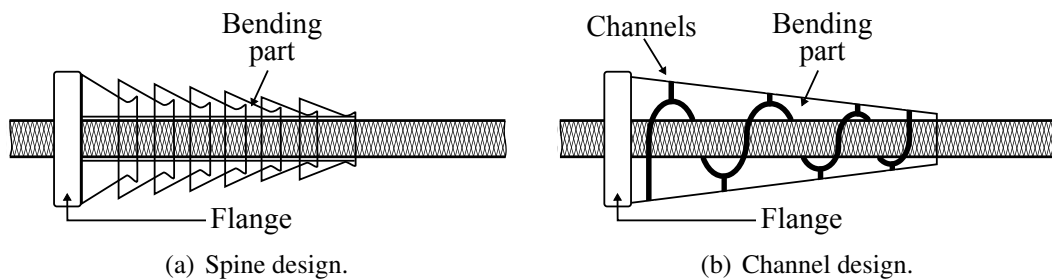
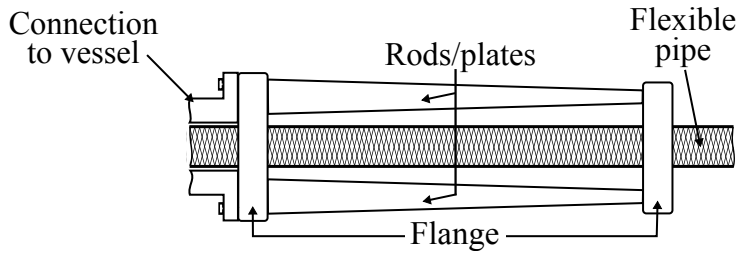


Figure 6.4

These designs are rejected as they are considered to be too complex to manufacture compared to a simpler design. The designs does not guarantee a solution to the temperature problem, consider for example figure 6.4(a), it is doubtful if the design has the ability to lower the temperature of the surface of the flexible pipe.

Another principle structure is proposed, based on these considerations, this is shown on figure 6.5



**Figure 6.5:** The developed principal structure.

The principal structure consist of two steel flanges, with the same function as the current design, and these are separated by rods or plates of steel, which provides the right bending behaviour of the structure. The rods/plates are distributed equally around the central axis and with enough space to ensure air or water to have direct contact with the surface of the pipe. Thus, the principal structure consists of two flanges and a number of separated rods or plates, and the structure is made of Stainless steel.

### 6.3.2 Quantitative Structure

The quantitative structure is setup next, and first, the shape of the rods/plates is determined by considering the cross sectional area of the current bend stiffener, see figure 6.2(a). The current bend stiffeners cross sectional area is both cylindrical and cone shaped, which gives the structure the right bending behaviour, however, is it selected to use a cone shaped rods, since this is a simple structure and has the same moment of inertia in all transverse directions, which is not the case with a plate.

The next step is to determine the number of rods and the spatial distribution of these, and therefore is the steel flange of the current design considered, see figure 6.6. There are 12 bolt holes in the flange of the current design, which are used to connect the current bend stiffener to the male connection to the vessel. It is required that the new design must be connected to the vessel in the same manner as the current design. Therefore, it is chosen to use the spatial distribution of the bolt holes in the current design as a basis for determination of the number of rods.

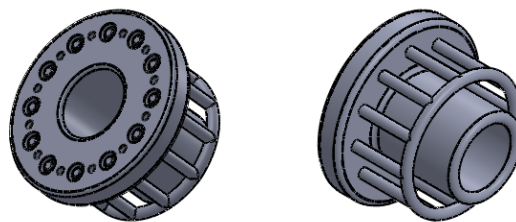


**Figure 6.6:** Design of the steel flange, drawn with inspiration from [46].

The spatial distribution of the bolt holes in the current design is shown on figure 6.7(a), and it is chosen to distribute an even number of rods symmetrically around the central axis of the bend stiffener. In order to place the rods symmetrically and to ensure a relatively similar moment of inertia in all directions, it is chosen to work with a number of rods from 4 to 12 rods. Only two rods will result in an relatively uneven distribution of the moment of inertia, and it is questionable if the diameter of one rod can be placed on the

## 6. Development of a Conceptual Design

area of the flange. However too many rods will cause rods with a relatively small diameter, which could lead to a buckling problem. The spatial distribution of the different number of rods are shown on figure 6.7(b) to figure 6.7(e), the dashed circles and the solid circles represent respectively the location of the rods and the bolt holes in the flange of the current design.

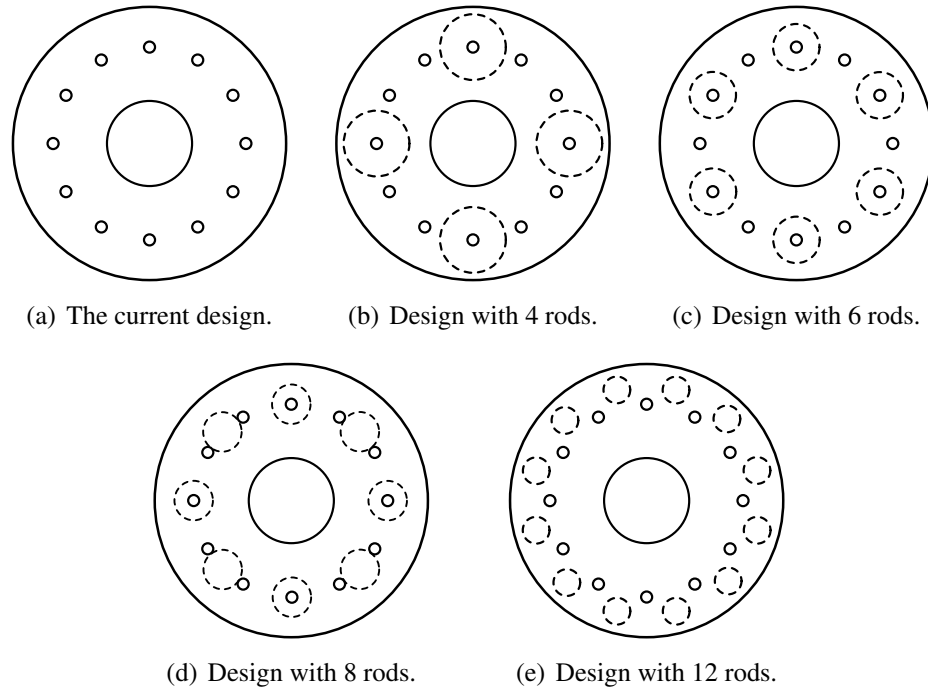


**Figure 6.7**

It is chosen to use the design with six rods, because the design with four rods will result in rods with a relatively large diameter compared to the other designs. The spatial distribution of the selected number of rods is shown on figure 6.7(c).

The design with eight rods is rejected, since the rods will be placed close to the bolt holes in the flange, and if the rods should be guided by the holes in the flange, the relative small material thickness between the holes could cause a weakness, see figure 6.7(d).

In the design with 12 rods, it is assumed that the rods can only be placed on the outside or the inside of the bolt holes, so the rods are in both cases placed close to the edge of the flange, where perhaps there is not enough material to absorb the bending of the rods. Therefore does the final quantitative structure consist of six cone shaped rods and two flanges as shown on figure 6.8.

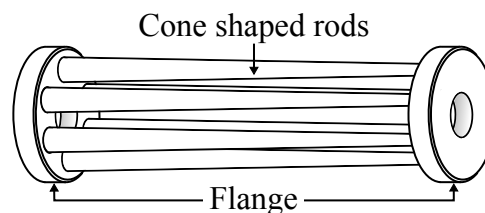


**Figure 6.8:** The quantitative structure.

### 6.3.3 Total Form

Dimensions are applied to the quantitative structure, to obtain the total form. It is selected to have a total form, which is almost set to the maximum limit of the design space, since optimization is used in the dimensioning of the new design. It is likely, that the total form has a too large mass and stiffness in relation to the stated requirements, however is it likely that the optimization procedure, will results in smaller dimensions and lesser mass. The total form is seen on figure 6.9.

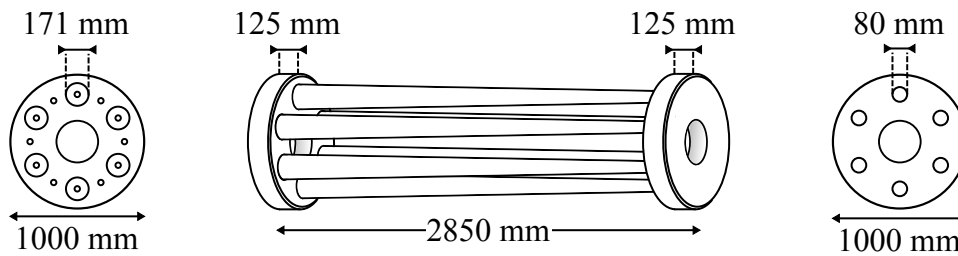


**Figure 6.9:** The total form.

To ensure a conservative initial design, it is chosen to have a total form with the same length as the current bend stiffener, while the outer diameter of the flanges is set to 1 m, this means that the initial outer diameter is set to have the maximum allowed dimensions stated in the requirements. The dimensions of the rods is selected, by stating that the sum of the six rods maximum diameter must be equal to half of the circumference of the circle which constitutes the bolt holes, which is equal to 171 mm, see figure 6.10.

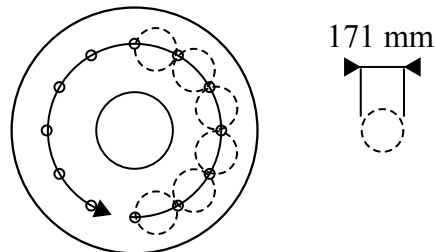


**Figure 6.10:** Diameter at the thick end of the rod.

By intuition are the small end of the rods selected to be 80 mm, and the width of the flanges is set to 125 mm. Later will this initial design be changed, for example by an optimization process, such that the design fulfils the requirements, and likely will the dimensions be smaller.

### 6.3.4 Detailed Design

The last step in the procedure is to design the details of links and connections. The detailed design is drawn in SolidWorks and shown on figure 6.11. The steel rods are placed inside each flange and mounted with bolts, see point 1 and 2 on figure 6.11. The bending moment is thereby transferred from each rod into the flange. It is also possible to assemble or disassemble the rods from the flanges, and it is hereby possible to replace a single part, if the bend stiffener should be damaged. These simple parts are also considered to be an advantage in the manufacturing process, as the steel rods can be manufactured by

## 6. Development of a Conceptual Design

a turning process, while the flanges can be produced by a milling/turning process, which are worldwide well known machining methods.

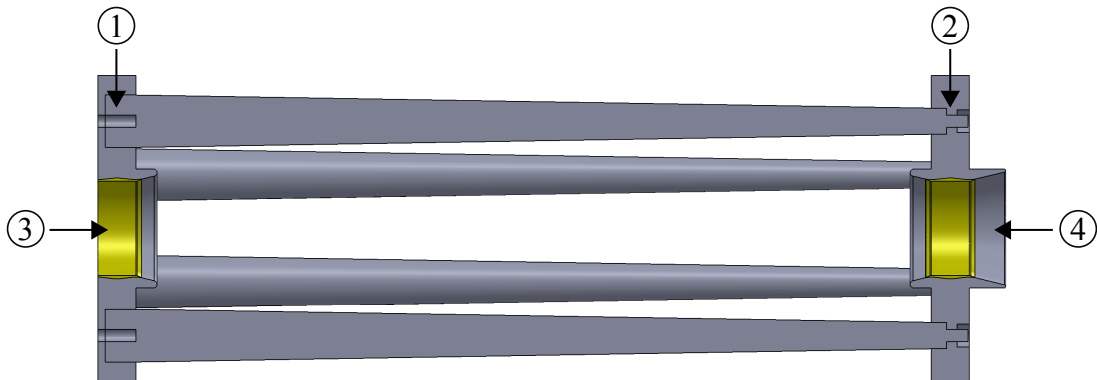


**Figure 6.11:** Cut through view of the detailed design.

The inner cylindrical area of the flanges are coated with polyurethane, in order to avoid damages and decrease wear of the outer polyamide sheath of the pipe, this is shown at point 3 on figure 6.11. The flanges are also expanded with collars, so the pipe does not bend around a sharp edge, which could cause damage of the outer layer, see point 4.

### 6.4 Presentation of The Initial Design Concept

The developed initial design is displayed on figure 6.12. The design allows air or water ventilation around the flexible pipe, which will solve the problem with the hydrolysis on the outer layer of the pipe. However, the design is still considered to be a concept, since the shape and dimensions must be refined and changed in order fulfil all the requirements.

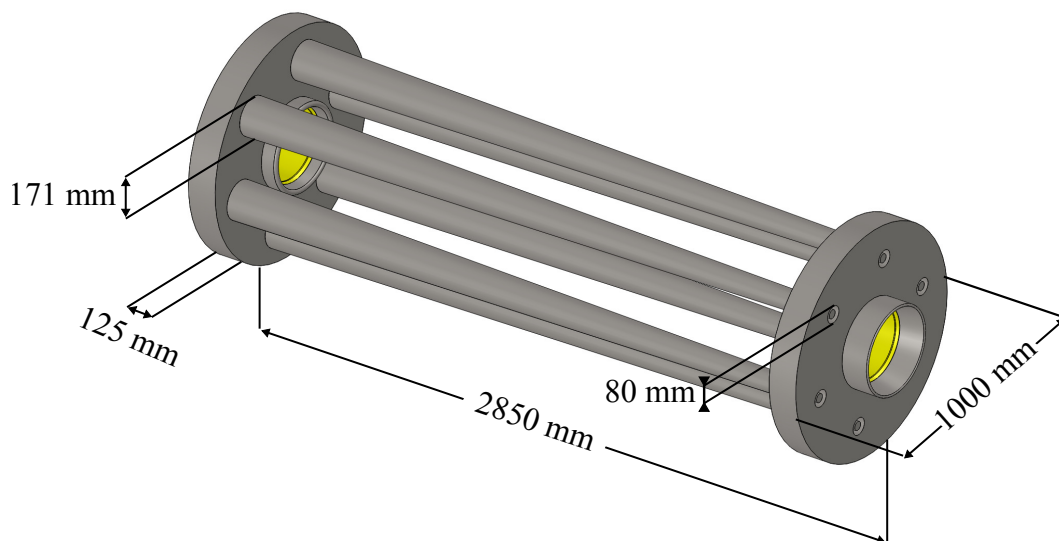


**Figure 6.12:** The initial design concept.

---

## **6.5 Summary**

A initial design has been setup by conducting the design process, which consist of four steps, where a basic design concept has been developed to the first design proposal. It is chosen to use stainless steel 304 AISI for the structure of the design, while polyurethane is used as a protection layer between the steel flanges and the flexible pipe. The initial design is evaluated and further developed in the next chapter.

## Initial Design Evaluation And Development

A design concept has been developed in the previous chapter, which is a series of intuitive ideas. This chapter describes how this initial design concept is evaluated and improved based on an optimisation process and simple static evaluations. This leads to a new developed and improved design concept which can be further optimized.

### Contents

---

7.1 Optimisation of Deflection Curve . . . . .	59
7.2 Design Changes due to Behaviour Issues . . . . .	60

---

### 7.1 Optimisation of Deflection Curve

The new conceptual design is optimized, in order to get the same mechanical behaviour as the current bend stiffener design. In order to do so, some dimensions are made variable and some are taken to be the same as the original dimensions. The flanges on the new design has been given the same dimensions as the current flange in the old design, where the radius in both ends of the conical rods are made variable, as it is the dimension of these rods which mainly governs the magnitude of the deflection. A very simple optimisation is made, where the geometry is modelled in Ansys APDL and the radii of the rods are used as design variables. The model is optimized towards the maximum deflection of the current bend stiffener, this deflection can be seen on figure 4.32. The objective function used for this simple optimisation is a least square function, where the residual of the deflection between the old and new design is calculated in each iteration. A more thorough description of the optimisation methods will be given later on. In this case, the initial dimensions used for the optimisation can be seen figure 6.9. The dimensions of the rods, shown on figure 6.9, are of course too large to give the desired deflection, and the optimisation then yields the following radii for the rods.

$$r_{rods} = 12.074 \text{ mm} \tag{7.1}$$

$$R_{rods} = 20.13 \text{ mm} \tag{7.2}$$

Where  $R_{rods}$  is the large radius nearest the vessel and  $r_{rods}$  is the one at the opposite end of the bend stiffener. These dimensions yields a deflection profile as shown on figure 7.1.

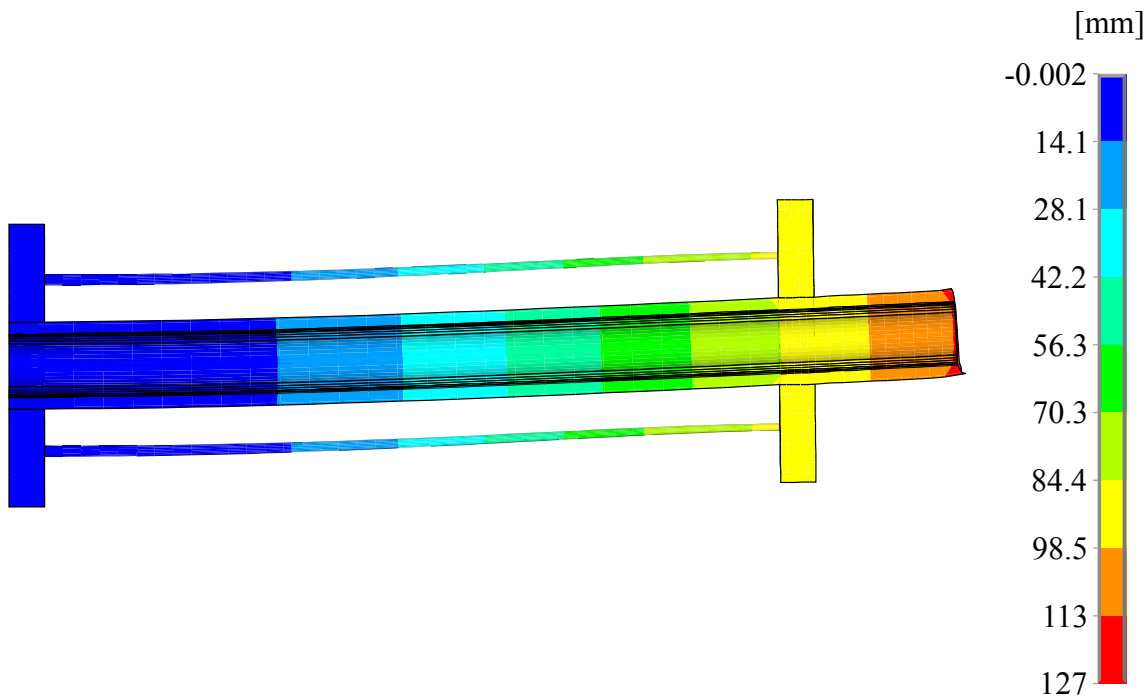


**Figure 7.1:** Deflection profile of the optimized initial design concept.

Figure 7.1 shows that the pipe and the bend stiffener does not follow each other very well in their deflection profile, as the new design allow some deflection of the pipe away from the neutral line of the bend stiffener. This is due to the two steel flanges which only supports the pipe in two small areas, one in each end. This allows for some rotation of the pipe inside the bend stiffener. Another issue can be seen from the shape of the deflected rods, which has a kind of s-shape. This is again due to the flanges which are too rigid, when applying a moment to the structure. One last issue which has a major influence on the behaviour of the structure is the surface pressure between the pipe and the flanges of the bend stiffener. It will cause a very high surface load, since these areas are the only ones supporting the pipe. These surface loads can cause wear and damage to the outer sheath of the pipe, and it can also prevent the pipe from travelling in its lengthwise direction through the bend stiffener. The design need some changes in order to deal with the aforementioned issues. These changes will be described in the next section.

## 7.2 Design Changes due to Behaviour Issues

It was seen from the previous section that the initial design proposal have some problems in its mechanical behaviour. The design is changed, in order to get rid of this unwanted behaviour. To do so, the current design from section 2.3 *Materials, Dimensions and Load Cases of The Current Bend Stiffener and Pipe* and the initial design concept are compared and the best intuitive concepts from both are merged into one design. The following list describes the concepts from each design which are taken on to a new design.

### Current Design

- *Polyurethane as a load transfer*

The polyurethane worked as a good load transfer between the pipe and bend stiffener, as it ensured a support of the pipe through the whole length of the bend stiffener. This distributes the surface loads to a large area and gives a soft connection to the pipe compared with steel.

- *Steel ring preventing separation of steel and polyurethane*

The flange on the current design has a steel grid, where the purpose is to grip in to the polyurethane and prevent a separation of the flange and the polyurethane. Especially the steel ring at the end of the grid is useful as it prevents the lengthwise tension force from separating the parts.

- *Polyurethane covering the flange to prevent environmental exposure*

When the polyurethane is covering the steel flange it protects the flange from the environment, and thereby corrosion, wear or other damages.

### Initial Design Concept

- *Conical steel rods for supplying stiffness*

The conical steel rods are a good alternative to the polyurethane for supplying the varying stiffness of the structure. This means that a less amount of polyurethane has to be used, and thereby decreases the insulating effect of the bend stiffener. The steel rods does also function as large cooling elements through the length of the bend stiffener.

A new conceptual design is developed with these four main concepts in mind. The new conceptual design seeks to keep the amount of polyurethane as low as possible, but still enough to function as the connection between the steel rods and the pipe. It is also sought to make a design where the flange, which is not connected to the vessel, is removed. The new conceptual design can be seen on figure 7.2.

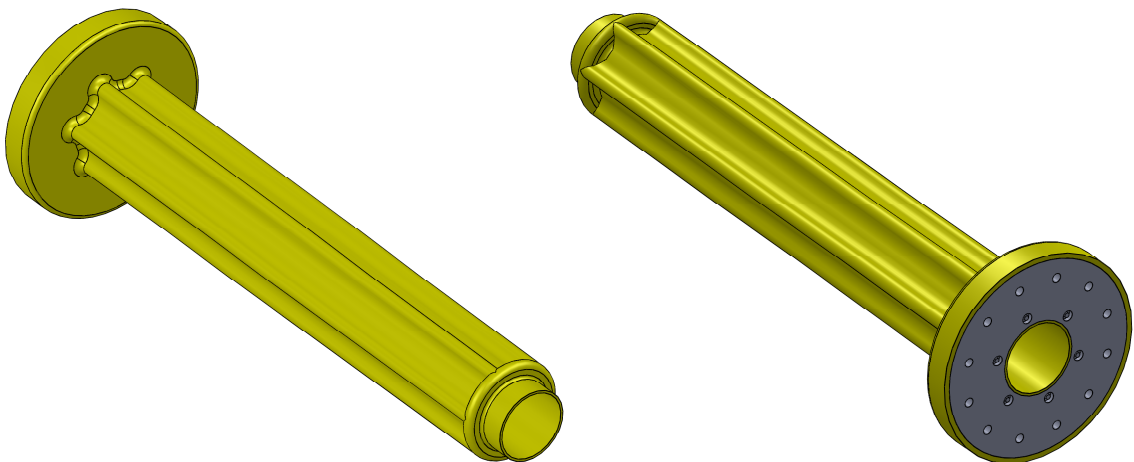


**Figure 7.2:** New conceptual design, this design consist of the best concepts from the current design and the initial design concept.

---

On the section cut shown in figure 7.3 can it be seen that the conical rods are surrounded by polyurethane and has no contact with the outer surface of the pipe, nor the environment.

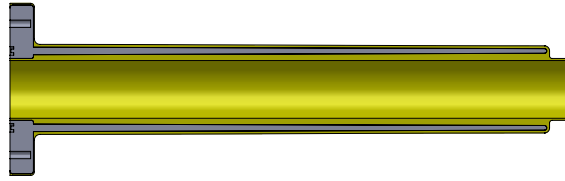


**Figure 7.3:** A section cut of the new conceptual design, where the conical steel rods are shown, surrounded by the polyurethane structure.

A ring is attached to the ends of the rods instead of the steel flange in the previous design proposal. This ring serves two purposes; preventing the tension force from separating the steel and polyurethane, and maintaining the distance between the rods so their deflection curves are identical on both side of the pipe. One issue with the ring, might be the relatively high pressure between the polyurethane and the steel ring, which might lead to damage of the polyurethane. The complete steel structure can be seen on figure 7.4.

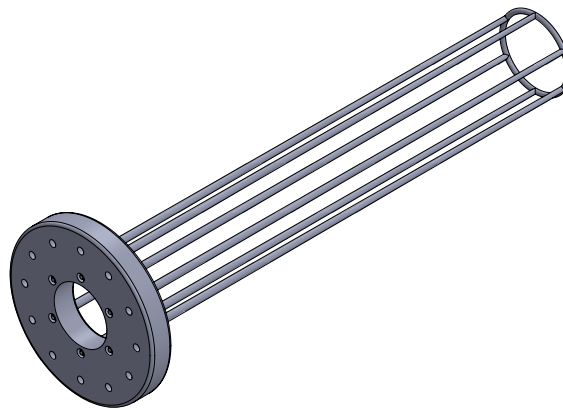


**Figure 7.4:** The new steel structure with flange, conical rods and a ring connecting the rods. This steel structure is moulded into the polyurethane part.

The idea is to place the steel part in a mould and mold the polyurethane around it. This design should prevent the behaviour issues seen from the previous design proposal, and in the same time lower the insulating effect compared to the design which is in use today. This new conceptual design will be optimized and evaluated in the next chapter.

## Final Design Optimisation and Development

The new design obtained in the previous chapter needs to be optimized towards the wanted behaviour, meaning that the first thing to do, is to ensure the same deflection profile, which is done by optimisation. This chapter will describe the theory used and how it is applied to the problem. Furthermore is the design checked for its insulating effect to ensure that the temperature requirement is fulfilled. The chapter ends with a refinement of the design, in order to avoid notches compromising the fatigue strength.

### Contents

---

<b>8.1 Optimisation</b> . . . . .	<b>63</b>
<b>8.2 Thermal Analysis of The Final Design</b> . . . . .	<b>66</b>
<b>8.3 Refinement of The Design</b> . . . . .	<b>70</b>
<b>8.4 Summary and Discussion</b> . . . . .	<b>71</b>

---

### 8.1 Optimisation

The new design is optimized in the same way as the design in the previous chapter. The optimisation is done in Matlab® in a combination with ANSYS® APDL. The design was optimized by using two design variables, which are the radii on the conical rods as seen on figure 8.1. The theory described in this section is based on the book called Numerical Optimization [44] and Introduction to Optimum Design [5].

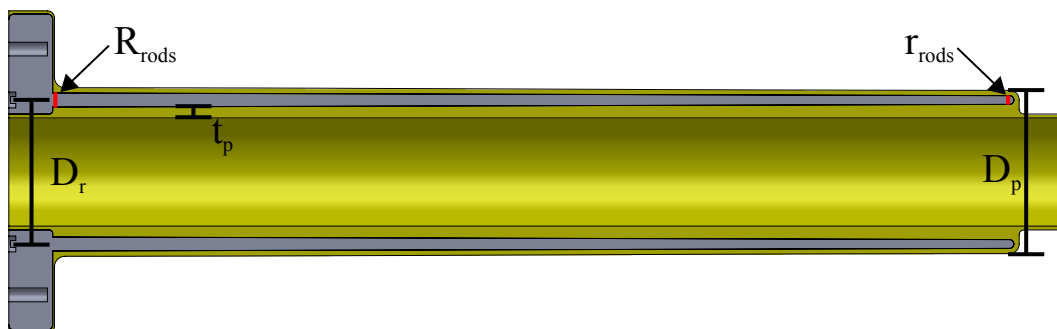


**Figure 8.1:** Design variables used in the optimisation marked with red. The dimensions which are indirectly affected by the design variables are marked with black.

The deflection profile is mainly governed by the radii of the rods, and these are directly changed through the optimisation, but also other dimensions are affected indirectly by the change of the radii of the rods, see figure 8.1. The circle on which the rods are placed

is changed as the rods are changed, and the outer diameter of the polyurethane part is changed indirectly together with the thickness of polyurethane between the rods and the pipe surface. The optimisation is done by comparing the deflection curves in each iteration, where 200 discretized points from the deflection of the old bend stiffener is compared to 200 points from the new design. This is illustrated on figure 8.2.

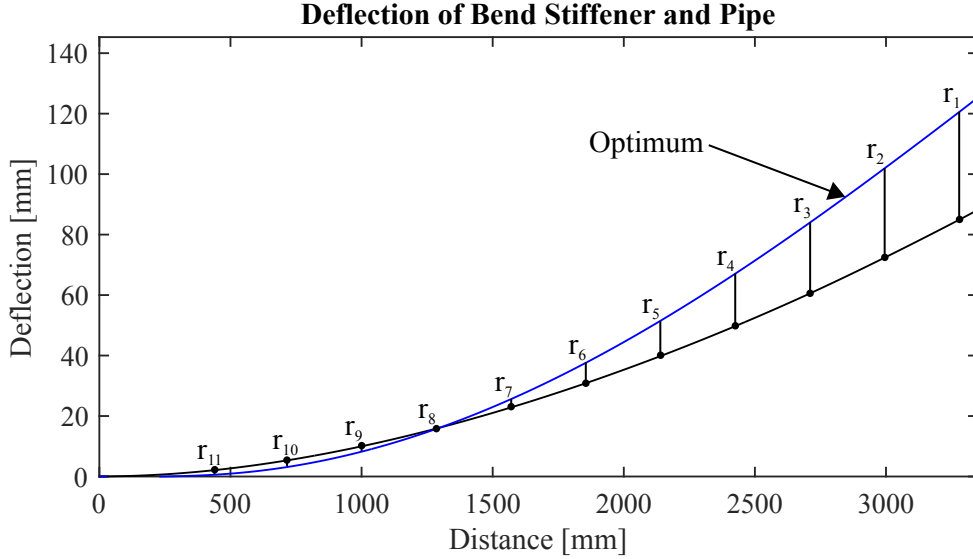


**Figure 8.2:** Optimisation of deflection curve with point residuals.

The blue line is the optimum, i.e. the deflection of the old bend stiffener design. A residual is calculated in each iteration for all 200 points,  $r_i$  as shown on the figure. These residuals are used to establish an objective function which should be minimized. This objective function is formulated as a least square expression, given as

$$f_{obj} = \sum_{i=1}^{200} \frac{1}{2} r_i^2 \quad (8.1)$$

The optimisation is gradient based, and therefore is the gradient calculated in the beginning of each iteration to determine the design sensitivity, and to determine the appropriate descent direction of the objective function. The gradient is calculated by forward difference approximation, where a small perturbation of the design variables is introduced in each direction. The optimisation algorithm is based on the *sqp* (Sequential Quadratic Programming) method. This method takes a general nonlinear problem and transform it into a QP subproblem. The general problem can be defined as the Langrangian

$$\mathcal{L}(\mathbf{x}, \boldsymbol{\lambda}) = f(\mathbf{x}) + \sum_{i=1}^m \lambda_i g_i(\mathbf{x}) \quad (8.2)$$

Where  $f$  is the objective function and  $g_i$  is the  $i^{th}$  inequality constraint equation and  $\lambda_i$  is the  $i^{th}$  Langrangian multiplier. This way of stating the Langrangian assumes that all

## 8. Final Design Optimisation and Development

---

constraints are inequalities. The idea of introducing the Langrangian is to convert the constraint problem to a unconstrained problem. The quadratic subproblem is obtained as

$$\min_{\mathbf{d} \in \mathbb{R}^n} \frac{1}{2} \mathbf{d}^T \mathbf{H}_k \mathbf{d} + \nabla f(\mathbf{x}_k)^T \mathbf{d} \quad (8.3)$$

subject to

$$\nabla g_i(\mathbf{x}_k)^T \mathbf{d} + g_i(\mathbf{x}_k) \leq 0 \quad (8.4)$$

Where  $\nabla$  denotes the gradient of the associated function,  $\mathbf{x}_k$  and  $\mathbf{H}_k$  are the design variable vector and the Hessian matrix at the  $k^{th}$  iteration of the subproblem, respectively.  $\mathbf{d}$  is a unit vector describing the feasible descent direction, and the solution for  $x_k$  is used to determine the next set of design variables.

$$\mathbf{x}_{k+1} = \mathbf{x}_k + \alpha_k \mathbf{d}_k \quad (8.5)$$

Where  $\alpha_k$  is the step size in the descent direction, which is determined by an appropriate line search method (e.g. golden section search). In each iteration is the Hessian matrix approximated and updated by a quasi-Newton based method. In the case of this optimisation, the BFGS (Broyden-Fletcher-Goldfarb-Shanno) method is used. A local minimum is reached when the KKT (Karush-Kuhn-Tucker) necessary conditions are fulfilled. These conditions for the Langrangian, stated in equation (8.2), are given as

$$\frac{\partial \mathcal{L}}{\partial x_i} = 0 \quad i = 1, \dots, n \quad (8.6)$$

$$\frac{\partial \mathcal{L}}{\partial \lambda_j} = g_j + s_j^2 = 0 \quad j = 1, \dots, m \quad (8.7)$$

$$\frac{\partial \mathcal{L}}{\partial s_j} = 2s_j \lambda_j = 0 \quad j = 1, \dots, m \quad (8.8)$$

Where  $\mathbf{s}$  is the slack variable vector containing all the slack variables used to convert all inequalities to equalities.  $n$  is the number of design variables and  $m$  is the number of inequality constraints. All this is evaluated in the software Matlab<sup>®</sup> and the algorithm needs an initial guess of the design variables, in order to start the iteration. The initial guess for this optimisation was given as

$$R_{rods} = 15.8 \text{ mm} \quad (8.9)$$

$$r_{rods} = 10.8 \text{ mm} \quad (8.10)$$

This guess was based on a brief study of the feasible region of the design space, as the design space seemed to have the global minimum in the vicinity of these values. If the optimisation reaches a local or a global minimum is very dependent on the initial guess, because a wrong initial guess can cause the optimisation to go towards a local minimum and get trapped in this minimum. After just four iterations from this guess, a minimum was found. This minimum came up with the following values for the design variables.

$$R_{rods} = 18.065 \text{ mm} \approx 18 \text{ mm} \quad (8.11)$$

$$r_{rods} = 6.6839 \text{ mm} \approx 6.5 \text{ mm} \quad (8.12)$$

These values results in a deflection curve as shown on figure 8.3.

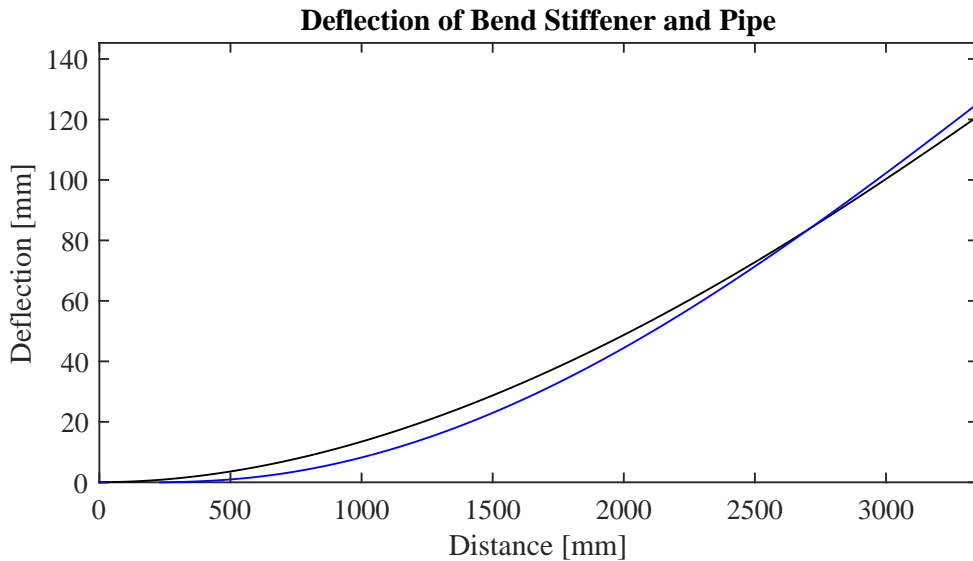


**Figure 8.3:** The optimized deflection curve. **Blue:** Deflection curve of the old bend stiffener design. **Black:** New bend stiffener design.

The behaviour of the two designs are very close on this figure, and the behaviour is assumed to be acceptable. These dimensions will be used in the design in further studies. The primary function to fulfill was the deflection, and the next which will be checked is the insulating effect. The temperature analysis is presented in the next section.

## 8.2 Thermal Analysis of The Final Design

This section describes how the thermal behaviour of the final design is evaluated using ANSYS Workbench<sup>®</sup>. Two steady state thermal analyses are conducted, both analyses are applied with natural convection, as convection has a cooling effect to the surface of the bend stiffener. The two models are similar set up, and the only difference is the different values for the natural convection. One analysis is conducted with convection to stagnant air, while the second analysis is completed with convection to water. Convection is the transfer of heat from the surface of the bend stiffener to the fluids surrounding the part. The fluids are in this case air or water. The expression for convective heat transfer is stated by equation (8.13).

$$q = hA(\Delta T) \quad (8.13)$$

Equation (8.13) is known as Newton's law of cooling. Here  $q$  is heat transferred per unit time, Watt, and  $A$  is area of the surface of the heat transferring part,  $m^2$ .  $\Delta T$  is the temperature difference between the surface and the fluid.

In equation (8.13),  $h$  is the convective heat transfer coefficient,  $\frac{W}{m^2} K$ . This coefficient depends on numerous factors, and some of those are flow velocity and viscosity of the

## 8. Final Design Optimisation and Development

surrounding fluid [7; 18]. The values for the used convective heat transfer coefficients are listed in equation (8.14) and equation (8.15).

$$h_{Air} = 5 \frac{W}{m^2 K} \quad (8.14)$$

$$h_{Water} = 1200 \frac{W}{m^2 K} \quad (8.15)$$

These values are default in ANSYS Workbench<sup>®</sup>, and are similar to the values normally used for these types of convective heat transfer [19]. The models are setup with symmetry planes, such that  $\frac{1}{3}$  of the bends stiffener with pipe is represented, see figure 8.4.

Two types of symmetry is used, cyclic symmetry planes and symmetry planes, shown on figure 8.4. Cyclic symmetry is used to simulate the entire bend stiffener with the pipe. The symmetry planes are used to simulate or 'mirror' the flexible pipe and the flange in the axial direction.

This is done to simulate the thermal conduction throughout the length of the pipe, and also the conduction between the vessel and the steel flange. It is assumed that the steel flange is suitable to constitute the connection to the vessel.

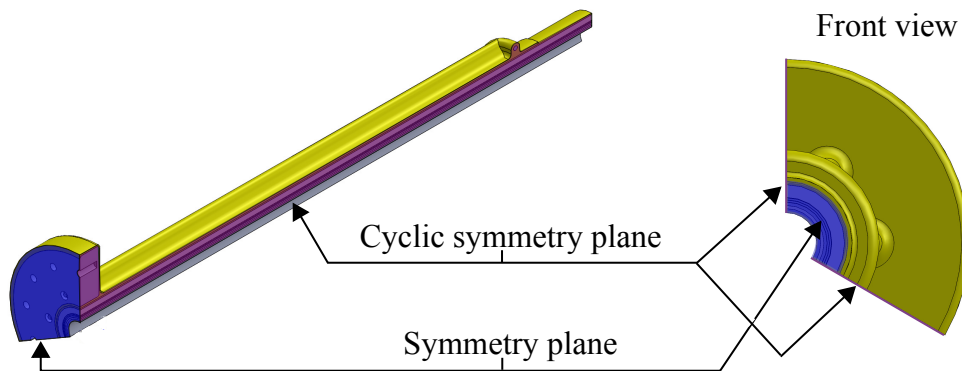


**Figure 8.4:** The cyclic symmetry planes and symmetry planes on the models. **Blue marking:** *Symmetry planes.* **Violet marking:** *Cyclic symmetry planes.*

The boundary conditions are shown on figure 8.5. The temperature of the inside area of the pipe is set to 130 °C, while the initial temperature is set to 25.3 °C. The initial temperature is chosen to have this value, as it represents a value in the high end of the temperature interval for both air and water stated in section 4.2 *Environment and Surroundings*. It is also the air temperature used in section 4.4.1 *Thermal Analysis*. Convection is applied to the surface of the bend stiffener and the pipe (The entire yellow part on figure 8.5).

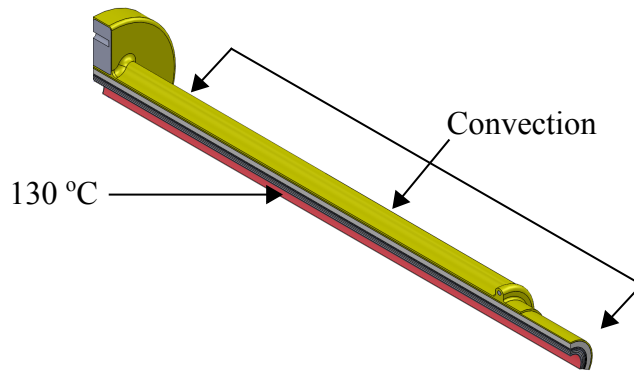


**Figure 8.5:** The boundary conditions on the model. **Red marking:** *The temperature inside the pipe.*

The results from the analysis with the convection of stagnant air is shown figure 8.6.

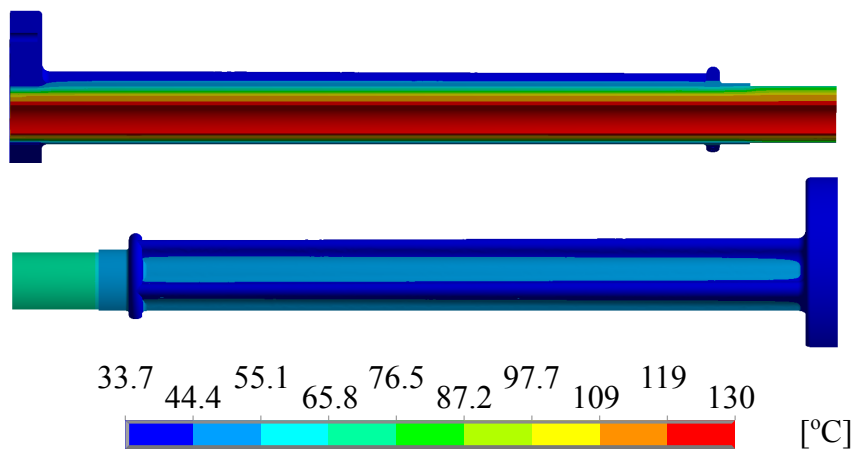


**Figure 8.6:** Results from the analysis with a convection of  $5 \frac{W}{m^2 K}$ .

From the results, it can be seen that the steel provides a relatively high cooling effect compared to the polyurethane. It is worth to notice the polyurethane has a temperature on the surface, that are 10 to 15 °C higher than the steel, even though the smallest thickness of the polyurethane between the rods is only 11 mm. To examine the temperature of the outer polyamide layer on the pipe, a path is defined on the outer circumference of the pipe, see figure 8.7.

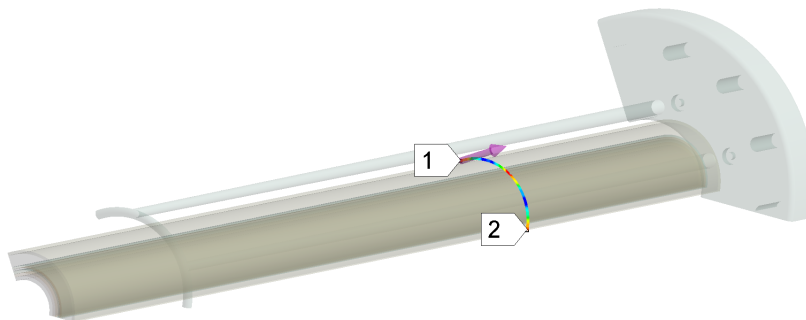


**Figure 8.7:** Path on the outer circumference of the pipe.

## 8. Final Design Optimisation and Development

From the path on the outer circumference of the pipe, the maximum temperature is determined. Based on the location of this temperature, a new path throughout the length of the bend stiffener is defined. This path are displayed on figure 8.8.



**Figure 8.8:** Path throughout the length of the bend stiffener.

The temperatures of the outer polyamide layer along the path is displayed on figure 8.9. The blue line defines the maximum allowed temperature.

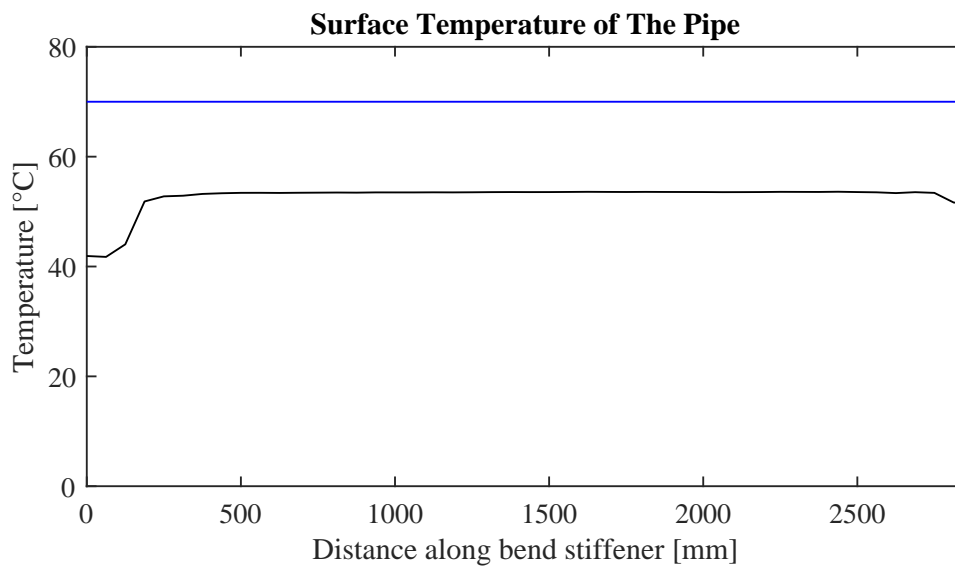


**Figure 8.9:** Temperature of the outer polyamide layer throughout the length of the bend stiffener. **Blue marking:** Maximum allowed temperature. **Black marking:** Temperatur of the outer layer

Next are the results with the convection of water displayed, see figure 8.10. As water has a higher convective heat transfer coefficient, the temperature affecting the surface of the pipe is lower.

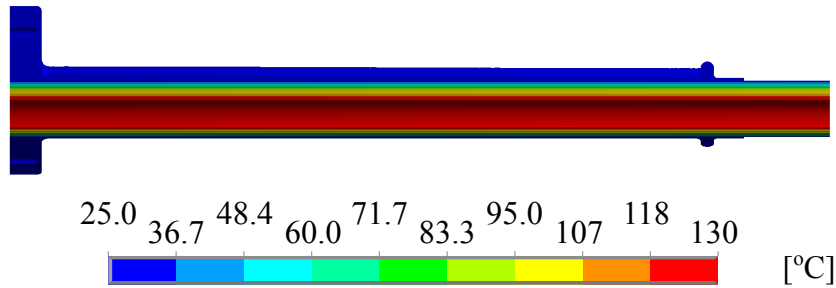


**Figure 8.10:** Results from the analysis with a convection of  $1200 \frac{W}{m^2 K}$ .

A path throughout the length of the bend stiffener is defined in a similar approach as described previously. The temperature of the outer layer of the pipe along the path is shown on figure 8.11.

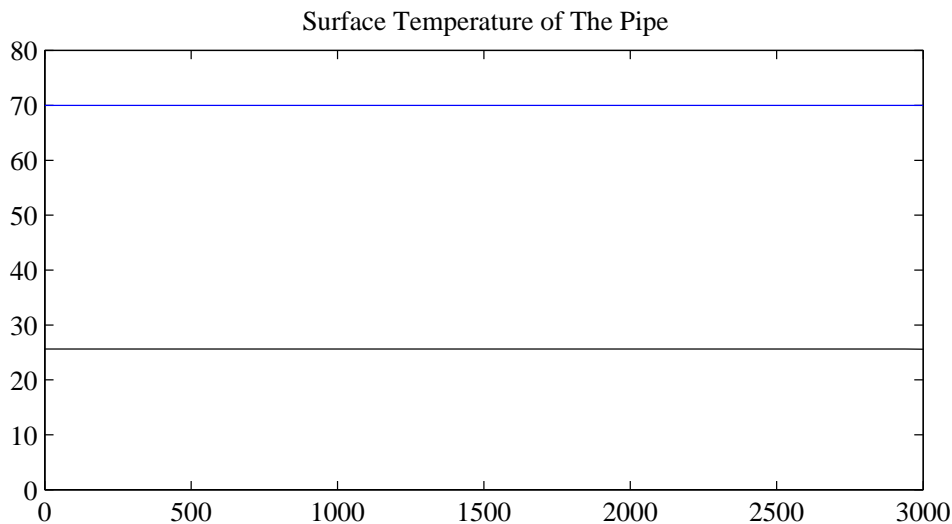


**Figure 8.11:** Temperature of the outer layer throughout the length of the bend stiffener. **Blue marking:** Maximum allowed temperature. **Black marking:** Temperatur of the outer layer.

Figure 8.10 and figure 8.11 shows clearly, the benefit of placing the bend stiffener in water from a thermal point of view. Based on the results, it can be concluded, that the design fulfils the requirement for the surface temperature of the flexible pipe as the temperature both in air and water is below  $70^\circ C$ .

In the next section, it is briefly explained how the new design is further improved.

### 8.3 Refinement of The Design

As the rods has been adjusted through the optimisation described earlier, the final details can be added to the design. The aim with this process is to change the design of the steel

structure, so the design has smooth contours and soft transitions, instead of sharp edges and notches. Notches and sharp edges can be fatal for the fatigue life. The changes are based on experience and intuition, the refined design is shown on figure 8.12.

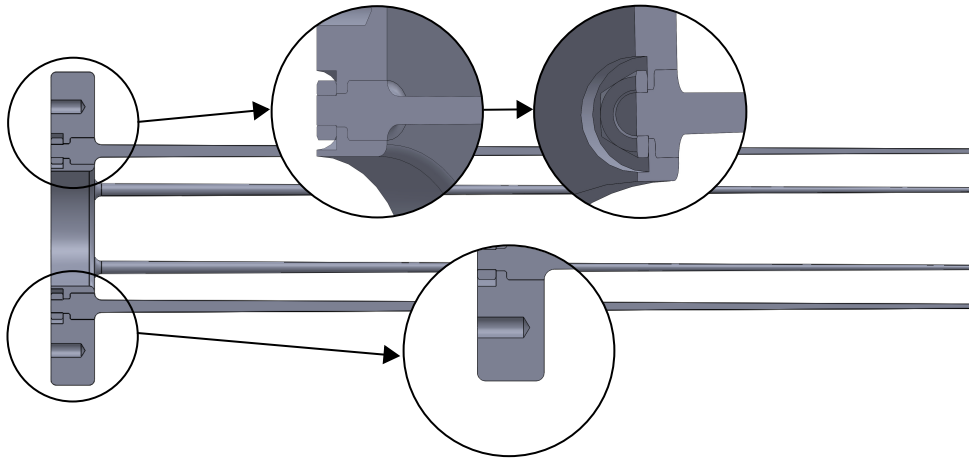


**Figure 8.12:** Refinements on the steel structure.

As illustrated on figure 8.12, edges are made with round contours, and the rods are designed with a notch radius to avoid relatively high stress concentrations. The notch radius is selected to be 20 mm. The rods are mounted to the flange with M42 bolts.

### 8.4 Summary and Discussion

This chapter describes how the design was optimized towards the desired behaviour and afterwards was the insulation effect of the optimized design evaluated. The two analyses showed that the design fulfilled both the behaviour and temperature requirement. In the end of this chapter was the design prepared for fatigue loads in the critical area of the conical rods in the vicinity of the flange. Until this point has now strength analysis been conducted, due to the fact that no equivalent model for the flexible pipe has been available. A pipe model was originally not a part of the scope for this project as the development of bend stiffener was supposed to have the main focus. However, since a pipe model is needed to evaluate static strength and fatigue life, a model for the pipe is developed in the next chapter.



## Analytical Modelling of the Bending Stiffness of a Flexible Pipe

It has been proven highly necessary to have a model describing the flexural behaviour of the flexible pipe, in order to evaluate the strength of the bend stiffener. This chapter will describe the derivation of an expression for an equivalent bending stiffness of the pipe.

### Contents

<b>9.1</b>	<b>Pipe Structure</b>	<b>73</b>
<b>9.2</b>	<b>Contribution from Polymer Layers</b>	<b>74</b>
<b>9.3</b>	<b>Contribution from Helical Steel Layers</b>	<b>75</b>
9.3.1	Bending Stiffness in No Slip Cases	75
9.3.2	Progression of Interlayer Sliding	78
9.3.3	Equivalent Stiffness including Bending and Torsional Effects of the Individual Helical Strips	80

### 9.1 Pipe Structure

The pipe is build of several layers of different materials, geometries and properties. As described in previous chapters, the pipe consist of polymer layers acting as fluid barriers and anti-wear layers. Steel layers are applied to give the desired strength in different directions. Some steel layers are maintaining the tensional strength and others are functioning as pressure armours. A brief review of the pipe, modelled in this report, is given below on figure 9.1.

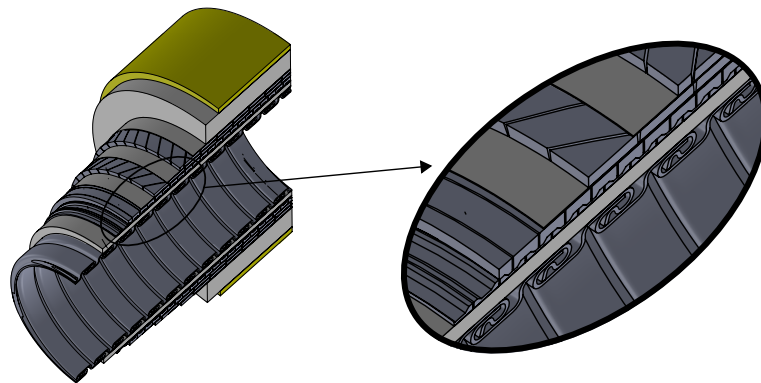


**Figure 9.1:** A cut through of the flexible pipe showing the different layers in the pipe structure.

The yellow and white layers are insulating, anti-wear and fluid barriers made of polyamide 11 (also called nylon 11). The grey layers are tensile and pressure armours made of steel. Material data and thickness of each layer can be seen in section 2.3 *Materials, Dimensions and Load Cases of The Current Bend Stiffener and Pipe*. The 3D drawing was originally drawn to establish a finite element model for the pipe properties, but due to time consuming complexity, this have to be a scope for future work. A drawing of the cross section of the helical steel layers is given below on figure 9.2, as they are used in the derivations through this section.

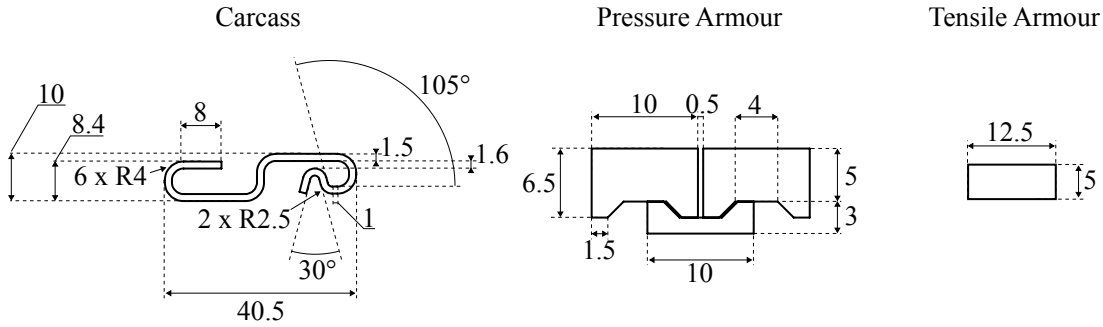


**Figure 9.2:** Cross section of the carcass, pressure armour and tensile armour in the flexible pipe. All dimensions are in mm.

The cross section of the pressure armour is assumed to be a rectangular with side lengths of 10 x 8 mm. Also the lay angle for these helical layers are important for the flexural stiffness of the pipe. These angles are listed in table 9.1.

**Table 9.1:** Lay angle for helical steel layers.

Layer	Lay Angle $\alpha_i$
Carcass	87.2°
Pressure Armour	85.5°
Inner Tensile Armour	35°
Outer Tensile Armour	35°

The lay angle is measured from the lengthwise axis of the pipe.

The most vital parts of the pipe, with respect to the bending stiffness, has been described and the stiffness derivation can begin.

## 9.2 Contribution from Polymer Layers

The modelling of the bending stiffness can be divided into to groups of contribution, those from the polymer layers and those from the helical steel layers. The contribution from the polymer layers is very simple to determine as they are considered as solid cylindrical

beams. The contribution can simply be taken from the moment-curvature relationship, given as

$$M_b = E_{poly} I_{poly} \kappa \quad (9.1)$$

Where  $M_b$  is the bending moment,  $E_{poly}$  and  $I_{poly}$  are Young's Modulus and the area moment of inertia of the cross sectional area of the polymer cylinders, respectively.  $\kappa$  is the curvature of the neutral axis, due to bending. The flexural stiffness is just the product of  $E_{poly}$  and  $I_{poly}$ .

### 9.3 Contribution from Helical Steel Layers

The stiffness contribution from the steel armours are much more complex as these are dependent on a wide range of parameters such as, internal and external pressure, friction, lay angle etc. The derivation of the stiffness contribution from these layers are divided into three parts; the first is the no slip case where there is no sliding between the layers, the second case is the intermediate zone between no slip and full slip, and the third part is the contribution due to local torsional effects while the pipe is bend. The full slip case is not considered as the contribution to the bending stiffness in this case is considered to be negligible. The derivations presented in this section is based on three papers on the modelling of flexural behaviour of flexible pipes. The first, written by J. A. Witz and Z. Tan in 1992, [62], is describing the bending moment before slip and discussing the case after slip and do also look into cases with extreme helical angles of the steel layers. The second paper is written by I. Kraincanic and E. Kebabze in 2001 [32], and deals with the slip initiation and progression, and seeks to describe the stiffness in these cases. A Ph.D. Thesis is supporting this paper and is also made by the one of the authors from the paper, E. Kebabze in 2000 [31]. The third, written by L. Dong, et al. in 2013 [16], is looking at the torsional effects of the helical layers occurring while bending the pipe.

#### 9.3.1 Bending Stiffness in No Slip Cases

The no slip case, is the case where no relative interlayer movement occurs, meaning that the friction force between to adjacent layers is greater than the normal force trying to move the layer in the axial direction. This part is mainly based on [62] and [31]. Only a quarter turn of the helical strips are considered to ease the derivations. This can be done because of symmetric and antisymmetric conditions. The idea is to describe a point on a helical strip, and be able to describe it before and after bending by using the assumption that plane cross sections remains plane after deformation. First of all is a helical trip considered in a local Cartesian coordinate system, see figure 9.3.

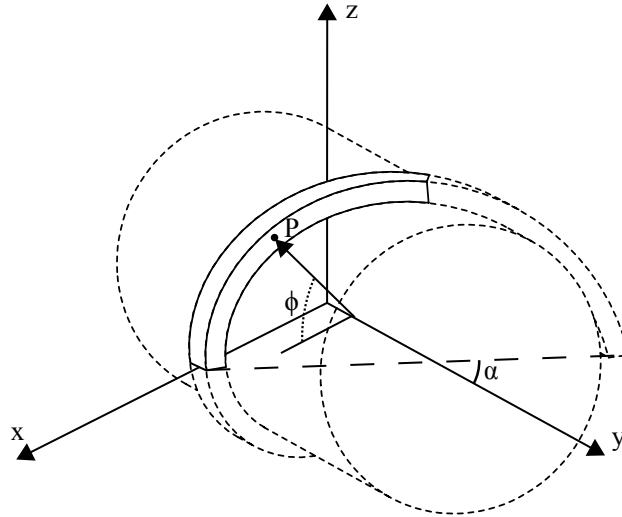


**Figure 9.3:** A helical strip with a local Cartesian coordinate system. Points lying on the centreline of the strip can be described by the radius and two angles. This figure is drawn with inspiration from [62]

As it is seen on the figure, the local coordinate system is placed in the centre of one turn of the helical strip. Any arbitrary point on the centreline can be described by the following expressions

$$x = R \cos \phi \quad y = \frac{R}{\tan \alpha} \phi \quad z = R \sin \phi \quad \phi \in \left[0, \frac{\pi}{2}\right] \quad (9.2)$$

Where  $R$  is the radius of the helical layer,  $\alpha$  is the lay angle and  $\phi$  is the angle between the  $xy$ -plane and the vector describing the point  $P$ . Since the derivation is performed on a no slip case, it is assumed that the strip remains bonded (read no sliding) to the adjacent layers under deformation. If the helical strip is subjected to a bending moment in the  $yz$ -plane, it is assumed that plane cross sections remains plane due to the absent of slip. It is sought to describe point  $P$  after deformation, denoted  $P^*$ , and the  $x$ -coordinate remains the same since it is a pure deformation in the  $yz$ -plane. See figure 9.4 for the deformed profile of the helical layer.

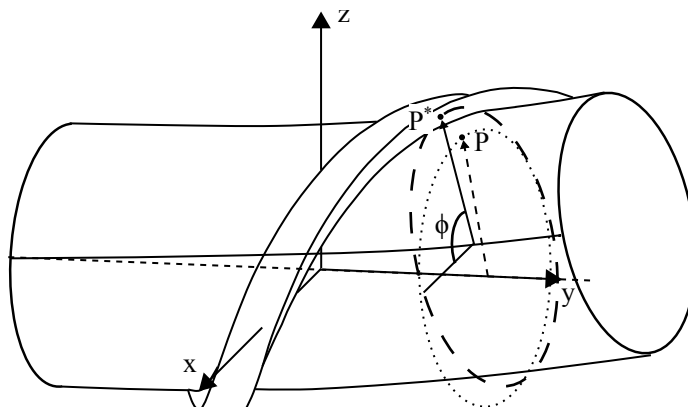


**Figure 9.4:** Deformed helical strip, the point  $P$  becomes  $P^*$  after deformation. This figure is drawn with inspiration from [62].

The point P\* can be expressed as following

$$x^* = R \cos \phi \quad (9.3)$$

$$y^* = \sin \left( \frac{R}{\tan \alpha} \phi \kappa \right) \frac{1}{\kappa} - R \sin \phi \sin \left( \frac{R}{\tan \alpha} \phi \kappa \right) \quad (9.4)$$

$$z^* = \left( 1 - \cos \left( \frac{R}{\tan \alpha} \phi \kappa \right) \right) \frac{1}{\kappa} + R \sin \phi \left( \frac{R}{\tan \alpha} \phi \kappa \right) \quad (9.5)$$

Where  $\kappa$  is the bending curvature of the neutral axis of the layer. The axial strain in the deformed helical tendon is given, based on the expressions for P and P\*. The strain expressed as a function of  $\phi$  is given as

$$\varepsilon(\phi) = \frac{ds^*}{ds} - 1 = \sqrt{\frac{dx^{*2} + dy^{*2} + dz^{*2}}{dx^2 + dy^2 + dz^2}} - 1 \quad (9.6)$$

By inserting and simplifying is the following expression obtained

$$\varepsilon(\phi) = \sqrt{1 - 2R \cos^2 \alpha \sin \phi \kappa + R^2 \cos^2 \alpha \sin^2 \phi \kappa^2} - 1 \quad (9.7)$$

This is highly nonlinear and can be simplified to a linear expression, by assuming small deflections, which yields

$$\varepsilon(\phi) = R \cos^2 \alpha \sin \phi \kappa \quad (9.8)$$

This expression is used to find the strain energy for one helical strip. The strain energy can be calculated from the expression for a rod undergoing axial tension, which is given by

$$U = \frac{1}{2} \int_0^S EA \varepsilon^2 ds \quad (9.9)$$

Where  $E$  is Young's Modulus and  $A$  is the cross sectional area and  $S$  is the length of the strip. The strip length can be expressed by using the lay angle and the length of the pipe,  $L$ .

$$S = \frac{L}{\cos \alpha} \quad (9.10)$$

Since the strain is expressed as a function of  $\phi$  in equation (9.8), a conversion of the integral is needed. The infinitesimal term  $ds$  is given by the following

$$ds = \frac{R}{\sin \alpha} d\phi \quad (9.11)$$

The strain energy is then expressed as

$$U = 4n \int_0^{\frac{\pi}{2}} \frac{1}{2} EA (R \cos^2 \alpha \sin \phi \kappa)^2 \frac{R}{\sin \alpha} d\phi \frac{\tan \alpha L}{2\pi R} \quad (9.12)$$

The expression is multiplied with four since the integral only describes the energy in a quarter of a turn of one strip, and  $n$  is the number of strips in the layer. The term in

the end,  $\frac{\tan \alpha L}{2\pi R}$ , is the number of revolutions of the strip in the entire length of the pipe. Evaluating the integral in equation (9.12) yields

$$U = \frac{1}{4}EAR^2 \cos^3 \alpha \kappa^2 nL \quad (9.13)$$

This expression inspires to make use of the principle of energy conversion, expressed as

$$\frac{dU}{d\kappa} = \frac{dW}{d\kappa} \quad (9.14)$$

$$W = M\kappa L \quad (9.15)$$

Where the latter expression describes the work done by the bending moment causing the same curvature. The use of these expressions yields the bending moment

$$M = \frac{1}{2}EAR^2 \cos^3 \alpha n\kappa \quad (9.16)$$

From which the equivalent stiffness in the no slip case can be obtained, based on  $M = EI\kappa$ .

$$EI_{ns} = \frac{1}{2}nEAR^2 \cos^3 \alpha \quad (9.17)$$

This stiffness is representative for small curvatures where no interlayer sliding occurs. The sliding will start to progress as the curvature increases. A prediction of this phenomena will be presented in the next section.

### 9.3.2 Progression of Interlayer Sliding

The interlayer sliding occurs as the curvature increases, and the limit between no sliding and initiation of sliding is denoted as a critical curvature  $\kappa_{cr}$ . Studies of this value have been going on for several decades and this section will present a method to predict this value and, more importantly, the stiffness progression in this intermediate zone between no slip and full slip of the layers in the flexible pipe. The methods in this section is based on [32], [31] and [16]. One of the distinctive characteristics of this intermediate zone is that after the sliding is initiated, only a part of the length of a helical strip will slide, while the rest is still in the no slip state. As the curvature increases, the length of the sliding part gradually increases until the entire tendon slips, and the layer is in the full slip state, at that point. This limit between the partial sliding and full slip, can be determined as  $\frac{\pi}{2}\kappa_{cr}$ . The minimum critical curvature, at which the sliding occurs, can be determined by considering the equilibrium configuration of a infinitesimal element of a helical tendon. By doing this the following expression can be obtained

$$\kappa_{cr}^{min} = \frac{\mu_i P_i + \mu_o P_o}{Et \sin \alpha \cos^2 \alpha} \quad (9.18)$$

$\mu_i$  and  $\mu_o$  are the inner and outer friction coefficients for a helical layer to adjacent layers, respectively. In the same way are  $P_i$  and  $P_o$  the inner and outer contact pressure, respectively.  $t$  is the thickness of the tendon in the radial direction of the pipe. From the consideration of this infinitesimal element, it can be shown that the minimum critical curvature is located at the tendons placed at the neutral axis, i.e.  $\phi = 0, \pi, 2\pi$ , etc. A relation between the global bending curvature and the critical angle at which the tendon

## 9. Analytical Modelling of the Bending Stiffness of a Flexible Pipe

slides, can also be determined by considering this infinitesimal element, by equating the friction force and the force increment over the element.

$$\kappa = \kappa_{cr}^{min} \frac{\phi_{cr}}{\sin \phi_{cr}} \quad (9.19)$$

The above expression does not allow for an explicit determination of the critical angle, however it can be approximated within a reasonable accuracy. This can be done by substituting the term  $\frac{\phi_{cr}}{\sin \phi_{cr}}$  with  $\frac{1}{\cos \frac{\phi}{\xi}}$ , where  $\xi$  can be determined from the boundary condition that  $\frac{\phi_{cr}}{\sin \phi_{cr}} = \frac{\pi}{2}$ , when  $\phi = \frac{\pi}{2}$ . This yields  $\xi = 1.7836$ , and the expression for the critical angle becomes

$$\phi_{cr} = \xi \arccos \frac{\kappa_{cr}^{min}}{\kappa} \quad (9.20)$$

This solution is off by approximately 0.7% compared to correct solution of  $\phi_{cr}$ . An important parameter, which will be used later on in the derivation, is the axial stress in the no slip part of the strip. This can be found from the expressions in the derivation of the no slip stiffness, and yields

$$\sigma_{ns} = ER\kappa \cos^2 \alpha \sin \phi \quad (9.21)$$

Another important parameter which is not derived, but taken directly from [16], is the axial stress in the sliding part of a strip.

$$\sigma_f = \frac{(\mu_i P_i + \mu_o P_o) R \phi}{t \sin \alpha} \quad (9.22)$$

The friction force is the only force balancing the axial stress after sliding occurs. From this point on and the rest of the derivation of the interlayer sliding stiffness progression, will the helical steel layers be considered as shells with same thickness as the tendons. However, their individual properties will still be taken into account. The bending moment, according to the stresses presented for the no slip and the slip region in equation (9.21) and (9.22), can be determined by

$$M = 4f_c \left( \int_0^{\phi_{cr}} \sigma_f + \right) \cos^2 \alpha R \sin \phi t R d\phi \quad (9.23)$$

$f_c$  is a fill factor to ensure the same cross sectional area for the equivalent shell compared to the layer of tendons. This fill factor is equal to the sum of arc lengths in between the tendons in the layer, and can be calculated as

$$f_c = \frac{nb}{2\pi R \cos \alpha} \quad (9.24)$$

Where  $b$  is the width of one strip in the layer. This can now be substituted into the moment expression, together with equation (9.21) and (9.22), and subsequently evaluating the integrals.

$$M = \frac{2nAR^2 \cos \alpha}{\pi} \left( \frac{\mu_i P_i + \mu_o P_o}{t \sin \alpha} (\sin \phi_{cr} - \phi_{cr} \cos \phi_{cr}) + \frac{1}{4} E \cos^2 \alpha \kappa (\pi - 2\phi_{cr} + \sin(2\phi_{cr})) \right) \quad (9.25)$$

This can be simplified to

$$M = \frac{4}{\pi} EI_{ns} \kappa_{cr} (\sin \phi_{cr} - \phi_{cr} \cos \phi_{cr}) + \frac{1}{\pi} EI_{ns} \kappa (\pi - 2\phi_{cr} + \sin(2\phi_{cr})) \quad (9.26)$$

The stiffness for the intermediate zone of no slip and full slip is found by differentiating equation (9.26).

$$EI_{ps} = EI_{ns} - \frac{EI_{ns}}{\pi} \left( 2\phi_{cr} - \sin(2\phi_{cr}) - \frac{4\xi \sin \phi_{cr}}{\tan\left(\frac{\phi_{cr}}{\xi}\right)} \left( \phi_{cr} \cos\left(\frac{\phi_{cr}}{\xi}\right) - \sin \phi_{cr} \right) \right) \quad (9.27)$$

This stiffness is valid for the partial slip zone and is characterized by the curvature interval  $\kappa \in \left] \kappa_{cr}, \frac{\pi}{2} \kappa_{cr} \right[$ . Until now the pipe stiffness has been treated in the no slip case and the partial slip case. However, these cases only includes the stiffness based on axial strains, which is acceptable when assuming small deformations and small lay angles for the helical layers. The next section describes a stiffness based on local curvature considerations of the helical tendons, which also include the effect of local torsion.

### 9.3.3 Equivalent Stiffness including Bending and Torsional Effects of the Individual Helical Strips

The geometry of helical layers are sensitive to bending, and the helical geometry changes during deformation of the pipe. These changes introduces local torsion and bending of the tendon, which is different from the effects determined by axial stiffness considerations. The deflection of a tendon is assumed to follow a loxodromic curve, which is stated by Svein Sævik in his Ph.D. thesis in 1992 [52]. Sævik proposed a description of the local curvatures of the tendon, based on this loxodromic curve and related the expressions to the global curvature of the pipe. The local curvatures are specified in three principal orthogonal directions, to which the global curvature is projected, by using trigonometric considerations of the loxodromic curve. The three directions can be seen on figure 9.5, where the three curvatures are drawn on a cross section of an undeformed helical tendon, in order to simplify the figure, as the understanding of the three directions does not change during deformation.

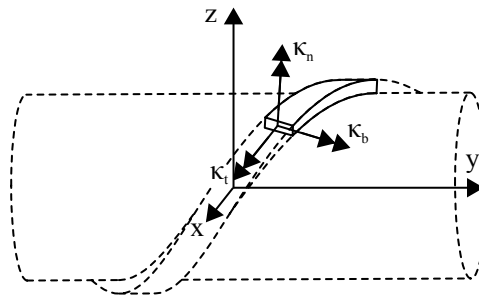


**Figure 9.5:** The global bending curvature is projected to three orthogonal local directions. This figure is drawn with inspiration from [62]

## 9. Analytical Modelling of the Bending Stiffness of a Flexible Pipe

The changes in the three curvatures during bending are according to Sævik, [52], given by

$$\Delta\kappa_n = -\kappa (1 + \sin^2 \alpha) \cos \alpha \cos \phi \quad (9.28)$$

$$\Delta\kappa_b = \kappa \cos^4 \alpha \sin \phi \quad (9.29)$$

$$\Delta\kappa_t = \kappa \sin \alpha \cos^3 \alpha \sin \phi \quad (9.30)$$

Where  $\kappa_n$ ,  $\kappa_b$  and  $\kappa_t$  are the curvatures in the normal, binormal and torsional directions of the cross section of a helical strip, respectively. The rest of the derivations in this section are based on the paper by Dong et al., [16]. The idea behind the derivations in this section is the same as in the no slip case, where the stiffness was based on the determination of the strain energy. The strain energy in this case is given as

$$U = \int_0^S \left( \frac{1}{2} EI_n \Delta\kappa_n^2 + \frac{1}{2} EI_b \Delta\kappa_b^2 + \frac{1}{2} GI_t \Delta\kappa_t^2 \right) ds \quad (9.31)$$

Where  $I_n$ ,  $I_b$  and  $I_t$  are the area moment of inertia corresponding to the three principal curvature directions presented on figure 9.5.  $G$  is the shear modulus of the tendon material. In the same manner as in the no slip case, can the strain energy be rewritten to the following expression.

$$U = \frac{2nL}{\pi \cos \alpha} \int_0^{\frac{\pi}{2}} \left( \frac{1}{2} EI_n \Delta\kappa_n^2 + \frac{1}{2} EI_b \Delta\kappa_b^2 + \frac{1}{2} GI_t \Delta\kappa_t^2 \right) d\phi \quad (9.32)$$

By using the energy conservation principle again, can the corresponding moment be obtained

$$M_{bt} = \frac{1}{2} n \left( EI_n (1 + \sin^2 \alpha)^2 \cos \alpha + EI_b \cos^7 \alpha + GI_t \sin^2 \alpha \cos^5 \alpha \right) \kappa \quad (9.33)$$

The stiffness is then given by

$$EI_{bt} = \frac{1}{2} n \left( EI_n (1 + \sin^2 \alpha)^2 \cos \alpha + EI_b \cos^7 \alpha + GI_t \sin^2 \alpha \cos^5 \alpha \right) \quad (9.34)$$

This stiffness takes into account the local effects of bending and torsion of the individual helical strips, while the pipe is undergoing a global bending moment. This stiffness expression, together with the one for polymer layers given in equation (9.1), has been used to determine an equivalent stiffness for the pipe described in section 2.3 *Materials, Dimensions and Load Cases of The Current Bend Stiffener and Pipe* and with the cross sections for the strips in the helical layers as shown on figure 9.2. By using these data the equivalent stiffness becomes

$$EI_{bt} \approx 117521 \text{ Nm}^2 \quad (9.35)$$

To model the pipe, an equivalent pipe is chosen as a solid rod with an radius of 154 mm, which yields an equivalent E-modulus of 266 MPa.



## Static Strength Analysis

This chapter is describing how the static analysis is carried out. The analysis is conducted in ANSYS® Workbench, as an nonlinear FE analysis.

### Contents

---

<b>10.1 Analysis Setup . . . . .</b>	<b>83</b>
<b>10.2 Results and Discussion of the Analysis . . . . .</b>	<b>84</b>

---

### 10.1 Analysis Setup

After pipe has been modelled, it has become very compliant, and therefore is it not possible to reach a converged result with a linear FE analysis, due to large deflections. Therefore is a geometrically nonlinear analysis conducted, with the use of quadratic elements. The model with loads are sketched on figure 10.1

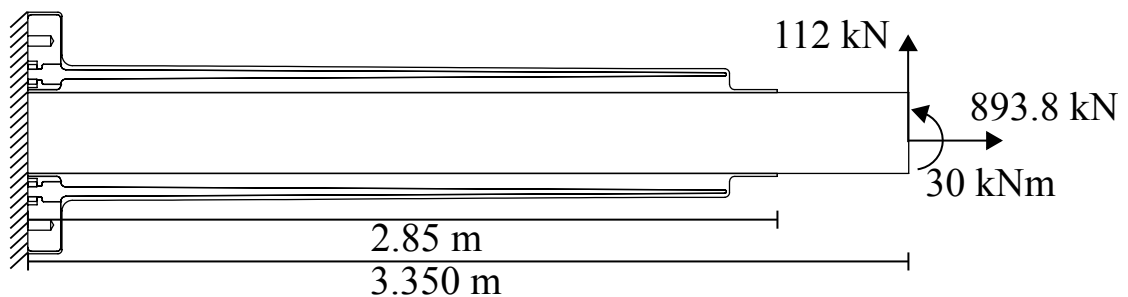


**Figure 10.1:** The load case used for the strength analysis.

Three different structural elements are used. For volumes which can be meshed using hexahedral elements is the SOLID186 used. This is a 20-node 3D element with three user accessible degrees of freedom, namely the three translational degrees of freedom, UX, UY and UZ as they are called in ANSYS®. The second element used in the model is called SOLID187, which is a 10-nodes 3D tetrahedral element, this is used for complex geometry regions where only free mesh with tetrahedrals is possible. The properties of this element are the same as the properties of SOLID186. The last element which is used in the model is SURF154 which is a 8-node surface element used on areas where loads are applied. The loads are distributed to this element as surface loads, by using the shape functions of the element to distribute the loads evenly over the surface. So this surface element works as a transition of loads between the external loads applied and the

---

structural 3D elements. Examples of areas where the different elements are applied can be seen on figure 10.2

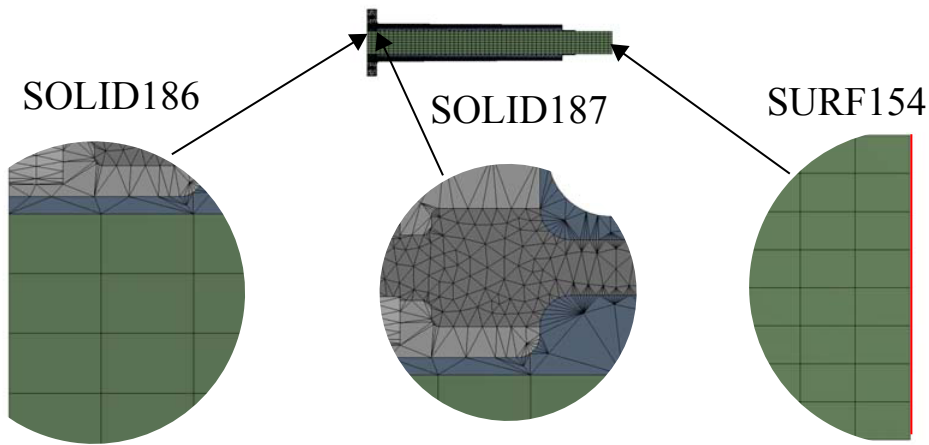


**Figure 10.2:** The different areas meshed with different elements.

The model is also modelled with symmetry conditions, which cuts the model in half. This decreases the computation time and the memory allocation during solving. Since this is a nonlinear analysis, a nonlinear solver is obviously required. ANSYS® has different types of nonlinear solvers, depending of the application. The one used in this analysis is a Newton-Raphson based iterative solver.

## 10.2 Results and Discussion of the Analysis

The model described in the previous section is solved, and the stresses and deflections are evaluated. Only the stresses in the bend stiffener are evaluated, as the pipe in the model is an equivalent pipe, with the only purpose of modelling the stiffness of the pipe. The deflection profile for the entire structure can be seen on figure 10.3

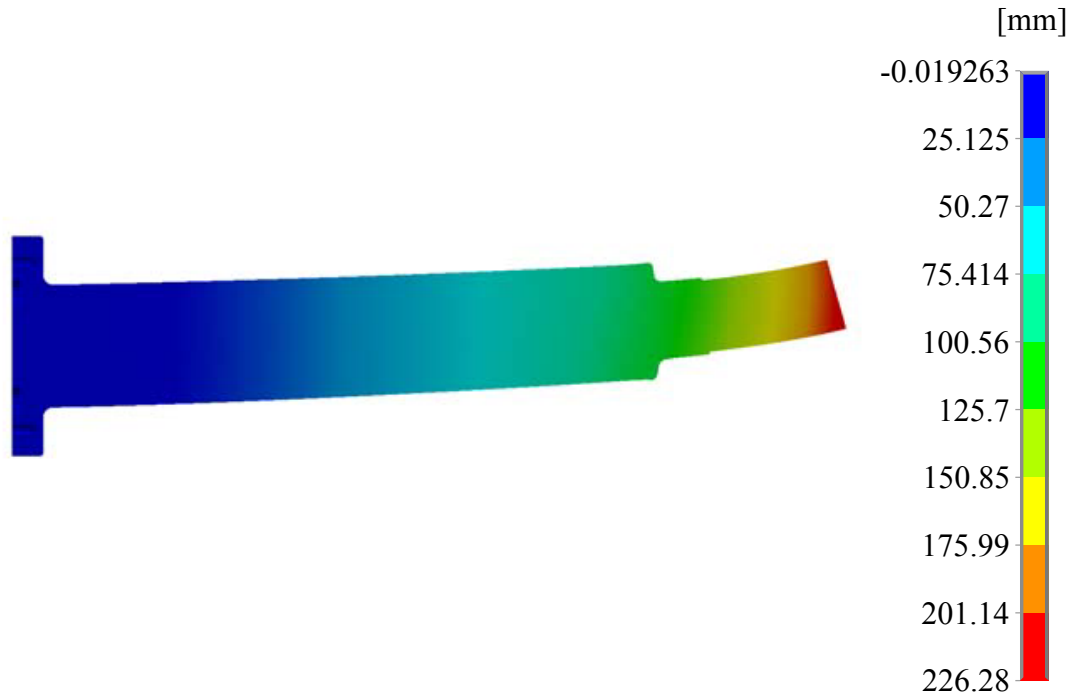


Figure 10.3: The deflection profile.

As it can be seen the deflection is very large, due to the very compliant pipe. The stresses of the critical area of the bend stiffener can be seen on figure 10.4.

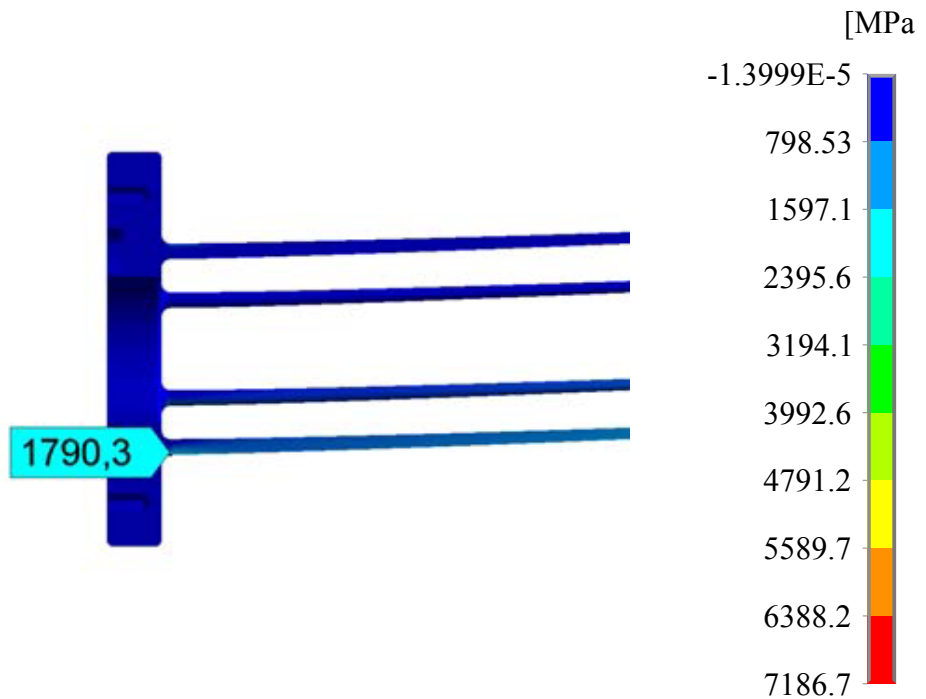


Figure 10.4: Stresses of the steel flange.

It is obvious that the stresses are enormously high in the steel structure, and that the structure will experience a lot of plastic deformation, and properly break before reaching

---

this high deformation state. It can be concluded with a high level of certainty that the design as it is right now cannot be dimensioned in a way so it gets the right strength, without compromising the deflection behaviour, which is undesirable. The reason that this was not discovered on an earlier stage is due to the missing pipe model, which was obtained in the very end of the project period.

## Conclusion and Discussion

A number of different models have been presented and a design procedure have been conducted. This chapter will conclude on the models and the outcome of the design procedure. Also the progress of the project will be discussed.

### Contents

---

<b>11.1 Modelling of the Current Bend Stiffener . . . . .</b>	<b>87</b>
<b>11.2 Design Procedure . . . . .</b>	<b>87</b>
<b>11.3 Optimisation of New Design and Strength Analysis . . . . .</b>	<b>88</b>
<b>11.4 Stiffness Modelling of the Pipe . . . . .</b>	<b>88</b>
<b>11.5 Overall Outcome of the Project . . . . .</b>	<b>89</b>

---

### 11.1 Modelling of the Current Bend Stiffener

The current bend stiffener used today, by National Oilwell Varco (NOV), have been modelled and analysed in order to determine the behaviour and highlight the flaws of this design. The structural behaviour, i.e. the deflection profile was determined by a finite element analysis and compared to an analytical beam model. The modelling of this was conducted with some success, as the models converged towards a common behaviour. The idea was to model the deflection without a pipe model, as this was not provided by the company, and it was originally not the scope of the project to model the pipe. It should be possible to obtain the same behaviour for the old and new design of the bend stiffener regardless of the type of pipe that was inserted to the model. Based on this idea a pipe modelled of solid layers was inserted, well knowing that this pipe was too stiff. This resulted in a deflection profile which could be used for optimizing the deflection of a new design later on. Another analysis conducted on the current bend stiffener was a thermal heat transfer analysis. The purpose of this analysis was to prove that the temperature at the surface of the pipe covered by the bend stiffener was actually a problem. It can be concluded that it indeed was a problem, even for a very optimistic case as described in section 4.4.1 *Thermal Analysis*.

### 11.2 Design Procedure

A new conceptual design based on the experience and requirements obtained through the first phase of the project. This design was a result of a extensive number of drawings and intuitive concepts. The design development followed a procedure developed by a mechanical engineer called Eskild Tjalve. He is, by some people in the industry and at the

---

universities, considered as one of the fathers of product design development. His procedure consist of a number of specific steps to be conducted. These steps were followed and a initial design concept was presented. The general behaviour of this design was evaluated and it was concluded that the design had some significant behaviour issues. Based on these experiences was a new design developed. This design was a combination of the old bend stiffener design from NOV and the previous developed conceptual design. The behaviour of the new combined design was acceptable and was further optimized.

### 11.3 Optimisation of New Design and Strength Analysis

The new design obtained in chapter 7 *Initial Design Evaluation And Development* was optimized towards a desired behaviour. This was done by using the same pipe model as in the analysis of the current bend stiffener. The optimisation was carried out in Matlab<sup>®</sup> and ANSYS<sup>®</sup>, by using a sqp (sequential quadratic programming) procedure. The optimisation succeeded and the behaviour of the new design was similar to the current design. The design was analysed using convection in a thermal analysis. This showed that the design fulfilled the temperature constraint. After almost a full project period without an equivalent pipe stiffness, it was decided to model the pipe and obtain a stiffness in that way (the discussion of this model is presented in the next section). The pipe model was used to evaluate the stresses in the bend stiffener, which was too high compared to the strength of the material. It was concluded that the design could not be dimensioned to carry so high loads without compromising the flexural behaviour, which is undesirable. Furthermore was a fatigue procedure setup and ready for evaluation of the fatigue life, but since the static stresses was too high there was no reason for doing any fatigue calculation. However, the fatigue procedure is presented in appendix D *Fatigue Evaluation*.

### 11.4 Stiffness Modelling of the Pipe

A pipe model was obtained in chapter 9 *Analytical Modelling of the Bending Stiffness of a Flexible Pipe*, based on a set of scientific papers. This chapter describes three ways of obtaining the stiffness of the pipe, depending on the amount of curvature. The first case modelled, was a no slip case where it was assumed that no interlayer sliding occurred, i.e. the axial strain did not exceed the friction resistance. The stiffness obtained in the no slip case is accurate for small curvatures of the pipe. As the curvature increases, slip starts to occur, which is called the partial slip case. The characteristics of this case is that only a part of a helical strip is sliding, while the rest is still in the no slip zone. The stiffness in this case is gradually decreasing as the curvature is increasing, due to the progression of the slip length of a tendon. When the tendons reach their full slip state, the stiffness is zero or so small that it can be neglected. The partial slip together with the no slip stiffness is good at predicting the stiffness as the curvature increases, but since the stiffness does only rely on axial effects, it does not take the local torsion and bending of the helical strips into account. The latter phenomena was modelled by assuming that the helical layers follows a loxodromic curve and that the local curvatures of the tendon can be obtained by projecting the global bending curvature to the local directions, by using the geometry considerations of a loxodromic curve. The stiffness was obtained by expressing the strain energy in means of the local curvatures, and convert it to a bending moment by the use of energy conversion and differentiation. This stiffness is considered to be

the most accurate, and therefore is this used as the stiffness approximation of the helical layers in the pipe, together with the stiffness contribution from the layers of polymer.

### **11.5 Overall Outcome of the Project**

The project leaves an open design proposal for further development, as the design proposal does not fulfill the strength requirements. The new design is good from a thermal point of view, as it actually lowered the temperature below the boundary. The further development can be carried on based on the experiences and models given in this report. All data which was not collected and accessible before this project are presented, i.e. all data needed for further development should be available in this report. This report does also provide an equivalent model of the flexible pipe, which makes it possible to evaluate a future design properly. The report does also provide a fatigue procedure for evaluating the fatigue life on a possible future steel design, but it should be noted that the procedure requires that there are no weldings in fatigue critical areas of the design.



## Future Work

This project forms a basis for future tasks to be conducted. The purpose of this chapter is to highlight some of the future tasks, which is considered to be important for the completeness of developing a new design of the bend stiffener.

### Contents

---

<b>12.1 New Design Proposals . . . . .</b>	<b>91</b>
<b>12.2 Load Scenarios and Experiments . . . . .</b>	<b>91</b>

---

#### 12.1 New Design Proposals

The design proposal in this report have some flaws, which needs a redesign in order to get rid of these flaws. There are several areas within the design which could be considered. One could consider changing the material, as there are great potentials in composites, for example. Another idea could be a pure steel design by taking advantage of a flexible geometry. Other geometries for a design with a combination of steel and polyurethane could also be proposed. Inspiration to new designs could be found in similar structures in the industry, e.g. bend restrictors which is used along the pipe at deeper levels of water.

#### 12.2 Load Scenarios and Experiments

A set of load scenarios have been given in this report. It can be discussed if this set of loads represents the total number of cycles that the structure is exposed to, during its lifetime. A new set of loads could be obtained by a literature study, as there are a lot of papers and theses containing statistics of waves and weather conditions causing the loads on these structures. Also several experiments could be established, in order to determine if the models in this report are correct. If a new design is developed, it could be tested if this design fulfills its purpose.



# Bibliography

- [1] 114  
**American Bureau of Shipping (ABS), Download d. 01-06-2015.**  
American Bureau of Shipping (ABS).  
*FATIGUE ASSESSMENT OF OFFSHORE STRUCTURES*, Download d. 01-06-2015.  
URL: [http://www.eagle.org/eagleExternalPortalWEB/ShowProperty/BEA%20Repository/Rules&Guides/Current/115\\_FatigueAssessmentofOffshoreStructures/Pub115\\_FAOS](http://www.eagle.org/eagleExternalPortalWEB/ShowProperty/BEA%20Repository/Rules&Guides/Current/115_FatigueAssessmentofOffshoreStructures/Pub115_FAOS).
- [2] 25  
**American Petroleum Institute, First edition March 2013, Errata 1 in January 2015.**  
American Petroleum Institute.  
*Specification for Flexible Pipe Ancillary Equipment (API SPECIFICATION 17L1)*, First edition March 2013, Errata 1 in January 2015.  
URL: [Canbeboughtat:http://www.techstreet.com/api/](http://www.techstreet.com/api/) Provided to this project by: National Oilwell Varco Denmark I/S.
- [3] 25  
**American Petroleum Institute, First edition March 2013.**  
American Petroleum Institute.  
*Recommended Practice for Flexible Pipe Ancillary Equipment (API RECOMMENDED PRACTICE 17L2)*, First edition March 2013.  
URL: [Canbeboughtat:http://www.techstreet.com/api/](http://www.techstreet.com/api/) Provided to this project by: National Oilwell Varco Denmark I/S.
- [4] 30  
**ANSYS, Download d. 11-12-2014.**  
ANSYS.  
*ANSYS Mechanical APDL Element Reference*, Download d. 11-12-2014.  
URL: <http://www.ansys.com/>.
- [5] 63  
**Arora, 2012.** Jasbir S. Arora.  
*Introduction To Optimum Design*. ISBN-13: 978-0-12-381375-6.  
Third Edition, Academic Press, Elsevier Inc.,  
2012.
- [6] 51  
**Ashby, 2005.** Michael F. Ashby.  
*Materials Selection in Mechanical Design*. ISBN: 978-0-7506-6168-3.  
Butterworth-Heinemann; 3 edition (February 9, 2005),  
2005.
- [7] 67  
**Atkins and Escudier, 2013.** Tony Atkins and Marcel Escudier.  
*Dictionary of Mechanical Engineering*. ISBN: 978-0199587438.  
Oxford University Press; 1 edition (June 10, 2013),  
2013.

- 
- [8] 12, 26  
**BASF, Download d. 16-03-2015.**  
BASF.  
*Elastollan® TPU Technical Data Sheet*, Download d. 16-03-2015.  
URL: <http://www2.basf.us/urethanechemicals/tpu/pdf/S60DN.pdf>.
- [9] 24  
**Blue Water Shipping, Download d. 14-04-2015.**  
Blue Water Shipping.  
*Cable reels to China*, Download d. 14-04-2015.  
URL: <http://www.bws.dk/news/news-archieve/2011/november/cable-reels-to-china.aspx>.
- [10] 52  
**Cambridge University Engineering Department, Download d. 01-05-2015.**  
Cambridge University Engineering Department.  
*Materials Data Book 2003*, Download d. 01-05-2015.  
URL: <http://www-mdp.eng.cam.ac.uk/web/library/enginfo/cueddatabooks/materials.pdf>.
- [11] 8  
**Chen, Download d. 16-03-2015.**  
Minghao Chen.  
*Fatigue analysis of flexible pipes using alternative element types and bend stiffener data*, Download d. 16-03-2015.  
URL: <http://ntnu.diva-portal.org/smash/get/diva2:507153/FULLTEXT01.pdf>. Norwegian University of Science and Technology. Master Thesis - 2011.
- [12] 108  
**Cook, Malkus, Plesha, and Witt, 2001.** Robert D. Cook, David S. Malkus, Michael E. Plesha, and Robert J. Witt.  
*Concepts and Applications of Finite Element Analysis*,. ISBN:978-0471356059.  
Wiley,  
2001. 4th Edition(October 17, 2001).
- [13] 2  
**Den Store Danske, Download d. 09-04-2015.**  
Den Store Danske.  
*Petrokemisk industri*, Download d. 09-04-2015.  
URL: [http://www.denstoredanske.dk/It%2c\\_teknik\\_og\\_naturvidenskab/Kemi/Petrokemi-\\_Jordolie%2c\\_benzin\\_og\\_asfalt/petrokemisk\\_industri](http://www.denstoredanske.dk/It%2c_teknik_og_naturvidenskab/Kemi/Petrokemi-_Jordolie%2c_benzin_og_asfalt/petrokemisk_industri).
- [14] 2  
**Den Store Danske, Download d. 09-04-2015.**  
Den Store Danske.  
*Solcelle*, Download d. 09-04-2015.  
URL: [http://www.denstoredanske.dk/It,\\_teknik\\_og\\_naturvidenskab/Elektronik,\\_teletrafik\\_og\\_kommunikation/Elektronik,\\_radio\\_og\\_tv/solcelle](http://www.denstoredanske.dk/It,_teknik_og_naturvidenskab/Elektronik,_teletrafik_og_kommunikation/Elektronik,_radio_og_tv/solcelle).
- [15] 114  
**DET NORSKE VERITAS (DNV), Download d. 01-06-2015.**  
DET NORSKE VERITAS (DNV).  
*Fatigue Design of Offshore Steel Structures*, Download d. 01-06-2015.  
URL: <https://exchange.dnv.com/publishing/codes/docs/2011-10/RP-C203.pdf>.
- [16] 75, 78, 79, 81  
**Dong, Huang, Zhang, and Liu, September 2013.**  
Leilei Dong, Yi Huang, Qi Zhang, and Gang Liu. *An Analytical Model To Predict the Bending Behaviour of Unbonded Flexible Pipes*.  
*Journal of Ship Research*, 57(3), 171–177,  
2013. School of Naval Architecture, Dalian University of Technology, Dalian, Liaoning Province, China.

## BIBLIOGRAPHY

---

- [17] 2  
**EHS today, Download d. 09-04-2015.**  
EHS today.  
*CSB to Hold Public Hearing Surrounding the Deepwater Horizon Explosion*, Download d. 09-04-2015.  
URL: <http://ehstoday.com/emergency-management/csb-hold-public-hearing-surrounding-deepwater-horizon-explosion>
- [18] 67  
**Engineering tool box, Download d. 02-06-2015.**  
Engineering tool box.  
*Convective Heat Transfer*, Download d. 02-06-2015.  
URL: [http://www.engineeringtoolbox.com/convective-heat-transfer-d\\_430.html](http://www.engineeringtoolbox.com/convective-heat-transfer-d_430.html).
- [19] 67  
**Engineers Edge, Download d. 02-06-2015.**  
Engineers Edge.  
*Convective Heat Transfer Coefficients Table Chart*, Download d. 02-06-2015.  
URL: [http://www.engineersedge.com/heat\\_transfer/convective\\_heat\\_transfer\\_coefficients\\_\\_13378.htm](http://www.engineersedge.com/heat_transfer/convective_heat_transfer_coefficients__13378.htm).
- [20] 114  
**Engineer's Handbook, Download d. 31-05-2015.**  
Engineer's Handbook.  
*Reference Tables - Surface Roughness Table*, Download d. 31-05-2015.  
URL: <http://www.engineershandbook.com/Tables/surfaceroughness.htm>.
- [21] 50  
**Europe, Download d. 30-04-2015.**  
Plastics Information Europe.  
*Price Details*, Download d. 30-04-2015.  
URL: <http://piweb.plasteurope.com/default.aspx?pageid=22222>.
- [22] 115, 117, 118  
**Fatemi, 2000.** Ali Fatemi.  
*Metal Fatigue in Engineering*. ISBN: 978-0471510598.  
Wiley-Interscience; 2 edition (December 1, 2000), 2000.
- [23] 116  
**Fatigue and Stress Analysis Lab - University of Waterloo, Download d. 31-05-2015.**  
Fatigue and Stress Analysis Lab - University of Waterloo.  
*An energy-based fatigue life model for proportional and nonproportional loading conditions*, Download d. 31-05-2015.  
URL: <https://uwaterloo.ca/fatigue-stress-analysis-lab/research-areas/energy-based-fatigue-life-model-proportional-and>.
- [24] 10  
**First Subsea, Download d. 16-02-2015.**  
First Subsea.  
*First Subsea*, Download d. 16-02-2015.  
URL: <http://www.firstsubsea.com/products/dbsc/image-gallery.html>.
- [25] 34, 37  
**Gere and Goodno, 2008.** James M. Gere and Barry J. Goodno.  
*Mechanics of Materials, SI Edition*. ISBN: 978-0495438076.  
Cengage Learning; 7 edition (July 14, 2008), 2008.

- 
- [26] 12  
**Grytå, Download d. 16-03-2015.**  
Gunhild Grytå.  
*Fatigue of Flexible Riser in Bend Stiffner Area*, Download d. 16-03-2015.  
URL: <http://www.diva-portal.org/smash/get/diva2:515357/FULLTEXT01.pdf>. NTNU Department of Marine Technology. Master Thesis - 2011.
- [27] 2  
**Ingeniøren, Download d. 18-03-2015.**  
Ingeniøren.  
*Knækket ventil lukker norsk Dong-plattform*, Download d. 18-03-2015.  
URL: <http://ing.dk/artikel/knaekket-ventil-lukker-norsk-dong-plattform-132342>.
- [28] 7  
**Jobindex.dk, Download d. 10-02-2015.**  
Jobindex.dk.  
*Virksomhedsprofil: National Oilwell Varco Denmark I/S (NOV Flexibles)*, Download d. 10-02-2015.  
URL: <http://www.jobindex.dk/company/2419/NOV%20Flexibles%20%28National%20Oilwell%20Varco%20Denmark%20I/S%29>.
- [29] 11, 12, 14, 15, 24, 26, 27, 29, 47  
**Johansen, Sørensen, and Lyckegaard, 2015.**  
Lean R. Johansen, Peter T. Sørensen, and Anders Lyckegaard.  
*Meeting with National Oilwell Varco Denmark I/S (NOV Flexibles)*,  
2015. Meeting date: 07-02-2015. Location: Fibigerstræde 14, 9220 Aalborg.
- [30] 107  
**Joseph Carloni, Julia Chen and Torres, Download d. 05-05-2015.**  
Jonathan Matheny Joseph Carloni, Julia Chen and Ashley Torres.  
*FEM Modeling of Instrumented Indentation*, Download d. 05-05-2015.  
URL: <http://slideplayer.com/slide/3190535/>.
- [31] 75, 78  
**Kebadze, 2000.** Elizbar Kebedze.  
*Theoretical modelling of unbonded flexible pipe cross-sections*.  
PhD Thesis, South Bank University, London, UK,  
2000.
- [32] 75, 78  
**Kraincanic and Kebedze, January 2001.**  
I. Kraincanic and E. Kebedze. *Slip initiation and progression in helical armouring layers of unbonded flexible pipes and its effect on pipe bending behaviour*.  
*Journal of Strain Analysis*, 36(3), 265–275,  
2001. South Bank University, London, UK.
- [33] 11  
**LICEngineering, Download d. 26-02-2015.**  
LICEngineering.  
*LICEngineering*, Download d. 26-02-2015.  
URL: <http://www.liceng.dk/files/phamlets/2.3.09.pdf>.
- [34] 107, 108, 109, 110, 111  
**Lund and Lindgaard, September 2013.**  
Erik Lund and Esben Lindgaard.  
*Course material for Course on Finite Element Methods*. pages 289–338,  
2013. Aalborg University (AAU). Department of Mechanical and Manufacturing Engineering.
- [35] 12, 26  
**MatWeb, Download d. 04-03-2015.**

## BIBLIOGRAPHY

---

- MatWeb.  
*304 Stainless Steel*, Download d. 04-03-2015.  
URL: <http://matweb.com/search/DataSheet.aspx?MatGUID=abc4415b0f8b490387e3c922237098da&ckck=1>.
- [36] 12, 26  
**MatWeb, Download d. 04-03-2015.**  
MatWeb.  
*316 Stainless Steel*, Download d. 04-03-2015.  
URL: <http://matweb.com/search/DataSheet.aspx?MatGUID=50f320bd1daf4fa7965448c30d3114ad>.
- [37] 12, 26  
**MatWeb, Download d. 16-03-2015.**  
MatWeb.  
*Arkema Group Rilsan® BESN P40 TL Nylon 11*, Download d. 16-03-2015.  
URL: <http://matweb.com/search/DataSheet.aspx?MatGUID=e65d08dfa6c94e47a53734e8d22a53ff>.
- [38] 12  
**MatWeb, Download d. 16-03-2015.**  
MatWeb.  
*BASF Elastollan S 60 D TPUR*, Download d. 16-03-2015.  
URL: <http://matweb.com/search/DataSheet.aspx?MatGUID=eafd984abb204718af1a6fea244f6498>.
- [39] 101  
**MatWeb, Download d. 25-02-2015.**  
MatWeb.  
*Shore (Durometer) Hardness Testing of Plastics*, Download d. 25-02-2015.  
URL: <http://www.matweb.com/reference/shore-hardness.aspx>.
- [40] 50  
**MetalPrices.com, Download d. 30-04-2015.**  
MetalPrices.com.  
*Stainless Steel*, Download d. 30-04-2015.  
URL: <http://www.metalprices.com/metal/stainless-steel/stainless-steel-flat-rolled-coil-304>.
- [41] 7, 8  
**National Oilwell Varco, Download d. 10-02-2015.**  
National Oilwell Varco.  
*Subsea Production Systems - Flexibles*, Download d. 10-02-2015.  
URL: <http://fps.nov.com/>.
- [42] 4  
**National Oilwell Varco, Download d. 14-04-2015.**  
National Oilwell Varco.  
*10 Reasons for Choosing Flexible Pipes*, Download d. 14-04-2015.  
URL: [https://www.nov.com/Segments/Completion\\_and\\_Production\\_Solutions/Subsea\\_Production\\_Systems/Flexibles/Products\\_and\\_Solutions/10\\_Reasons\\_for\\_Choosing\\_Flexible\\_Pipes.aspx](https://www.nov.com/Segments/Completion_and_Production_Solutions/Subsea_Production_Systems/Flexibles/Products_and_Solutions/10_Reasons_for_Choosing_Flexible_Pipes.aspx).
- [43] 24  
**National Oilwell Varco, Download d. 14-04-2015.**  
National Oilwell Varco.  
*National Oilwell Varco Completes Flexible Pipe Acquisition*, Download d. 14-04-2015.  
URL: <http://www.nov.com/news.aspx?archive=2344>.
- [44] 63  
**Nocedal and Wright, 2006.** Jorge Nocedal and Stephen J. Wright.  
*Numerical Optimization*. ISBN-13: 978-0387-30303-1.  
Springer Science+Business Media, LLC.,  
2006.

- 
- [45] 114, 117, 118  
**Norton, 2010.** Robert L. Norton.  
*Machine Design: International Version.* ISBN: 978-0131384385.  
Pearson Education (US); (February 4, 2010),  
2010.
- [46] 9, 10, 13, 14, 15, 16, 31, 42, 54, 115  
**NOV and Lyckegaard, 2015.**  
National Oilwell Varco Denmark I/S NOV and Anders Lyckegaard. *e-mail*,  
2015. Data, images and photographs distributed by NOV Flexibles, see e-mail correspondence on  
Appendix CD.
- [47] 2  
**Office of Energy Efficiency and Renewable Energy - US, Download d. 09-04-2015.**  
Office of Energy Efficiency and Renewable Energy - US.  
*History of Wind Energy*, Download d. 09-04-2015.  
URL: <http://energy.gov/eere/wind/history-wind-energy>.
- [48] 12, 26  
**Osswald and Menges, 2003.** Tim A. Osswald and Georg Menges.  
*Materials Science of Polymers for Engineers.* ISBN: 978-1-56990-348-3.  
Hanser Publications; Second edition (March 1, 2003),  
2003.
- [49] 101  
**Pro Cal Inc., Download d. 25-02-2015.**  
Pro Cal Inc.  
*Shore Hardness Scale*, Download d. 25-02-2015.  
URL: [http://www.pcimfg.com/wp-content/uploads/2014/03/Shore\\_Hardness\\_Scale.jpg](http://www.pcimfg.com/wp-content/uploads/2014/03/Shore_Hardness_Scale.jpg).
- [50] 101  
**Product Development Notebook, Download d. 25-02-2015.**  
Product Development Notebook.  
*Durometer*, Download d. 25-02-2015.  
URL: [http://www.pdnotebook.com/wp-content/themes/thesis\\_151/images/durometer.gif](http://www.pdnotebook.com/wp-content/themes/thesis_151/images/durometer.gif).
- [51] 22  
**Royal Netherlands Meteorological Institute, Download d. 24-02-2015.**  
Royal Netherlands Meteorological Institute.  
*Annual overview world weather - January-December 2014*, Download d. 24-02-2015.  
URL: [http://www.knmi.nl/klimatologie/annual\\_overview\\_world\\_weather/index.cgi?var=t2m\\_ghcncams\\_w&mon1=dec&year1=2014&anomalie=nee&kort=ja&expert=nee&type=kaartwereld](http://www.knmi.nl/klimatologie/annual_overview_world_weather/index.cgi?var=t2m_ghcncams_w&mon1=dec&year1=2014&anomalie=nee&kort=ja&expert=nee&type=kaartwereld).
- [52] 80, 81  
**Sævik, 1992.** Svein Sævik.  
*On stresses and Fatigue in Flexible Pipes.*  
PhD Thesis, Department of Marine Structures, The University of Trondheim, Trondheim, Norway,  
1992.
- [53] 24  
**Sanmar Chain International, Download d. 26-02-2015.**  
Sanmar Chain International.  
*FPSO / FPU / MOPU*, Download d. 26-02-2015.  
URL: [http://www.sci-chain.com/?page\\_id=236](http://www.sci-chain.com/?page_id=236).
- [54] 1  
**SBC Energy Institute, Download d. 13-04-2015.**  
SBC Energy Institute.  
*Wind Power*, Download d. 13-04-2015.  
URL: <https://www.sbc.slb.com/SBCInstitute/Publications/Wind.aspx>.

## BIBLIOGRAPHY

---

- [55] 3  
**subsea, Download d. 08-05-2015.**  
subsea.  
*Unbonded Flexible Risers - Recent Field Experience and Actions for Increased Robustness*, Download d. 08-05-2015.  
URL: [http://www.ptil.no/getfile.php/PDF/Rapporter/4Subsea\\_%20PSA-Norway\\_Flexibles-rev5.pdf](http://www.ptil.no/getfile.php/PDF/Rapporter/4Subsea_%20PSA-Norway_Flexibles-rev5.pdf).
- [56] 12, 26  
**T&D Reid Brothers, Download d. 16-03-2015.**  
T&D Reid Brothers.  
*Rilsan® Polyamide 11 in Oil & Gas*, Download d. 16-03-2015.  
URL: <http://www.reidbrothers.co.uk/upload/HCL-Smart-Band-Hybrid---RISLAN-Polyamide-11-in-Oil-and-Gas.pdf>.
- [57] 49  
**Tjalve, 1976.** Eskild Tjalve.  
*Systematisk udformning af industriprodukter : vÅrktøjer for konstruktøren*. ISBN: 87-500-1697-0.  
Akademisk Forlag,  
1976.
- [58] 2  
**Wikipedia, Download d. 09-04-2015.**  
Wikipedia.  
*Deepwater Horizon oil spill*, Download d. 09-04-2015.  
URL: [http://en.wikipedia.org/wiki/Deepwater\\_Horizon\\_oil\\_spill](http://en.wikipedia.org/wiki/Deepwater_Horizon_oil_spill).
- [59] 7  
**Wikipedia, Download d. 10-02-2015.**  
Wikipedia.  
*National Oilwell Varco*, Download d. 10-02-2015.  
URL: [http://en.wikipedia.org/wiki/National\\_Oilwell\\_Varco](http://en.wikipedia.org/wiki/National_Oilwell_Varco).
- [60] 2  
**Wikipedia, Download d. 09-04-2015.**  
Wikipedia.  
*Oliekrise*, Download d. 09-04-2015.  
URL: <http://da.wikipedia.org/wiki/Oliekrise#Baggrund>.
- [61] 23  
**Wikipedia, Download d. 24-02-2015.**  
Wikipedia.  
*Seawater*, Download d. 24-02-2015.  
URL: <http://en.wikipedia.org/wiki/Seawater>.
- [62] 75, 76, 80  
**Witz and Tan, 1992.**  
J. A. Witz and Z. Tan. *On the Flexural Structural Behaviour of Flexible Pipes, Umbilicals and Marine Cables*.  
Marine Structures, 5, 229–249,  
1992. Elsevier Science Publishers Ltd., England.
- [63] 26  
**World Weather Online, Download d. 10-03-2015.**  
World Weather Online.  
*Rio De Janeiro Monthly Climate Average, Brazil*, Download d. 10-03-2015.  
URL: <http://www.worldweatheronline.com/Rio-De-Janeiro-weather-averages/Rio-De-Janeiro/BR.aspx>.



# Appendix A

## Shore hardness scale

In this appendix, the Shore hardness scale is described. It is common to use two levels on the Shore hardness scale, A and D. Where A covers hardness interval for soft materials like rubber, while D covers harder materials [39].

To illustrate the difference between the Shore A and D scale, plastic products with different hardness are set up, and the hardness values are compared, see figure A.1.

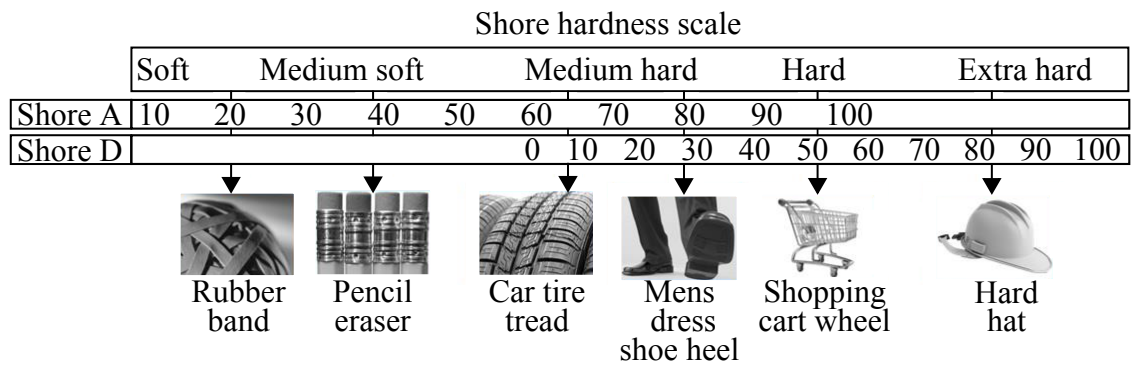


**Figure A.1:** Overall Shore hardness scala for plastic products [49; 50]

From figure A.1 it is seen that the polyurethane used in the bend stiffener is relatively hard.



## Preliminary Finite Element Model

This appendix describes the setup of a preliminary finite element model, see figure B.1. The model is not used because as it required greater computing power, but the knowledge gained from the modelling procedure is used to setup the used model described in section 4.4.2 *Deflection Analysis*. The main idea with the model, is to divide the model into mostly square or rectangular volumes, so partly quadratic shaped elements could be used. The remaining curved volumes could then be meshed with tetrahedral shaped elements. As the used model, is the preliminary model also setup with symmetry condition, the symmetry plane is shown on figure B.1.

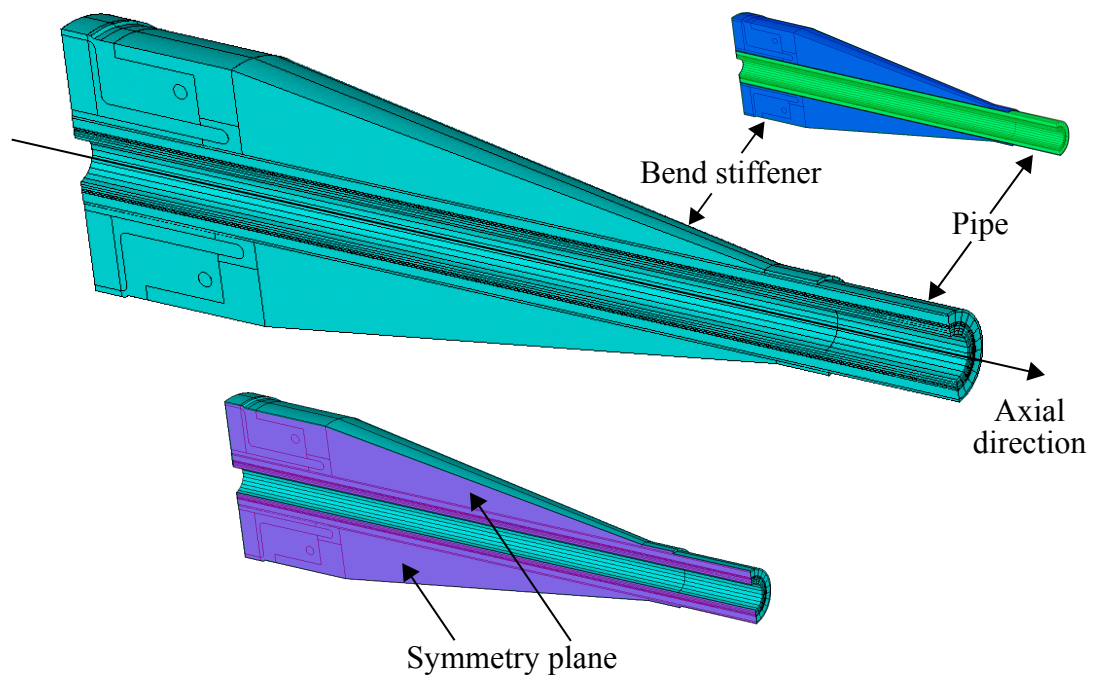


**Figure B.1:** The preliminary model of the bend stiffener with the flexible pipe. **Blue marking:** The bend stiffener. **Green marking:** The flexible pipe. **Violet marking:** The used symmetry plane.

To setup the preliminary model, the cross sectional area of both the bend stiffener and the pipe is drawn, and compared to the used model, consist the cross sectional area of the preliminary model of smaller areas, and these were partly square or rectangular shaped. The curved areas are highlighted on figure B.2, the rest of the areas are square or rectangular shaped.

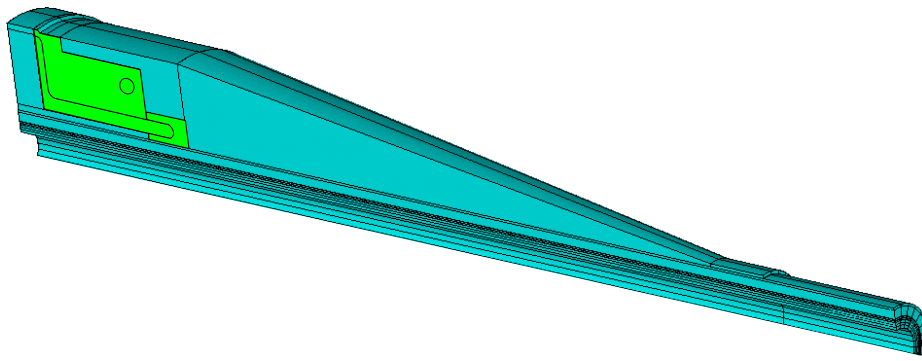


**Figure B.2:** Cross sectional area of the preliminary model. **Green marking:** *Curved areas*

The model is created by rotating the cross sectional area around the axial direction by  $15^\circ$  to generate one volume. Then 11 extra volumes is generated so all the volumes constitute 180 degrees of the bend stiffener and the pipe, this procedure for only the bend stiffener is shown on figure B.3(a) and figure B.3(b).

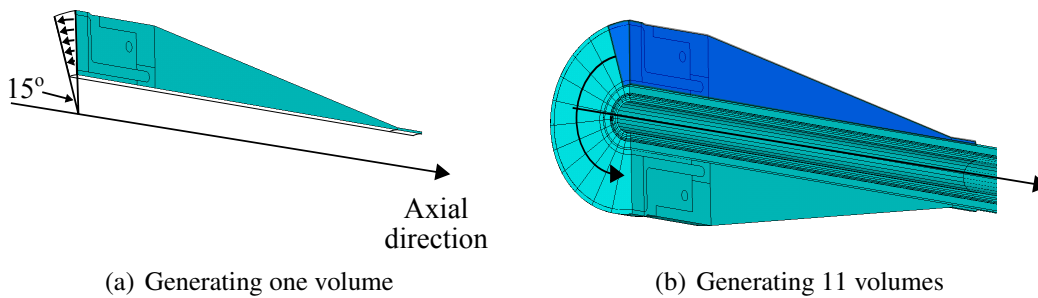


**Figure B.3:** Volume generating procedure for the bend stiffener. **Blue marking:** *One volume*

Hereafter is the steel structure modelled and applied inside the bend stiffener. The steel structure also consisted of individual volumes. The discretization of the model are conducted with partly mapped or sweep mesh. Examples of meshed curved, square and rectangular areas are shown on figure B.4. This also shows the use of the quadratic and tetrahedral shaped elements.

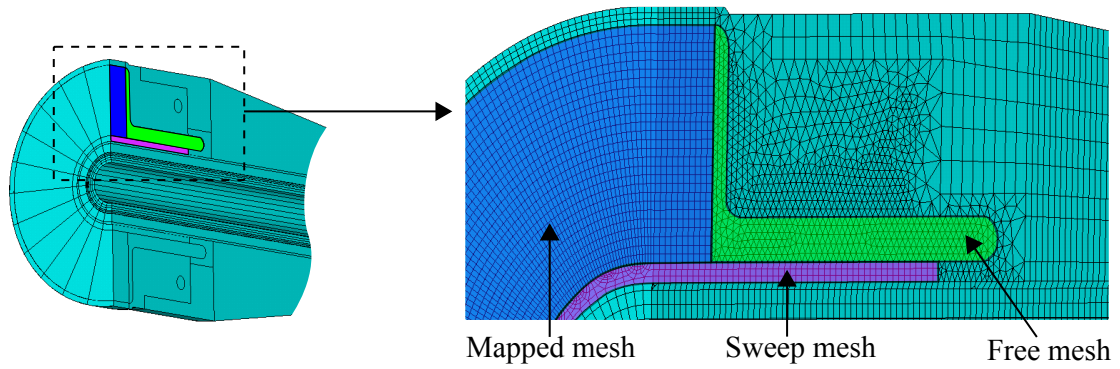


**Figure B.4:** Example of curved, square and rectangular areas, and volumes which are meshed with different shaped elements. The mapped and sweep mesh are conducted with quadratic shaped element, while tetrahedral shaped element are used in the free mesh. **Blue marking:** *Mapped mesh*. **Green marking:** *Free mesh*. **Violet marking:** *Sweep mesh*

The model consisted of over 200 small volumes, which made the model complex to setup, change and refine, but it also required high computing power. Therefore is this model rejected and it is chosen to setup a simpler model, that consist of few volumes.



## The Theory of FE Contact Formulations

A contact problem is a nonlinear problem, because the stiffness is a function of the contact between the bodies. This nonlinear problem is typically solved by the Newton Raphson algorithm, where the load is applied in steps. To explain the contact problem stated in FEA, figure C.1(a), figure C.1(b) and figure C.1(c) are considered. The two bodies in a contact are called the contactor and the target, see figure C.1(a). The idea is to simulate the contact between the contactor and the target by interface elements that work on the surface of each body. The interface elements are activated when the gap between the contactor and the target is within a certain tolerance, the contact is shown on figure C.1(b). The interface elements are applied on the surface of the contactor and the target, and the elements work as a constraint, ensuring that the bodies do not penetrate each other as shown on figure C.1(c). This also means that the interface elements ensure that displacements of the contactor and the target follow each other [34].

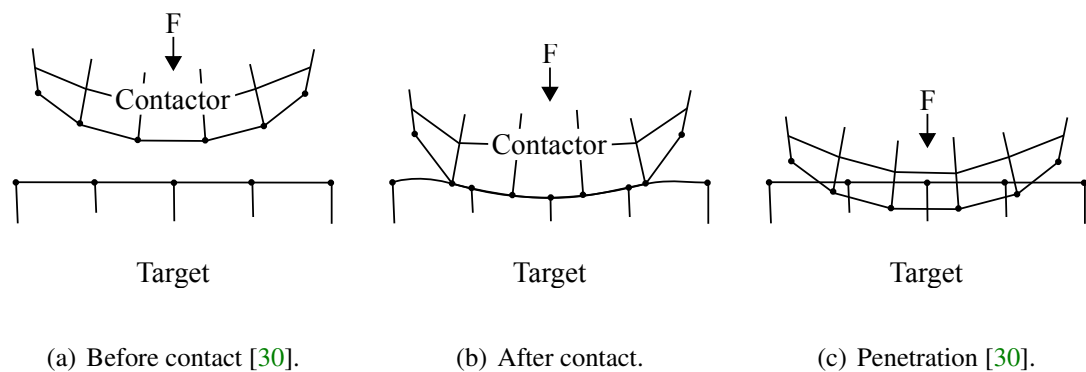


**Figure C.1**

So considering a contact problem, two conditions must be fulfilled. The first condition is that the bodies, which are in contact, must not penetrate each other, in other words there must be compatibility between the bodies. The second condition is momentum conservation, meaning that the total momentum before contact is equal to the momentum after contact. There are two typical methods to formulate a contact problem, the Penalty method and the Lagrange multiplier method, but the normally used FE formulation is a combination of these methods, called the augmented Lagrangian method. The augmented Lagrangian method is an iterative procedure using the Penalty method, and in this procedure the pressure and frictional stresses are augmented with the Lagrangian method, which ensures no penetration [34].

The Penalty method adds a constraint in terms of an artificial stiffness in order to formulate a function that prevents penetration of the bodies. So when the bodies are within a certain

tolerance, the artificial stiffness will be applied, and the contact between the bodies can be simulated. To explain the Penalty method, two situations are considered, the situation before contact and the situation after contact, these are shown on figure C.2(a) and figure C.2(b) [34].

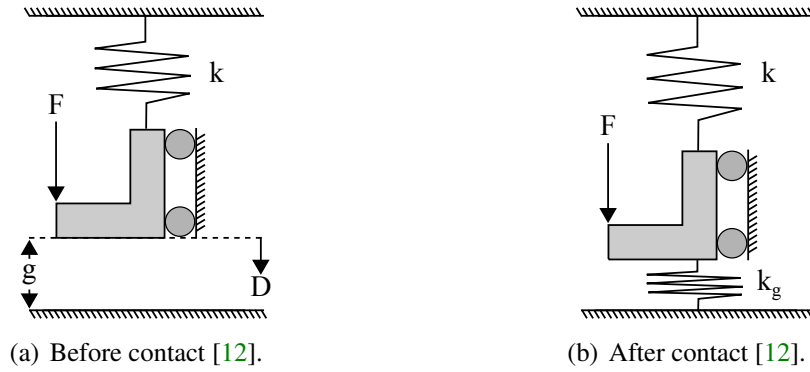


Figure C.2

On figure C.1(a), a L-shaped block is connected to a spring with the stiffness,  $k$ . The subsurface and the L-shaped block are separated by a gap,  $g$ , and the block is affected by a Force,  $F$ , which leads to a displacement,  $D$ . As long as the displacement is smaller than the gap, the systems force equilibrium is stated by  $F = kD$ . If the displacement becomes larger than the gap, due to the load, the system is applied with a artificial stiffness ( $k_g$ ), this is shown on figure C.1(b). So the force before contact is expressed by equation (C.1), while the force after contact is stated by equation (C.2) [34; 12].

$$F = kD \text{ for } D < g \quad (C.1)$$

$$F = (k + k_g)D \text{ for } D \geq g \quad (C.2)$$

The artificial stiffness works, so it is zero, when the displacement is smaller than the gap, and it has a magnitude when the displacement crosses the gap, this behaviour is shown on figure C.3, and the non linear behaviour of the problem is thereby seen.

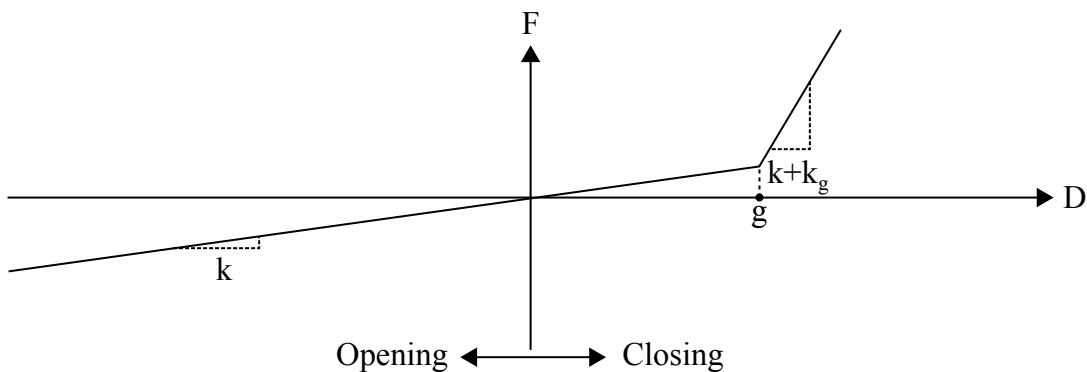


Figure C.3: Force/displacement curve [12].

The setting of the artificial stiffness is associated with some difficulties, if the stiffness do not have a proper magnitude, compatibility between the bodies will not be ensured,

### C. The Theory of FE Contact Formulations

however will the method ensures conservation of momentum. The stiffness has normally a large magnitude in order to enforce the constrain that ensures no penetration of the bodies. With the Lagrange multiplier method is the contact formulated with a force constraint in order prevent the penetration. The Lagrange multiplier method is formulated as

$$F = kD \text{ for } D < g \quad (\text{C.3})$$

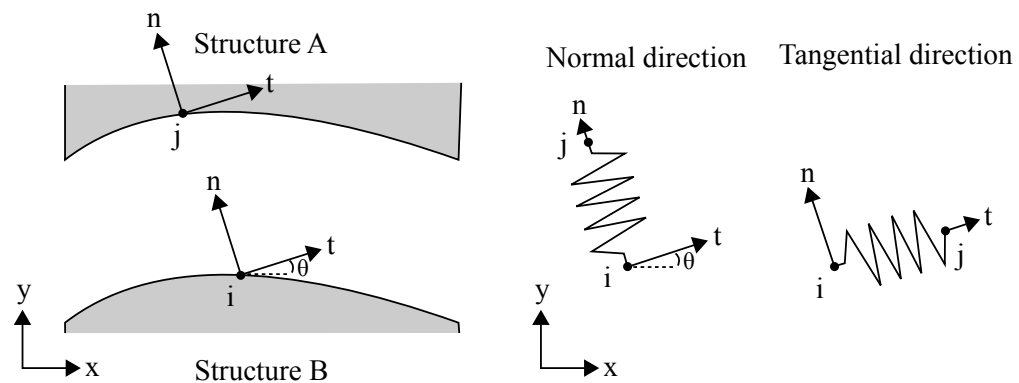
$$\begin{bmatrix} k & 1 \\ 1 & 0 \end{bmatrix} \begin{Bmatrix} D \\ \lambda \end{Bmatrix} = \begin{Bmatrix} F \\ g \end{Bmatrix} \text{ for } D \geq g \quad (\text{C.4})$$

And this leads too

$$D = g \quad (\text{C.5})$$

$$F = kD + \lambda \Leftrightarrow \lambda = F - kD \quad (\text{C.6})$$

The Lagrange multiplier method ensures compatibility, but conservation of momentum is not necessary fulfilled. The following text describes a Penalty based 2D interface element, this element is alike the one used by ANSYS. To described the element a contact problem between two structures is considered, see figure C.4(a). On figure C.4(a) are the structures A and B divided by a gap, the purpose is to formulated a interface element that describes the contact between node j and i on structure A and B. As it is a 2D contact problem, the element between node j and i must represent the two parallel surfaces that can be in contact, which is a pair in the normal direction, denoted as n, and another in the tangential direction, t. The element has the orientation  $\theta$ , and the element can be considered as two springs acting in normal direction and tangential direction, see figure C.4(b) [34].



(a) The normal and tangential direction of the nodes on the two surfaces [34]. (b) The two springs in normal direction and tangential direction [34].

**Figure C.4**

With the springs is it possible to formulate the contact between structure A and B, in both normal direction as well as the tangential direction. As contact in two directions are include in the element, must the force in each direction be described. When the normal force is positive (tension), the gap will be larger, and no contact will be established. If the normal force is negative (compressive), contact will be established, and the normal

displacements and forces will be related by the spring stiffness,  $k_n$ . If  $k_n$  is very large compared to the force, will the displacement of node j be equal to node i. The infinitesimal displacements in normal direction, defined for the local coordinate system, are for node j and i are denoted as  $v_{Lj}$  and  $v_{Li}$ , and the change in the displacements in the normal direction,  $\Delta v$ , is given by

$$\Delta v = v_{Lj} - v_{Li} + Gab \quad (C.7)$$

since the expression above contains the gap between the structures, will the gaps influence be considered. If there are no gap, will the compressive force immediately cause a displacement in the normal direction, shown by C.5(a). However if there are a opening or a gap, will the gab in equation (C.7) be larger than zero, meaning that the gap must be closed before the spring effect is activated, which is illustrated on figure C.5(b). If the gab in equation (C.7) is negative, it means that the contact is applied with a preload, so the spring is stretched and the compressive force must overcome the preload in order to close the gap, this is shown on figure C.5(c).

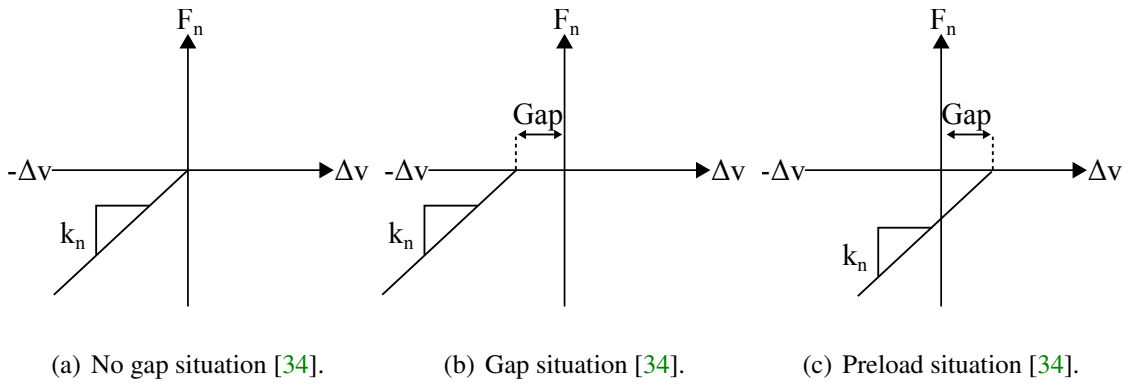


**Figure C.5:** Force/displacement curve for the normal direction.

Next will the force in the tangential direction be considered. The tangential force is only defined when the normal force is compressive, and is expressed by Coulomb friction, which is given by the friction coefficient,  $\mu$ . As long as the tangential force is smaller than the normal force multiplied with  $\mu$ , no sliding of the surfaces occurs equation (C.8), while the sliding situation is given by equation (C.9). The relative displacement in the tangential direction ( $\Delta u$ ) is stated by equation (C.10). In this expression are  $u_{Lj}$  and  $u_{Li}$  the infinitesimal displacements in tangential direction, and  $U_{slide}$  is the accumulated amount of sliding.

$$|F_t| \leq \mu |F_n| \quad (No \ sliding) \quad (C.8)$$

$$|F_t| > \mu |F_n| \quad (Sliding \ occurs) \quad (C.9)$$

$$\Delta u = u_{Lj} - u_{Li} - U_{slide} \quad (C.10)$$

The relation between the normal force, the tangential force and  $U_{slide}$  is shown on figure C.6.

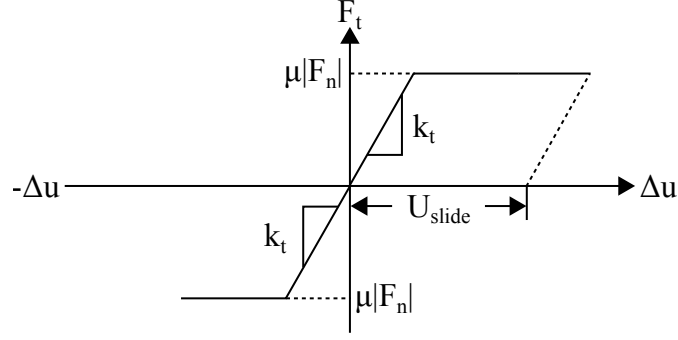


**Figure C.6:** Force/displacement curve for the tangential direction [34].

Since the forces in the local coordinate system is determined, the local stiffness matrix can be setup by considering the local element equilibrium, see equation (C.11). In equation (C.11), the element force vector,  $F_L$ , and the element displacement vector,  $\Delta_L$  are expressed by the forces and displacements in the normal and tangential direction for each node as shown in equation (C.12) and equation (C.13). Thereby can the element stiffness matrix be setup as shown in equation (C.14).

$$\{F_L\} = [K_L] \{\Delta_L\} \quad (C.11)$$

$$\{F_L\} = \{F_{ti} \ F_{ni} \ F_{tj} \ F_{nj}\}^T \quad (C.12)$$

$$\{\Delta_L\} = \{u_{Li} \ v_{Li} \ u_{Lj} \ v_{Lj}\}^T \quad (C.13)$$

$$[K_L] = \begin{bmatrix} k_t & 0 & -k_t & 0 \\ 0 & k_n & 0 & -k_n \\ -k_t & 0 & k_t & 0 \\ 0 & -k_n & 0 & k_n \end{bmatrix} \quad (C.14)$$

To formulate the equations in the global coordinate system, the 2D transformation matrix,  $[T]$ , is used and this stated by equation (C.15).

$$[T] = \begin{bmatrix} \cos(\theta) & \sin(\theta) & 0 & 0 \\ -\sin(\theta) & \cos(\theta) & 0 & 0 \\ 0 & 0 & \cos(\theta) & \sin(\theta) \\ 0 & 0 & -\sin(\theta) & \cos(\theta) \end{bmatrix} \quad (C.15)$$

$\cos(\theta)$  and  $\sin(\theta)$  are determined by the used of the elements shape functions. The global element force and displacement vectors can now be expressed as shown by equation (C.16) and equation (C.17). It can be shown that the global element stiffness can be written as shown in equation (C.18)

$$\{F_G\} = \{F_{xi} \ F_{yi} \ F_{xj} \ F_{yj}\}^T = [T]^T \{F_L\} \quad (C.16)$$

$$\{\Delta_G\} = \{u_{xi} \ v_{xi} \ u_{yj} \ v_{yj}\}^T = [T]^T \{\Delta_L\} \quad (C.17)$$

$$[K_G] = [T]^T [K_L] [T] \quad (C.18)$$

---

The user must define the following parameters

1. Nodes i and j
2. Normal stiffness
3. Tangential stiffness
4. Friction coefficient
5. Initial value of the gap
6. Convergence measures

To setup a proper contact problem, can be associated with some difficulties, as the above quantities might be unknown.

## Fatigue Evaluation

The aim of this appendix is to describe how fatigue of the steel structure inside the bend stiffener is calculated. The evaluation of the designs resistance to fatigue is based on stress-life (S-N) methods for proportional multiaxial stresses and the Palmgren-Miner linear damage hypothesis. The following section describes how a corrected S-N curve is determined, and represented by Basquin's equation. Afterwards, the considerations behind the selected approach are outlined. At the end of the chapter, the approach for the fatigue calculations is introduced.

### D.1 The Setup of a Corrected S-N Curve

In the approach for the fatigue calculations, a corrected S-N curve is used. This curve is expressed by Basquin's equation, equation (D.1).

$$S_{N_f} = A(N_f)^B \quad (D.1)$$

In equation (D.1),  $S_{N_f}$  is the fatigue strength,  $N_f$  is the fatigue life, and the letter A is a coefficient presenting the value of  $S_{N_f}$  at one cycle. B is the slope of S-N curve on a log-log graph. To setup Basquin's equation representing a corrected S-N curve, the uncorrected endurance limit for the stainless steel,  $S_{e'}$ , is calculated as shown in equation (D.2) and equation (D.3). In equation (D.2),  $S_{ut}$  is the ultimate tensile strength.

$$S_{e'} = 0.5 \cdot S_{ut} \quad (D.2)$$

$$S_{e'} = 0.5 \cdot 505MPa = 252.5MPa \quad (D.3)$$

The calculated uncorrected endurance limit,  $S_{e'}$ , is corrected by the factors for the axial load in table D.1, as all the multiplied corrected factors, for axial load has a lower value than the multiplied corrected factors for a bending load.

**Table D.1:** The used correction factors.

Loads	$C_{Load}$	$C_{Size}$	$C_{Surf}$	$C_{Temp}$	$C_{Reliab}$	Total
Bending	1	0.9	0.95	1	0.868	0.742
Axial	0.7	1	0.95	1	0.868	0.577

The values for correction factors for  $C_{load}$  and  $C_{size}$  are simply based on the type of loading and the size of the machine part. The machine part is the rod at the critical region, displayed with blue on figure D.3.

$C_{Surf}$  is set to 0.95, corresponding to a surface finish of  $125 \mu in$ , which is a widely used value for a turning manufacturing process [20].  $C_{Temp}$  is set to 1, as the temperature is below  $450^\circ C$ , while the value of  $C_{Reliab}$  chosen to represent a reliability of 95 %. This value is selected as it is common to use a reliability for welded offshore steel structures of 97.7% [1; 15; 45].

The corrected endurance limit,  $S_{e'}$ , is calculated, and the slope of the S-N curve is determined by Basquin's equation, as shown on equation (D.4) and equation (D.6).

$$S_{ut} = S_{ut}(1)^B \quad (D.4)$$

$$S_e = S_{ut}(10^6)^B \quad (D.5)$$

$$B \approx -0.09 \quad (D.6)$$

$$(D.7)$$

Hereby is Basquin's equation representing the used S-N curve set up as shown in equation (D.8).

$$S_{Nf} = 505 \text{Mpa}(N_f)^{-0.09} \quad (D.8)$$

The drawn S-N curve is displayed on figure D.1. The dashed line illustrates the uncorrected S-N curve.

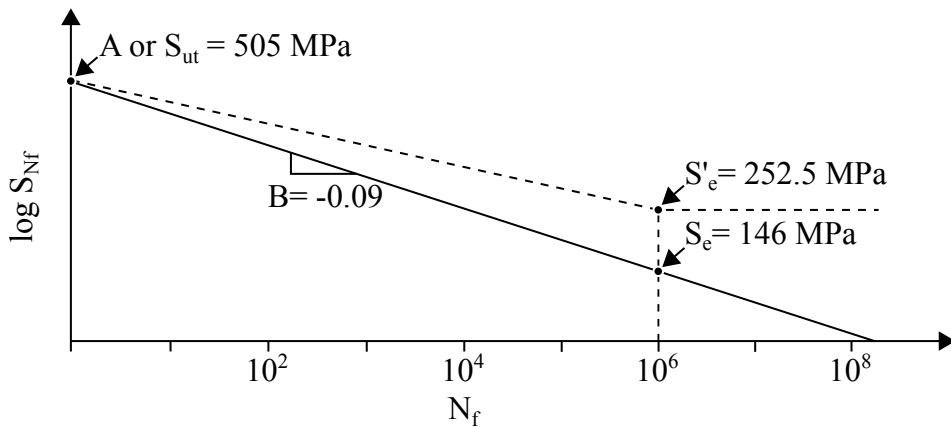


**Figure D.1:** The corrected S-N curve.

Next, the considerations behind the selected approach are described.

## D.2 Considerations and the Overall Approach

The approach is based on considerations about the loads, regions with notches and the selection of a fatigue criteria. Therefore, this section begins with a description of the loads and regions of the structure, which are particularly sensitive to fatigue. In the last part of this section, the overall steps of the approach are described. The loads are listed in table D.2. The load cycle for each load case is represented by an upper and lower limit. All loads with a maximum value are listed as the upper limit, and all minimum values are denoted as the lower limit, see table D.2

**Table D.2:** Load cases - Bend stiffener and pipe assembly

Load Case	No. of Cycles	Min. Tens.	Max. Tens.	Tens. Range	Min. Shear	Max. Shear	Shear Range	Min. Mom.	Max. Mom.	Mom. Range
		Lower	Upper		Lower	Upper		Lower	Upper	
-	-	kN	kN	kN	kN	kN	kN	kNm	kNm	kNm
1	1065600	1100	1300	200	-30.7	20.65	51.35	-74.4	69.01	143.41
2	586000	1080	1320	240	-35.09	26.51	61.6	-89.05	82.84	171.89
3	267000	1060	1340	280	-39.23	32.5	71.73	-103.7	94.83	198.53
4	80000	1050	1350	300	-41.21	35.54	76.55	-111.1	100.2	211.4
5	1000	933.1	1463	529.9	-67.43	83.04	150.47	-223.2	170.2	393.4
6	400	893.8	1491	597.2	-112	160.5	272.5	-405.2	288	693.2

All tension forces are along the x-axis, shear forces are along the z-axis and all moments are around the y-axis, see the axes on figure 2.15. All data in this table are from [46].

There are six load cases with a total number of 2 million load cycles, and the design must be able to withstand these cycles. The load tests are intended to imitate the load cycles, which could affect the bend stiffener under operational conditions, throughout the required lifetime. However, the correlation between the test and the real load cycles under operational conditions is uncertain. It is therefore chosen to setup a conservative approach.

The loads in one cycle are proportional, meaning that the amplitudes of the stresses peaks simultaneously, while nonproportional loading is when the loads are out of phase. An example of stress as a result of proportional and nonproportional loading are shown on figure D.2. On the figure, an element affected by a normal stress,  $\sigma_x$ , and shear stress,  $\tau_{xy}$  is shown. If the loads are proportional, the stresses are in phase, such that the stresses peaks simultaneously at time A, B and C. Under nonproportional loading the stresses are out of phase, and in the case on the figure, the normal stress is constant while the shear stress cycles [22].

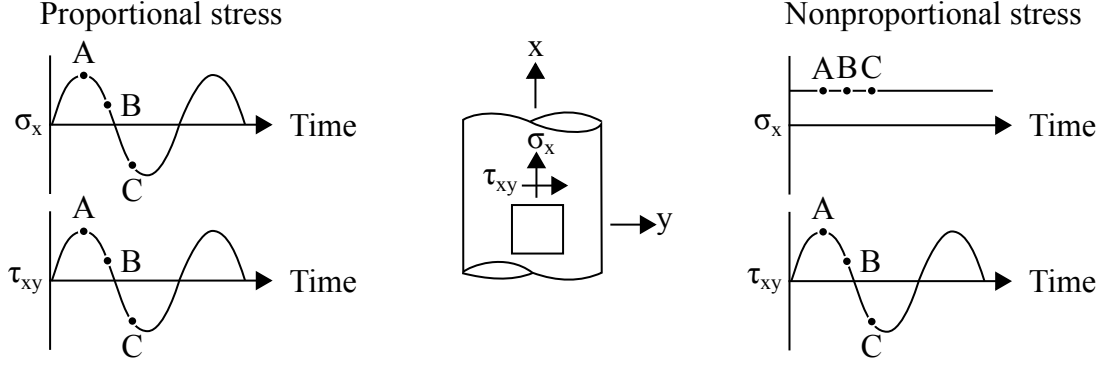


**Figure D.2:** Proportional and nonproportional loading [23].

The steel structure inside the new design contains notches, and these regions are particularly sensitive to fatigue. The main critical region of the structure is therefore considered to be in the interface between the rods and the flange, this region is highlighted with blue on figure D.10.

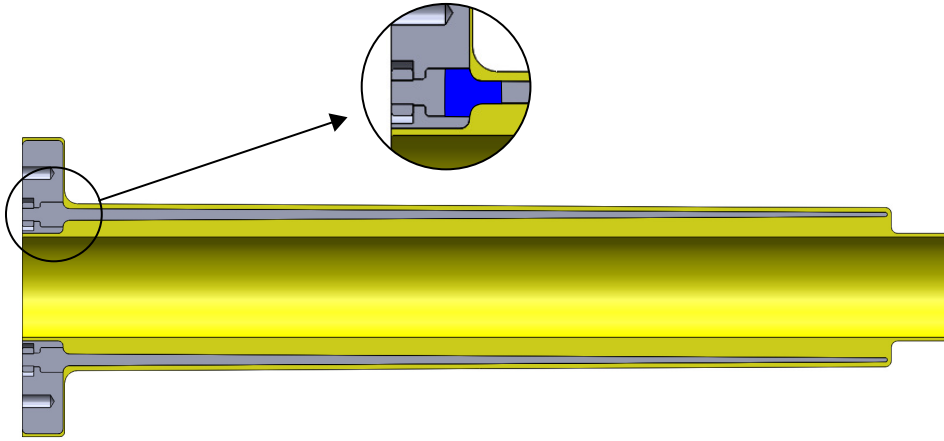


**Figure D.3:** Critical region of the structure.

Based on these considerations, the fatigue analysis is setup. The overall idea is to gather stresses from FE static analysis of each load cycle, and afterwards calculate an equivalent alternating and mean stresses using the Von Mises criteria. The equivalent alternating and mean stress are denoted as  $\sigma'_a$  and  $\sigma'_m$ . See Von Mises criteria for the alternating and mean stress in equation (D.9) and (D.10).

$$\sigma'_a = \sqrt{\frac{(\sigma_{x_a} - \sigma_{y_a})^2 + (\sigma_{y_a} - \sigma_{z_a})^2 + (\sigma_{z_a} - \sigma_{x_a})^2 + 6(\tau_{xy_a}^2 + \tau_{yz_a}^2 + \tau_{zx_a}^2)}{2}} \quad (\text{D.9})$$

$$\sigma'_m = \sqrt{\frac{(\sigma_{x_m} - \sigma_{y_m})^2 + (\sigma_{y_m} - \sigma_{z_m})^2 + (\sigma_{z_m} - \sigma_{x_m})^2 + 6(\tau_{xy_m}^2 + \tau_{yz_m}^2 + \tau_{zx_m}^2)}{2}} \quad (\text{D.10})$$

In equation (D.9), the  $\sigma_{x_a}$ ,  $\sigma_{y_a}$  and  $\sigma_{z_a}$  are the alternating normal stresses. The  $\sigma_{x_m}$ ,  $\sigma_{y_m}$  and  $\sigma_{z_m}$  are the normal mean stresses.  $\tau_{xy_a}$ ,  $\tau_{yz_a}$  and  $\tau_{zx_a}$  are the alternating shear stresses,

while the  $\tau_{xy_m}$ ,  $\tau_{yz_m}$  and  $\tau_{zx_m}$  are the mean shear stresses. With the equivalent alternating and mean stresses are the damage from each load case determined by a corrected S-N curve, and by Palmgren-Miner damage hypothesis is a total damage obtained. The safety factor for fatigue is set to ten, as described in section 2.3.3 *Load Cases*. The safety factor is applied by lowering the allowable damage with a factor of ten.

The Von Mises criteria is normally used for ductile materials. Ductile materials has over 5% elongation before fracture in a tensile test, such as stainless steel 304 [45]. The selection for the Von Mises criteria is based on considerations about the widely used criterias for fatigue calculation for elements in a multiaxial stress condition. The considered criterias are: The maximum principal stress criteria and the Sines Method. The maximum principal stress criteria is displayed in equation (D.11), where  $\sigma_{1_a}$  is the principal alternating nominal stress. This criterion is based on the concept that failure occurs, when a the maximum principal stress in a element subjected to multiaxial stresses exceeds the maximum normal strength for the material in a tension test. The maximum principal stress criterion is normally used for brittle materials like cast iron. The other criteria is the Sines method, in this method the equivalent alternating stress is calculated as in the Von Mises criteria, the Sines method is shown iequation (D.12). Equivalent stress methods, such as Von Mises criteria, should only be used for proportional loading, and where the principal axes directions remain the same during the load cycle. [45; 22].

$$\sigma'_a = \sigma_{1_a} \quad (\text{D.11})$$

$$\sqrt{2}S_{Nf} = \sqrt{\frac{(\sigma_{x_a} - \sigma_{y_a})^2 + (\sigma_{y_a} - \sigma_{z_a})^2 + (\sigma_{z_a} - \sigma_{x_a})^2 + 6(\tau_{xy_a}^2 + \tau_{yz_a}^2 + \tau_{zx_a}^2)}{2} + m(\sigma_{x_m} + \sigma_{y_m} + \sigma_{z_m})} \quad (\text{D.12})$$

In equation (D.12), m is a coefficient indicating the influence of the mean stress and  $S_{Nf}$  is uniaxial fully reversed fatigue strength. The coefficient m can be determined by experiments, and a value of 0.5 is normally used. The Sines method do not take shear mean stresses into account, and the Von Mises criteria is considered to be more conservative than Sines method [45; 22]. The Von Mises method is mainly chosen because the criteria is conservative, compared to Sines method, and the method includes all stresses [22]. As the criteria is selected, the following section describes the steps of the approach.

### D.3 The Approach for The Fatigue Calculations

The following section describes the used approach to estimate the damage caused by the cycling loads.

1. FE static analysis of each upper and lower limit of each load case are conducted. Based on these analyses, the regions on the steel structure subjected to maximum Von Mises stresses are located.

- 
2. From the FE analysis, the nodal stress solutions covering the critical region of the structure are written to text files. Thereby will 12 data files be written, each file will contain data from the same critical region.
  3. The data are imported in to MatLab, where the stress range for each element for each load case is calculated. In the equations below the  $\Delta\sigma_{1\ Element}$ , is the stress range tensor for load case 1, specified by the selected element, while  $\sigma_{1U\ Element}$  and  $\sigma_{1L\ Element}$  is the upper and lower stress tensor specified the particular element. As there are six load cases, there are also six stress range tensors.

$$\Delta\sigma_{1\ Element} = \sigma_{1U\ Element} - \sigma_{1L\ Element} \quad (D.13)$$

$$\Delta\sigma_{2\ Element} = \sigma_{2U\ Element} - \sigma_{2L\ Element} \quad (D.14)$$

$$\vdots \quad (D.15)$$

$$\Delta\sigma_{6\ Element} = \sigma_{6U\ Element} - \sigma_{6L\ Element} \quad (D.16)$$

4. The Von Mises stresses for all stress ranges are calculated.
5. The specific element with the largest Von mises stress for each load case is determined. Thereby is it possible that six different elements are picked out, one for each load case. If different elements are picked out, the approach for the fatigue calculation is conducted for every element. Thereby, the element with the maximum damage is sought.
6. Based on one element number, the upper and lower stress tensor for each load case are setup, and the principal stresses and their directions are determined.
7. The directions for the principal stresses are compared, in order to control if the directions remain fixed through the load cycle.
8. Based on the upper and lower stress tensor, an alternating and mean tensor are calculated. The index,  $i$ , indicates the specific load case.

$$\sigma_{ai\ Element} = \frac{(\sigma_{iU\ Element} - \sigma_{iL\ Element})}{2} \quad (D.17)$$

$$\sigma_{mi\ Element} = \frac{(\sigma_{iU\ Element} + \sigma_{iL\ Element})}{2} \quad (D.18)$$

9. As compressive mean stresses has a beneficial effect on fatigue, these should be included in the calculations. However, if these negative values are inserted in the Von Mises criteria, the compressive mean stresses will be calculated as a mean tensile stress, because these are raised to the second power. An example is  $\tau_{xym}^2$ . Therefore, all the compressive mean stresses in the mean stress tensor is set to zero. This is assumed to make the calculations more conservative [45; 22].

10. With the alternating and mean tensor, the equivalent alternating and mean stresses for load case,  $\sigma'_{ai}$  and  $\sigma'_{mi}$ , are calculated using Von Mises criteria.

$$\sigma'_{ai} = \sqrt{\frac{(\sigma_{xa} - \sigma_{ya})^2 + (\sigma_{ya} - \sigma_{za})^2 + (\sigma_{za} - \sigma_{xa})^2 + 6(\tau_{xya}^2 + \tau_{yza}^2 + \tau_{zxa}^2)}{2}} \quad (\text{D.19})$$

$$\sigma'_{mi} = \sqrt{\frac{(\sigma_{xm} - \sigma_{ym})^2 + (\sigma_{ym} - \sigma_{zm})^2 + (\sigma_{zm} - \sigma_{xm})^2 + 6(\tau_{xym}^2 + \tau_{yzm}^2 + \tau_{zxm}^2)}{2}} \quad (\text{D.20})$$

11. The fatigue strength,  $S_{Nfi}$ , and the fatigue life,  $N_{fi}$ , of each load case is determined using the modified Goodman equation, equation (D.21), and Basquin's equation for the corrected S-N curve, equation (D.22).

$$\frac{\sigma'_{ai}}{S_{Nfi}} + \frac{\sigma'_{mi}}{S_{ut}} = 1 \quad (\text{D.21})$$

$$S_{Nfi} = 505\text{Mpa}(N_{fi})^{-0.09} \quad (\text{D.22})$$

12. The damage of each load case is gathered to one total damage,  $D_{PM}$ , by the Palmgren-Miner linear damage hypothesis, equation (D.23). To include the safety factor, the allowable sum of the damages is set to  $\frac{1}{10}$ .

$$D_{PM} = \sum \frac{n_i}{N_{fi}} = \frac{n_1}{N_{f1}} + \frac{n_2}{N_{f2}} + \dots + \frac{n_6}{N_{f6}} = \frac{1}{10} \quad (\text{D.23})$$

As mentioned earlier, the procedure is conducted for every element with a maximum stress range in order to determine the maximum damage on the structure.



# **Annex-CD**

Below is the contents of the enclosed CD:

**D.4 Report (pdf-version)**

**D.5 Optimisation Scripts**

**D.6 Thermal Models**

**D.7 Nonlinear Stress Analysis**

**D.8 3D Pipe Model**

**D.9 New Design 3D Model**

**D.10 Fatigue Script**